# PREPARATION OF POLY(METHYL METHACRYLATE-*CO*-BUTYL ACRYLATE)/ORGANOPHOSPHATE MODIFIED MONTMORILLONITE NANOCOMPOSITES


SANIT SIRAPANICHART



A THESIS SUBMITTED IN FULFILLMENT

OF THE REQUIREMENT FOR THE DEGREE OF

MASTER OF SCIENCE IN NANOSCIENCE AND NANOTECHNOLOGY

COLLEGE OF NANOTECHNOLOGY

KING MONGKUT'S INSTITUTE OF TECHNOLOGY LADKRABANG

2012

KMITL-2012-NT-M-001-001

| | |
|---|---|
| **หัวข้อวิทยานิพนธ์** | การเตรียมวัสดุประกอบนาโนระหว่างพอลิเมทิลเมทา-คริเลต-โค-บิวทิลอะคริเลตกับมอนต์มอริลโลไนต์ปรับปรุงโครงสร้างด้วยออแกโนฟอสเฟต |
| **นักศึกษา** | นายสานิตย์ สิระปาณิชาติ |
| **รหัสประจำตัว** | 51064607 |
| **ปริญญา** | วิทยาศาสตรมหาบัณฑิต |
| **สาขาวิชา** | นาโนวิทยาและนาโนเทคโนโลยี |
| **พ.ศ.** | 2555 |
| **อาจารย์ที่ปรึกษาวิทยานิพนธ์** | ผศ.ดร.ภัทธาวุธ มนต์วิเศษ |
| **อาจารย์ที่ปรึกษาวิทยานิพนธ์ร่วม** | ผศ.ดร.ปุณณมา ศิริพันธ์โนน<br>รศ.ดร.จิติ หนูแก้ว |


## บทคัดย่อ


งานวิจัยนี้เป็นการเตรียมฟิล์มของวัสดุประกอบนาโนระหว่างพอลิเมทิลเมทาคริเลต-โค-บิวทิลอะคริเลตกับมอนต์มอริลโลไนต์ที่แทรกสอดด้วยเตตระบิวทิลฟอสโฟเนียม (P(MMA-*co*-BA)/P-MMT) โดยใช้เทคนิคการหล่อแบบสารละลาย พอลิเมอร์ร่วม P(MMA-*co*-BA) ถูกสังเคราะห์ขึ้นผ่านปฏิกิริยาพอลิเมอไรเซชันแบบสารละลาย และใช้เบนโซอิลเปอร์ออกไซด์เป็นตัวริเริ่ม P-MMT ถูกดัดแปรโครงสร้างด้วยเตตระบิวทิลฟอสโฟเนียมโบรไมด์ (TBPB) ผ่านปฏิกิริยาการแลกเปลี่ยนประจุบวก ซึ่งพบว่า P-MMT มีระยะห่างระหว่างระนาบ *001* ($d_{001}$) กว้างกว่า Na-MMT และมีปริมาณของ TBPB ที่แทรกอยู่ในชั้นของ P-MMT ประมาณ 9.3% โดยน้ำหนัก จากนั้นทำการขึ้นรูปวัสดุประกอบนาโน P(MMA-*co*-BA)/P-MMT โดยหล่อเป็นแผ่นฟิล์มด้วยเทคนิค doctor blade ปริมาณของ P-MMT (1, 2, 3, และ 6 เปอร์เซนต์โดยน้ำหนัก) และสูตรของพอลิเมอร์ร่วม (M9B1, M8B2, M7B3, และ M6B4) ของวัสดุประกอบได้ถูกปรับเปลี่ยน พบว่าตำแหน่งพีกของระนาบ *001* ของวัสดุประกอบที่มีปริมาณของ P-MMT ที่ 1 และ 2 เปอร์เซนต์โดยน้ำหนัก มีการเลื่อนตำแหน่งของพีก ไปยังตำแหน่ง 2θ ที่ต่ำลงเล็กน้อย แสดงให้เห็นว่าวัสดุประกอบที่เตรียมได้นี้ มีโครงสร้างเป็นวัสดุประกอบนาโนแบบแทรกตัว (Intercalated nanocomposite structure) เป็นส่วนใหญ่ และยังคงมีอนุภาคของ P-MMT บางส่วนที่รวมตัวกันอยู่ในเนื้อของวัสดุประกอบ ภาพถ่ายสัณฐานวิทยาของวัสดุประกอบ P(MMA-*co*-BA)/P-MMT ที่มีปริมาณของ P-MMT อยู่ 2% โดยน้ำหนัก ด้วยกล้องจุลทรรศน์อิเล็กตรอนแบบส่องผ่าน (TEM) ได้ยืนยันให้เห็นถึงโครงสร้างแบบแทรกตัวของวัสดุประกอบนาโนนี้ วัสดุประกอบนาโน P(MMA-*co*-BA)/P-MMT ที่เตรียมได้มีเสถียรภาพทางความร้อนดีกว่า P(MMA-*co*-BA) สำหรับสูตร M6B4 มีอุณหภูมิการสลายตัว

สูงสุดเมื่อเติม P-MMT ลงไป 3% โดยน้ำหนัก แต่ในขณะที่สูตร M7B3, M8B2, และ M9B1 มีอุณหภูมิการสลายตัวสูงสุดเมื่อเติม P-MMT ลงไป 1% โดยน้ำหนัก นอกจากนี้ยังพบว่าไม่มีความแตกต่างอย่างมีนัยสำคัญระหว่างอุณหภูมิเปลี่ยนสถานะคล้ายแก้ว ($T_g$) ของพอลิเมอร์ร่วมกับวัสดุประกอบนาโนที่มีพอลิเมอร์ร่วมสูตรเดียวกัน ในกรณีที่เติม P-MMT ในปริมาณที่น้อย (1-2% โดยน้ำหนัก) ความแข็งแรงดึงและค่ามอดูลัสของยังของวัสดุประกอบนาโนที่เตรียมได้มีค่าสูงกว่า P(MMA-*co*-BA) และยังพบว่าค่าความแข็งแรงดึงและค่ามอดูลัสของยังของวัสดุประกอบนาโนจะเพิ่มขึ้นตามปริมาณการเติม P-MMT แต่อย่างไรก็ตาม ค่าความแข็งแรงดึงและค่ามอดูลัสของยังของวัสดุประกอบนาโนจะลดลง เมื่อเติม P-MMT ในปริมาณที่มากขึ้น แผ่นฟิล์ม P(MMA-*co*-BA)/P-MMT ที่เตรียมได้นี้ มีความโปร่งใสและมีสมบัติการป้องกันรังสียูวี โดยเฉพาะอย่างยิ่งในช่วงของรังสียูวี-บี ฟิล์มวัสดุประกอบนาโน P(MMA-*co*-BA)/P-MMT มีเสถียรภาพทางความร้อนและสมบัติเชิงกลที่ดีกว่าฟิล์มวัสดุประกอบ P(MMA-*co*-BA)/unmodified-MMT

**คำสำคัญ :** วัสดุประกอบนาโน, มอนต์มอริลโลไนต์, ออแกโนเคลย์, ออแกโนฟอสเฟต, พอลิเมทิลเมทาคริเลต-โค-บิวทิลอะคริเลต, การหล่อแบบสารละลาย

| | |
|---|---|
| **Thesis Title** | Preparation of Poly(methyl methacrylate-*co*-butyl acrylate)/Organophosphate Modified Montmorillonite Nanocomposites |
| **Student** | Mr. Sanit Sirapanichart |
| **Student ID** | 51064607 |
| **Degree** | Master of Science |
| **Program** | Nanoscience and Nanotechnology |
| **Year** | 2012 |
| **Thesis Advisor** | Asst.Prof.Dr. Pathavuth Monvisade |
| **Thesis Coadvisor** | Asst.Prof.Dr. Punnama Siriphannon |
| | Assoc.Prof.Dr. Jiti Nukeaw |


**Abstract**

This research involves preparation of poly(methyl methacrylate-*co*-butyl acrylate)/tetrabutylphosphonium modified montmorillonite (P(MMA-*co*-BA)/P-MMT) nanocomposite films by using simple solution casting technique. P(MMA-*co*-BA) was synthesized *via* solution polymerization using benzoyl peroxide as an initiator. P-MMT was modified by cation exchanging with tetrabutylphosphonium bromide (TBPB). The d-spacing ($d_{001}$) of the P-MMT was higher than that of Na-MMT. The content of TBPB in P-MMT was about 9.3 wt%. P(MMA-*co*-BA)/P-MMT nanocomposite films were fabricated by doctor blade technique. The P-MMT contents (i.e. 1, 2, 3, and 6 wt%) and the copolymer formulas (i.e. M9B1, M8B2, M7B3, and M6B4) of the composites were varied. The composites containing 1 and 2 wt% of P-MMT showed slightly shifted of the $d_{001}$ peak to lower 2θ, indicating mostly intercalated nanocomposite structure occurred with some agglomerate particles. The intercalated nanostructure of P(MMA-*co*-BA)/P-MMT 2% composites was observed in TEM micrograph. The nanocomposites had better thermal stability than their virgin polymer. The highest $T_{d\text{-}10\%}$ of the M6B4 series was at 3 wt% addition of P-MMT (M6B4-P3) whereas the highest $T_{d\text{-}10\%}$ of the M7B3, M8B2, and M9B1 systems were at 1 wt% addition of P-MMT. There was no significant difference between $T_g$ of the copolymers and their nanocomposites. Tensile strength and Young's modulus of nanocomposites were higher than those of their original copolymer. In case

of low concentration of P-MMT addition (1-2 wt%), the higher of P-MMT loading, the higher tensile strength and Young's modulus were obtained. However, the tensile strength and Young's modulus of the nanocomposites decreased at higher content of P-MMT. The P(MMA-*co*-BA)/P-MMT nanocomposite films showed the high transparency and screening ability in UV region, especially in the UV-B range. P(MMA-*co*-BA)/P-MMT nanocomposites showed better thermal stability and mechanical properties than those of the P(MMA-*co*-BA)/unmodified-MMT composite films.

**Keywords:** Nanocomposites; Montmorillonite; Organoclay; Organophosphate; Poly(methyl methacrylate-*co*-butyl acrylate); Solvent casting

# ACKNOWLEDGMENTS

It would not have been possible to write this thesis without the help and support of the kind people around me, to only some of whom it is possible to give particular mention here.

Above all, I would like to express my deepest appreciation to my dearest mother and sisters for their unequivocal support throughout, love, care, and encouragement, as always, for which my mere expression of thanks likewise does not suffice.

This thesis would not have been possible without the help, support and patience of my advisors, Asst.Prof.Dr. Pathavuth Monvisade, Asst.Prof.Dr. Pumnama Siri-phannon, and Assoc.Prof.Dr. Jiti Nukeaw. The good advice and friendship of them has been invaluable on both an academic and a personal level, for which I am extremely grateful. Special thanks to the thesis committees, Assoc.Prof.Dr. Taweechai Amorn-sakchai, Dr. Pitiporn Thanomngam, and Dr. Darinee Phromyothin, for reading and criticizing my thesis manuscript.

I would like to express my gratitude to all professors who have invaluable knowledge and taught me while I was studying at the King Mongkut's Institute of Technology Ladkrabang.

I would like to acknowledge the financial, academic and technical support of the National Nanotechnology Center (NANOTEC), NSTDA, Ministry of Science and Technology, Thailand, through its program of Center of Excellence Network.

Special thanks to Scientific Instruments Service Center, faculty of science, KMITL, for them help in XRD, XRF, TGA, and UV-vis analysis. Thanks also to the department of chemistry, faculty of science, KMITL, for instrumental process and instrument analysis.

Last, but by no means least, I would like to give the great thanks to all of my lovely friends, especially Miss Piyaphan Pannasri, Mr. Suebpong Suebwongnat and Miss Apichaya Jianprasert, and the scientists at the department of chemistry, KMITL, and the college of KMITL Nanotechnology, who have been always taking care, helping, and encouraging throughout.

For any errors or inadequacies that may remain in this work, of course, the responsibility is entirely my own.

Mr.Sanit Sirapanichart

# TABLE OF CONTENTS

# TABLE OF CONTENTS (CONTINUED)

# TABLE OF CONTENTS (CONTINUED)

# LIST OF TABLES

# LIST OF FIGURES

# LIST OF FIGURES (CONTINUED)

Figure Page

# LIST OF FIGURES (CONTINUED)

Figure Page

# LIST OF FIGURES (CONTINUED)

Figure Page

# SYMBOLS AND ABBREVIATIONS

| | |
|---|---|
| TBPB | : Tetrabutylphosphonium bromide |
| MMA | : Methyl methacrylate |
| BA | : Butyl acrylate |
| PMMA | : Polymethyl methacrylate |
| PBA | : Polybutyl acrylate |
| P(MMA-*co*-BA) | : Copolymer of methyl methacrylate and butyl acrylate |
| MMT | : Montmorillonite |
| Na-MMT | : Sodium-montmorillonite |
| S-MMT | : Swelled-montmorillonite |
| P-MMT | : Tetrabutylphosphonium intercalated montmorillonite |
| uMMT | : Unmodified montmorillonite |
| P(MMA-*co*-BA)/P-MMT | : Composites between poly(methyl methacrylate-*co*-butyl acrylate) and tetrabutylphosphonium intercalated montmorillonite |
| $M_xB_y$-$P_z$ // $M_xB_y$-$U_z$ | : Formula of the composites between poly(methyl methacrylate-*co*-butyl acrylate) and tetrabutylphosphonium intercalated montmorillonite with varying its compositions |

Where; M = methyl methacrylate

B = butyl acrylate

P = P-MMT

U = uMMT

# SYMBOLS AND ABBREVIATIONS (CONTINUED)

x, z, y = a number representing the concentration to which they are subscripted

| | |
|---|---|
| GPC | : Gel permeation chromatography |
| XRD | : X-ray diffractometer |
| XRF | : X-ray Fluorescence spectrometer |
| DSC | : Differential scanning calorimeter |
| TGA | : Thermogravimetric analysis |
| TEM | : Transmission electron microscopy |
| $T_{d\text{-}10\%}$ | : Decomposition temperature at 10% weight loss |
| $T_g$ | : Glass transition temperature |
| $d_{001}$ | : Distance between *001* plane of MMT |
| $\overline{M}_w$ | : Weight average molecular weight |
| $\overline{M}_n$ | : Number average molecular weight |
| *MWD* | : Molecular weight distribution |

# Chapter 1
# Introduction

## *1.1 Introduction*

Nanocomposites are a promising new class of materials containing filler with at least one dimension in the nanometer scale. In the recent years, polymer/layered inorganic nanocomposites have been extensively studied because of their excellent properties, such as enhanced mechanical properties, increased thermal stability and conductivity, improved gas barrier properties and reduced flammability [1-3].

Poly(methyl methacrylate), PMMA, is one of the most widely use of acrylate polymers. It is often preferred on account of its moderate properties, especially its clarity and outstanding outdoor weathering, easy handling and processing, and low cost [4]. These impressive properties make PMMA to be an economical alternative to polycarbonate (PC) when extreme strength is not necessary. However, PMMA usually behaves in a brittle manner when loaded, resulting in restriction of PMMA application. Thus, to vary from its original applications, the copolymerization between MMA and a monomer, which its polymer has glass transition temperature ($T_g$) lower than room temperature, e.g., butyl acrylate polymers (PBA), are suggested. Generally, the PBA is considered as a colorless transparent rubbery polymer in ambient temperature, thus, it is commonly used in the copolymer to alleviate the brittleness of the final product [5]. However, the presence of a rubbery part in the structure will lower the mechanical properties of that polymer. Therefore, various types of inorganic nanoparticles have been added into PMMA matrix to enhance the mechanical properties [1,6-7]. Among the inorganic nanoparticles, the montmorillonite (MMT) clays receive considerable interest because their structure exhibit stiffness, strength and dimensional stability in two dimensions, rather than one. The efficiency of MMT to modify the properties of the polymer is primarily determined by the degree of its dispersion in the polymeric matrix.

The improvement of dispersion stability is the most significant characteristics of nano-inorganic/polymer composites. In order to achieve a good dispersion and

dispersion stability of the inorganic nanoparticles into the polymer, it is necessary to modify them to be more organophilic and compatible to the polymer. Most of the commercially available organo-MMTs are produced by exchange of alkali or alkali earth cations in the interlayer space of MMT with alkyl ammonium salts. However, the alkyl ammonium modified MMTs are thermally unstable above 250 °C [8-12]. For this reason, other cations, e.g., phosphonium, pyridinium and imminium, have also been used due to their higher thermal stability [13].

Phosphonium compounds are widely used as stabilizers in many applications, such as flame retardants for textiles and paper, stabilization agents for polyacrylonitrile fibers exposed to sunlight, heat stabilizers for nylon, etc [12-15]. Thus, the use of phosphonium salts as organic modifiers to MMT may further enhance the thermal and flammability properties of polymer nanocomposites.

Therefore, in this work, the preparation of nanocomposite films between poly(methyl methacrylate-*co*-butyl acrylate) and tetrabutylphosphonium intercalated montmorillonite (P(MMA-*co*-BA)/P-MMT) by solution casting technique and their characterization were investigated. The effects on the properties of the nanocomposite films by varying compositions of MMA:BA in the copolymers and amount of P-MMT loading were also studied.

## *1.2 Objectives*

1. To prepare the P(MMA-*co*-BA)/P-MMT nanocomposite film by solution casting technique.
2. To study the properties of P(MMA-*co*-BA)/P-MMT nanocomposite films influenced by the compositions of MMA:BA in the copolymer formulas and the contents of P-MMT addition.

## *1.3 Scopes of study*

1. Preparation of P-MMT from MMT and tetrabutylphosphonium bromide (TBPB) using agitation technique *via* cation exchange reaction.
2. Synthesis of P(MMA-*co*-BA) copolymers with different weight ratios of MMA:BA monomer, i.e., 9:1, 8:2, 7:3 and 6:4, *via* solution polymerization

with the presence of 0.1 wt% of benzoyl peroxide (with respect to the total weight of MMA and BA monomers). Molecular weight of the copolymers was determined by gel permeation chromatography (GPC).

3. Preparation of P(MMA-*co*-BA)/P-MMT nanocomposite films by solution casting technique with varying the copolymer formulas and concentrations of P-MMT, i.e., 1, 2, 3 and 6 wt% (with respect to the weight of P(MMA-*co*-BA) copolymers).
4. Characterization of the nanocomposite films by X-ray diffractometer (XRD), X-ray fluorescence spectrometer (XRF) and thermogravimetric analyzer (TGA).
5. Identification effects due to the compositions of MMA:BA monomers and the amount of P-MMT loading on the properties of the nanocomposite films, i.e., thermal property by using differential scanning calorimeter (DSC), optical property by using UV-Visible spectrometer (UV-vis), morphology by using transmission electron microscopy (TEM), and mechanical properties by using universal testing machine.

## *1.4 Expected results*

1. Getting experiences and knowledge about preparation of the P(MMA-*co*-BA)/P- MMT nanocomposite film.
2. The P(MMA-*co*-BA)/P-MMT nanocomposite films can be successfully prepared.
3. The suitable recipe for preparation of the P(MMA-*co*-BA)/P-MMT nanocomposite film can be suggested.

# Chapter 2
# Theory and Literature Reviews

## *2.1 Clays [16-20]*

Clays are composed of hydrous aluminium phyllosilicate minerals which include variable amounts of structural water and have, typically, particle size less than 2 μm in diameter. Clays are generally formed by the chemical weathering of silicate-bearing rocks by carbonic acid, but some are formed by hydrothermal activity. Clays are distinguished from other small soil particles, such as silt, by their smaller size, flake or layered shape, affinity for water and tendency toward high plasticity.

### *2.1.1 Physical characteristics of clays*

- Clay minerals tend to form microscopic to sub microscopic crystals.
- They can absorb water or lose water from simple humidity changes.
- When mixed with limited amounts of water, clays become plastic and are able to be molded and formed.
- When water is absorbed, clays will often expand as the water fills the spaces between the stacked silicate layers.
- Due to the absorption of water, the specific gravity of clays is high variable and is lowered with increased water content.
- The hardness of clays is difficult to determine due to the microscopic nature of the crystals, but the hardness is usually about 2-3 and many clays give a hardness of 1 in field tests.
- Clays tend to form from weathering and secondary sedimentary processes with only a few examples of clays forming in primary igneous or metamorphic environments.
- Clays are rarely found separately and are usually mixed not only with other clays but with microscopic crystals of carbonates, feldspars, micas and quartz.

### *2.1.2 Grouping*

There are four main groups of clays:

- Kaolinite [$Al_2Si_2O_5(OH)_4$]
- Montmorillonite-smectite
  [$(Ca, Na, H)(Al, Mg, Fe, Zn)_2(Si, Al)_4O_{10}(OH)_2 - nH_2O$]*
- Illite [Clay-mica, $(K, H)Al_2(Si, Al)_4O_{10}(OH)_2 - nH_2O$]*
- Chlorite

*(*where n represents the variable amount of water)*

### *2.1.3 Montmorillonite (MMT)*

**Montmorillonite** is a very soft phyllosilicate mineral that typically forms in microscopic crystals, forming clay. The crystalline structure of the MMT is a "flake" particle shape, which resembles a corn flake, as shown in Fig. 2.1. These flakes are extremely small, ranging in long dimension from 10 micrometers to 0.01 micrometers. Hundreds of such flakes aggregate to form a thin particle. The MMT is importantly considered as a material that can offer a high respect ratio and large surface area, for instance, one gram of the MMT has a surface area about 750 $m^2$, thus, its twelve grams have a surface area that can covers an entire football field.

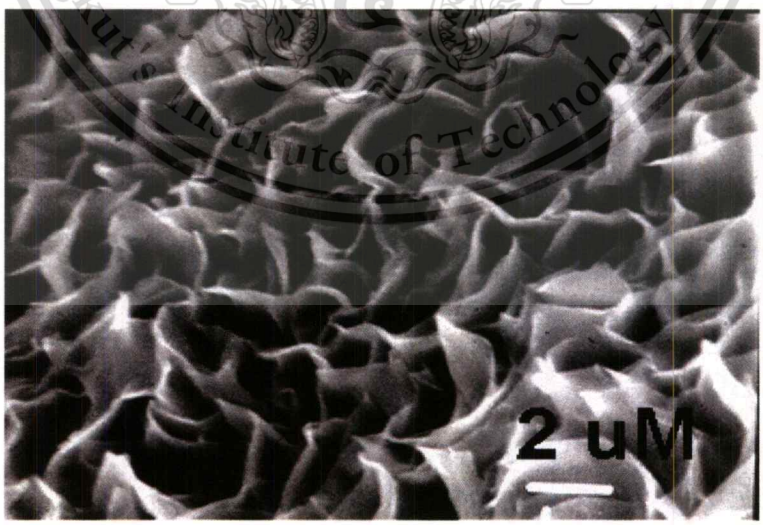


**Fig. 2.1** Flake-like shape of montmorillonite [21]

Typically, the MMT, a member of the smectite family, is 2:1 clay, meaning that it has 2 tetrahedral sheets sandwiching a central octahedral sheet, shown in Fig. 2.2. It is always electrically unbalanced by substitutions of aluminum (III) by magnesium (II), iron (II), or calcium (II). This results in a negative charge deficiency on the surface of layers that must be balanced externally by cations that weakly held near the tetrahedral layers, which in turn are exchangeable. The quantity of cations required to create a net charge balance is called *"the exchangeable cation capacity (CEC)"*. The most prominent exchangeable cations are sodium, calcium, magnesium, and potassium, respectively.

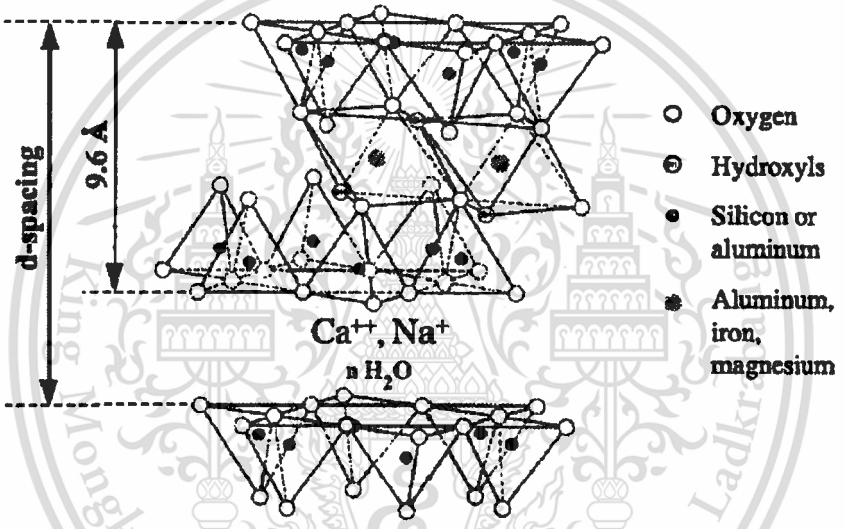


**Fig. 2.2** Basic structure of 2:1 clay minerals [17]

Generally, due to exchangeability of the MMT toward the cations and water moleclues and its extremely high aspect ration and surface area, thus, it is importantly considered as an excellent and widely used absorbent. Therefore, the MMT has been generally used for wastewater treatment, used in cosmetics, has reputed therapeutic effects, and also used in animal feeds as an anti-caking agent. According to current research, it indicates that the MMT or bentonite has the ability to bind mycotoxins in the digestive system of animals as well as several bacteria in-vitro.

Moreover, the MMT is also used in the oil drilling industry as a component of drilling mud, making the mud slurry viscous which helps in keeping the drill bit cool and removing drilled solids. It is also used as a soil additive to hold soil water in

drought prone soils, to the construction of earthen dams and levees and to prevent the leakage of fluids. It is also used as a component of foundry sand and as a desiccant to remove moisture from air and gases.

## *2.2 Modification of MMT [1,8-15]*

According to the nature of the MMTs, 2:1 clay, they are commonly a hydrophilic inorganic compound whereas polymer contains mainly hydrophobic group. Thus, MMT used in nanocomposite fabrication is necessary to modify with an organic modifier to be more organophilic and compatible to the polymer. Most of the commercially available organo-MMTs are produced by exchange of alkali or alkali earth cations in the interlayer space of MMT with alkyl ammonium salts or other cations, e.g., phosphonium, pyridinium and imminium that have also been used due to their higher thermal stability, while, the alkyl ammonium modified MMTs are thermally unstable above 250 °C.

## *2.3 Organophosphorus compounds [22-24]*

**Organophosphorus compounds** are degradable organic compounds containing carbon-phosphorus bonds (apart from phosphate and phosphite esters), primarily used in pest control as an alternative to chlorinated hydrocarbons which persist in the environment. However, phosphorus shares group 5 in the periodic table with nitrogen, thus, phosphorus compounds and nitrogen compounds are somewhat related.

Naturally, phosphorus can adopt oxidation states as −3, −1, +1, +3 and +5. Especially at oxidation state +5, quaternary phosphonium salts, such as, tetraphenylphosphonium bromide, hexadecyl tributyphosphonium bromide and tetrabutylphosphonium bromide, etc., they are great technological importance as flame retardant agents and plasticizers. Particularly, tetrabutylphosphonium bromide (TBPB) when used as MMT modifier, it shown enhancement of the thermal stability up to 350°C, almost equivalent to tetraphenylphosphonium MMT. This is due to the high thermal stability of tetrabutylphosphonium cation. Molecular structure of the TBPB is shown in Fig. 2.3. Thus, in other words, the use of quaternary phosphonium salts as organic modifiers to layered silicates may further enhance the thermal stability and flame retardancy of polymer nanocomposites. Nevertheless, the stability of

phosphonium MMT is substantially decreased (70–80 °C) with regard to the parent phosphonium salt. By the way, it is recognized that degradation pathways and thermal stability depend on molecular structure.

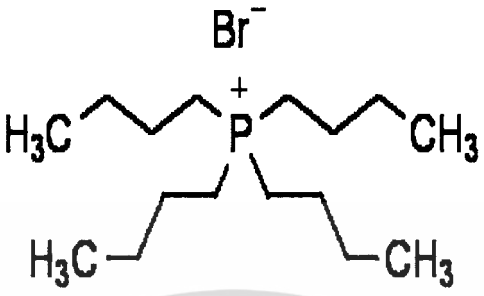


**Fig. 2.3** Molecular structure of tetrabutylphosphonium bromide [25]

Along with the well-known properties of organophosphorus compound, i.e., increase of flame retardancy and heat stabilization, there many researches are developed and some related works are summarized as following;

Wei Xie *et al.* [26] studied on the thermal stability of quaternary phosphonium modified montmorillonites. Organically modified layered silicates (OLS) with high thermal stability are critical for synthesis and processing of polymer layered silicate nanocomposites (PLSN). In the current study, the non-oxidative thermal degradation chemistry of alkyl and aryl quaternary phosphonium-modified montmorillonites (P-MMT) was examined using TGA combined with pyrolysis/GC-MS. The morphology evolution at elevated temperature was investigated using *in-situ* high-temperature X-ray diffraction (XRD) and Fourier transform infrared spectroscopy (FTIR). The onset decomposition temperature *via* TGA of these P-MMTs ranged from 190 to 230 °C. The initial degradation of the alkyl P-MMTs follows potentially two reaction pathways - $\beta$-elimination [$E_\beta$] and nucleophilic displacement at phosphorus [$S_N(P)$] - reflecting the multiple environments of the surfactant in the silicate. Aryl P-MMT decomposition proceeds *via* either a reductive elimination through a five-coordinate intermediate or radical generation through homologous cleavage of the P-phenyl bond. Overall, the interlayer environment of the montmorillonite has a more severe effect on stability of the phosphonium surfactant than previously reported for ammonium-modified montmorillonite (N-MMT). Nonetheless, the overall thermal stability of P-MMT is

higher than that of N-MMT. These observations indicate that, in addition to their conventional purpose as stabilizers, phosphonium salts offer unique opportunities for melting processing polymer layered silicate nanocomposites.

Youngchul Lee *et al.* [27] worked on preparation and characterization of epoxy/clay nanocomposites. Epoxy/clay nanocomposites have been prepared using Montmorillonite (MMT) ion-exchanged with various organic cations; hexadecyltributyl phosphonium ion, octadecyltrimethyl ammonium ion, methyl tallow bis-2-hydroxyl ammonium ion and dimethyl hydrogenated tallow (2-ethylhexyl) ammonium ion. The resulting nanocomposites were found to show exfoliated clay structure by using transmission electron microscope (TEM) and X-ray diffractometry (XRD). The flame retarding property of 5wt% clay/epoxy nanocomposites was found to be enhanced when compared with that of the original epoxy without clay.

Hua Ren *et al.* [28] studied on synthesis and properties of a phosphorus-containing flame retardant epoxy resin based on bis-phenoxy (3-hydroxy) phenyl phosphine oxide. A reactive phosphorus-containing compound, bis-phenoxy (3-hydroxy) phenyl phosphine oxide (BPHPPO) was first successfully synthesized to produce the phosphorus-containing flame retardant epoxy resin (BPHPPO-EP). The chemical structures were characterized from FTIR, MS, NMR spectra and elemental analyses. Thermal degradation behaviors and flame retardant properties of the cured epoxy resins were investigated from the thermogravimetric analysis (TGA) and the limiting oxygen index (LOI) test using 4,4-diaminodiphenylsulfone (DDS) as curing agent. The high char yields and the high limiting oxygen index values were found to certify the great flame retardancy of this phosphorus-containing epoxy resin.

Patel H.A. *et al.* [23] studied on preparation and characterization of phosphonium montmorillonite with enhanced thermal stability. Quaternary phosphonium cations, i.e., tetrabutylphosphonium, hexadecyl tributylphosphonium; tetradecyl tributylphosphonium, tetraphenylphosphonium, methyl triphenyl-phosphonium, ethyl triphenylphosphonium and propyl triphenylphosphonium, were intercalated into montmorillonite (MMT) rich bentonite of Indian origin, by ion exchange reaction. The phosphonium MMT were characterized by Fourier transform infrared spectroscopy (FTIR), powder X-ray diffraction analysis (PXRD), particle size distribution (PSD) and thermogravimetric analysis (TGA). The phosphonium cations

significantly influenced the particle size distribution. The longer alkyl chain, the finer particles were formed. The tetrabutylphosphonium and tetraphenylphosphonium MMT showed enhanced thermal stability (300–400 °C) and may be potentially useful materials for melt processing of polymer/layered silicates nanocomposites.

## *2.4 Poly(methyl methacrylate), PMMA [4]*

**PMMA,** or poly(methyl 2-methylpropenoate) is a colorless transparent amorphous thermoplastic polymer. The PMMA is synthesized from methyl methacrylate monomer *via* free radical vinyl polymerization, as illustrated in Fig 2.4.

The PMMA is well known for its excellent clarity (up to 92% of glasses) and UV resistance, thus, it is used extensively for optical applications, such; lenses, light covers, glazing (particularly in aircraft), light pipes, meter covers, bathroom fittings, outdoor signs, skylights, baths, toys. Moreover, the PMMA also has another advantage over glass; it is more transparent than glass when thickness works are required. Whenever glass windows are made too thick, they become difficult to see through. While, PMMA windows can be made as much as 13 inches (33 cm) thick, they are still perfectly transparent.

Furthermore, the PMMA is also found in paint. Acrylic latex paints often contain the PMMA suspended in water. Unfortunately, it is slightly dissolve in water, so dispersing it in water requires another polymer to make it compatible with water. By the way, it is more than just plastic and paint. Often, lubricating oils and hydraulic fluids tend to get really viscous and even gummy when they get really cold. When a little bit of PMMA is dissolved in these oils and fluids, they do not get viscous in the cold, and machines can be operated down to -100 °C.

In addition, the PMMA still has some more advantage properties, such as, good abrasion resistance, hardness and stiffness, low water absorption, low smoke emission, good track and arc resistance. But it also has poor solvent resistance, low continuous used temperature of approx. 50 °C, poor fatigue resistance, notch sensitive properties and behaves in a brittle manner when loaded (Glass transition temperature ($T_g$) of PMMA is 85-165 °C, atactic).

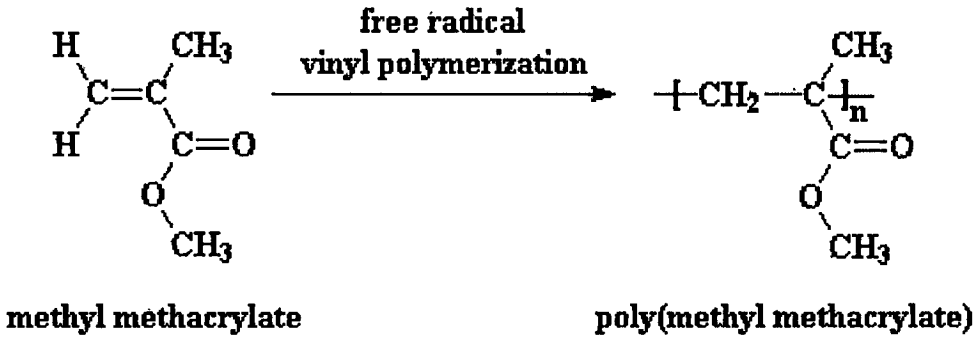


**Fig. 2.4** Polymerization reaction of methyl methacrylate monomer *via* free radical vinyl polymerization [4]

## *2.5 Poly(butyl acrylate), (PBA) [5]*

**PBA** or poly(n-butyl acrylate) is a member of acrylate polymers, a colorless transparent amorphous polymer, and a kind of thermoplastic polymers, like PMMA. Molecular structure of PBA is shown in Fig 2.5.

For preparation of the PBA, butyl acrylate monomer is required to synthesize practically *via* emulsion polymerization to obtain less cross-linked PBA. Through this technique, it is usually rapid and gives high molecular weight polymer in a system of low viscosity. The safety hazard and expense of flammable solvents are eliminated. Anyway, solution polymerization can be commonly used to produce it as well.

By the way, general characteristic of the PBA is a tacky, rubbery polymer, an elastomer, even if, its tackiness decreases with increase in molecular weight. For the physical properties of PBA, it has glass transition temperature at -45 °C, density of 1.08 g/cm$^3$ and refractive index of 1.47 at 25 °C. In addition for the properties of PBA, it has medium permeability to gases, fair to good tear resistance, good abrasion resistance, and also, reasonable insulation property. Commonly, PBA can be stable up to approx. 300 °C, good heat ageing property, and it decomposes only under extreme heat, 300-500 °C. According to the notably elastomeric properties of the PBA, it is actually used in architectural paints, coating and lacquers, radiation-curable system, application in papers, leather and textile industries, and adhesive and sealing compounds. More than that, it is ordinarily used as a good soft monomer in general copolymer, helping the copolymer to alleviate the brittleness.

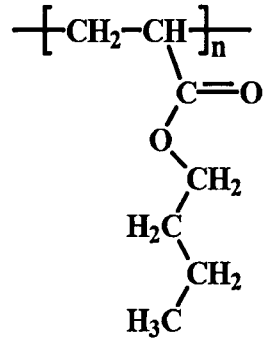

**Fig. 2.5** Molecular structure of poly(n-butyl acrylate) [5]

## *2.6 Composites [29]*

**Composites** are composed of two categories of constituent materials, i.e., matrix and reinforced phase. The matrix normally surrounds and supports the reinforced phase by maintaining their relative positions. The reinforced materials impart their special mechanical and physical properties to enhance the matrix properties. A synergism creates material properties unavailable from the individual constituent materials. The wide variety of matrix and strengthening materials allows designing various products and/or structures.

## *2.7 Polymer-Clay Nanocomposites [1-3,30-34]*

Nanocomposites are a type of composites containing filler that has at least one dimension in the range of nanometer. Most of the nanocomposites can be produced by using metal particles, colloids, and smectic-clay minerals. Since Toyota's pioneering work had been reported on polymer-clay nanocomposites, these kinds of nanocomposites have been extensively studied because of their excellent properties, such as enhanced mechanical properties, increased thermal stability and conductivity, improved gas barrier property, and reduced flammability with the presence of only small amount of nanoclay fillers.

Dispersion of clay minerals in a polymer matrix is categorized into three types, as shown the schematic in Fig. 2.6;

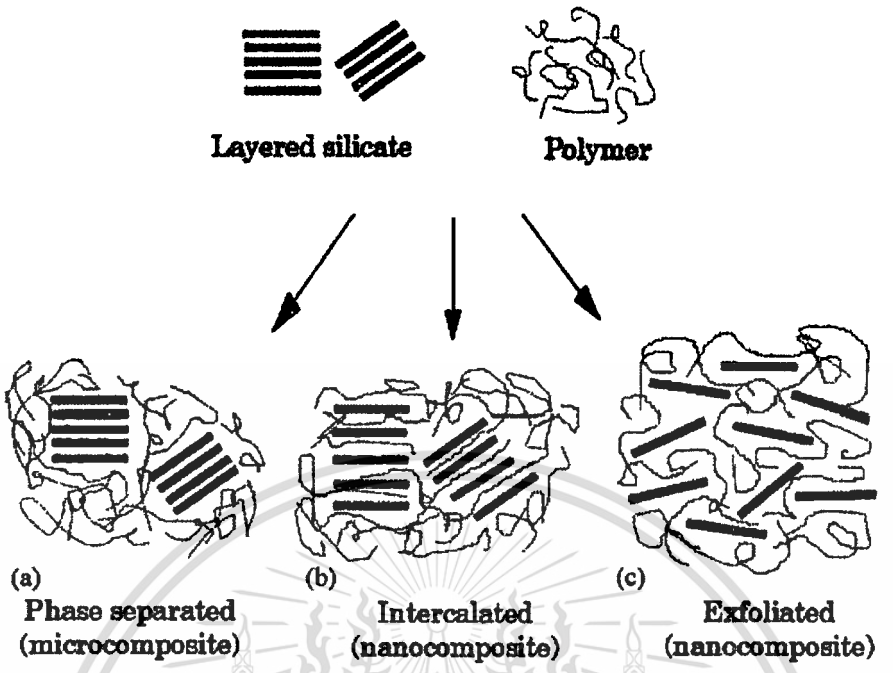


**Fig. 2.6** Schematic of three main types of polymer-clay composites; (A) conventional composite, (B) intercalated nanocomposite and (C) exfoliated nanocomposite [1]

➢ *Conventional composites* contain the existing clay tactoids in original aggregated state with a non-intercalated polymer chain along the silicate layers. The clay tactoids are simply dispersed as a segregate phase.

➢ *Intercalated nanocomposites* are formed by the insertion of one or more polymer chains into the clay galleries resulting in a well ordered multilayer with alternating polymer chains and nanoscale inorganic layers, owing to the spatial confinement of the polymer between the dense clay layers.

➢ *Exfoliated nanocomposites* can be obtained by separating a single silicate layer in the polymer matrix with the average distance of each layer depending on the clay content. The clay contents in exfoliated nanocomposite are usually much lower than those in the intercalated nanocomposite; however, the exfoliated nanocomposite is more desirable than the intercalated one because of the stronger synergistic effects between polymer matrix and silicate layers.

Generally, X-ray diffraction (XRD) is the principal method that has been used to examine the types of dispersion of clay-containing polymeric nanocomposites *via* the calculation of interlayer spacing or so called $d_{001}$-*spacing*. The $d_{001}$ is calculated from the Bragg's law equation as shown below;

$$n\lambda = 2(d_{001}) \sin\theta$$

Where n is an integer, θ is the angle of incidence (or reflection) of the X-ray beam, and λ is the X-ray wavelength. Most X-ray machines use Cu-K$\alpha_1$ radiation with λ = 0.1540562 nm.

From Fig 2.7, the more penetrating of polymer chain into the clay galleries, the broader characteristic peak of MMT will be obtained. Besides, for the peak in XRD pattern of the intercalated nanocomposite, it will be broader and shifted to lower 2θ due to the insertion of one or more polymer chains into the *001* plane of the clay layers causing wider interlayer spacing, as illustrated in Fig 2.7(b). Moreover, if the insertion of the polymer chains into the *001* plane of the clay layers destroys the tactoids of the MMT, resulting in the exfoliated nanocomposite, the peak of MMT in XRD pattern will disappear as shown in Fig 2.7(c).

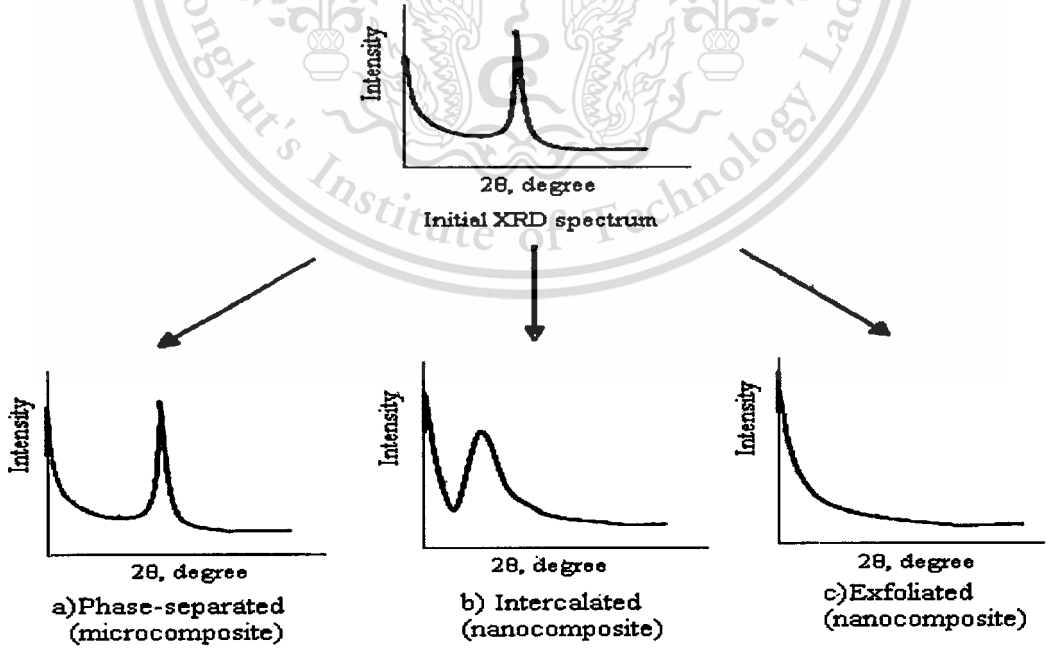


**Fig 2.7** Schematic of XRD patterns of polymer-clay composites; (a) Conventional composite, (b) Intercalated nanocomposite and (c) Exfoliated nanocomposite [1]

## *2.8 Processing of Polymer-Clay Nanocomposites [1,35]*

There are three main methods are commonly used in order to fabricate polymer-clay nanocomposites that are;

- *Melt processing*

The layered silicate is mechanically mixed with the solid polymer matrix in the molten state elevated temperatures. Under these condition and if the layer surfaces are sufficiently compatible with the selected polymer, the polymer can be inserted into the interlayer space and form either an intercalated or an exfoliated nanocomposite. This method has great advantages than others. First, this method is environmentally benign due to the absence of organic solvents. Second, it is compatible with current industrial process, such as extrusion and injection molding. However, processing temperature should be controlled to avoid the decomposition of the organic modifier.

- *Solution casting*

In the solution casting method, the organoclay is dispersed and/or swelled using a solvent in which the polymer is soluble. The entropy gained by desorption of solvent molecules, this allows the polymer chains to diffuse between the silicate sheets after evaporation of the solvent, the sheet reassembles, sandwiching the polymer to form an ordered, multilayered structure. Actually, it is quite difficult to find a solvent that correspond to both of the organoclay and the polymer, hence, this leads to sedimentation and bad dispersion problems of the organoclay. To relieve these problems, before casting, the mechanical mixing is necessary. Moreover, for the problem after the evaporation of solvent, there is some trace of solvent that may be trapped in finished nanocomposite, causing some misrepresentative properties.

- *In-situ polymerization*

It is similar to the solution method except that the role of the solvent is replaced by a polar monomer solution. The layered silicate is swollen within the liquid monomer, or a monomer solution, so that the polymer formation can occur between the intercalated sheets. This is merit point of this technique, which is higher possibility to obtain exfoliated sheets and wider interlayer spacing. Besides, this technique is considered as a solvent-free method, harmless to the surroundings. Nevertheless, there still have some disadvantages, which are, firstly, the rapid sedimentation of organoclay

due to the very low viscosity of the monomer causing more agglomerate of clay particles by enclosed with the polymer chains, secondly, the built-up heat during polymerization leading to the decomposition of the organic modifier then following by the collapse of interlayer spacing, and for the last one, the shrinkage of the completed nanocomposite because of the different between the density of the monomer and polymer system after polymerization. Therefore, agitation and literature reviews may be needed to support this method.

## *2.9 Related literature reviews*

Tomohiro YAMAGUCHI and Eisuke YAMADA, [36] concerned about preparation and properties of clay/SEBS intercalated composites. Clay/polystyrene-*b*-poly(ethylene-*co*-butylene)-*b*-polystyrene triblock copolymer (SEBS) intercalated composites were prepared by melt-blending. The clays were a pristine montmorillonite (Mt) and three organically modified montmorillonites (organo-Mts) with different amounts of distearyldimethylammonium (D18) cation. The amounts of D18 were 50, 70 and 100% of the cation exchange capacity (denoted as D18Mt(50), D18Mt(70) and D18Mt(100), respectively). The clay/SEBS composites were characterized by field-emission scanning electron microscopy (FE-SEM), X-ray diffraction analysis (XRD). The dynamic mechanical analysis (DMA) and the tensile properties were also examined. The size of agglomerated clay particles decreased with the increasing amount of D18. The FE-SEM image of D18Mt (100)/SEBS revealed that the clay particles were dispersed at the sub-m m level (100–500 nm). The XRD patterns suggested that the SEBS chains were inserted into the interlayers of the organo-Mts. The DMA curves indicated that the addition of the organo-Mts produced an increase in the storage modulus in the rubbery plateau region, but a slight decrease in the glass transition temperature of the polystyrene domains. The tensile properties of the organo-Mt/SEBS composites were higher than those of the unmodified Mt/SEBS. D18Mt (100)/SEBS displayed an improved tensile modulus, tear strength and hardness compared to pure SEBS, without sacrificing the tensile strength and elongation at break.

S I Marras *et al.* [37] studied on surfactant-induced morphology and thermal behavior of polymer layered silicate nanocomposites. Poly(L-lactic acid) nanocomposites were prepared by the addition of montmorillonite modified with various loadings of hexadecylammonium cation. The influence of alkylammonium on the morphology and surface charge of the clay was investigated by X-ray diffraction (XRD) analysis and electrokinetic measurements, respectively. The structural characteristics of the inorganic-organic hybrids were studied by XRD, transmission electron microscopy (TEM) and atomic force microscopy (AFM). Thermal analysis was carried out by thermogravimetric analysis (TGA) under constant nitrogen flow and under air. The results showed that high concentration of surfactant present in the clay greatly increases clay's dispersibility into the matrix and this substantially improves the thermal stability of the pristine polymer.

Christine M. Moore *et al.* [38] concerned about effect of mixture casting phosphonium salts with Nafion® on the proton exchange capacity and mass transport through the membranes. This research examined how the physical properties of Nafion® were affected by mixture casting Nafion® with quaternary phosphonium salts. Quaternary phosphonium salts could be mixture cast with commercially available Nafion® suspension to form membranes with decreased proton exchange capacity and altered mass transport of cations, anions and neutral species through the membrane. Since quaternary phosphonium salts were similar in size and hydrophobicity to quaternary ammonium salts, the mass transport of cations, anions and neutral species through tetraethylphosphonium bromide and tetrabutylphosphonium treated Nafion® was similar to tetraethylammonium bromide and tetrabutylammonium treated Nafion®, respectively. Although there was no statistically significant difference between transports through tetrabutylphosphonium bromide treated Nafion® membranes and tetrabutylammonium bromide treated Nafion® membranes, there was a detectable difference for the transport of ferricyanide, methyl viologen and tetramethyl-phenylenediamine through tetraethylphosphonium bromide treated Nafion® membranes. The difference was consistent with the fact that tetraalkylphosphonium bromides were slightly larger than tetraalkylammonium bromides, so the resulting pore size for a tetraalkylphosphonium bromide treated Nafion® membrane was larger than the pore size for a tetraalkylammonium bromide treated Nafion® membrane. The proton exchange capacity of tetraalkylphosphonium bromide treated membranes was larger

than tetraalkylammonium bromide treated membranes. This data was expected since phosphonium salts were less hydrophobic than the ammonium salts and would have a lower affinity for the sulfonic acid exchange sites. Overall, this research indicates that quaternary phosphonium bromide salts could be employed to further tailor the physical and chemical properties of Nafion® membranes.

Tsung-Yen Tsai *et al.* [39] investigated in morphology and properties of poly(methyl methacrylate)/clay nanocomposites prepared by in-situ solution polymerization. After the organic modification by ionic exchanging with amine salts, the organoclay becomes more hydrophobic and compatible than pristine clay with methyl methacrylate monomer. The modified clays are characterized by wide angle X-ray diffraction (WAXRD). The powdered X-ray diffraction and transmission electron microscopy (TEM) techniques were employed to study the morphology of the PMMA/clay nanocomposites which indicate that the modified clays were dispersed in PMMA matrix to form both exfoliated and intercalated PMMA/modified clay nanocomposites. The thermal and mechanical properties were measured by thermogravimetric analysis (TGA) and differential scanning calorimetry (DSC). The thermal stability of PMMA was increased and depended on clay loading. The Tg of the PMMA/clay nanocomposites increases with the clay content. This result can be explained that the motion of the PMMA chains is restricted by the clay layers. Gas permeability analyzer (GPA) shows the excellent gas barrier property of the nanocomposites which is in good agreement with the morphology. The optical property was measured by UV–vis spectroscopy which shows the good optical clarity and UV resistance.

Ray-Yi Lin *et* al. [40] concerned about preparation of porous PMMA/$Na^+$–montmorillonite ($Na^+$–MMT) cation-exchange membranes for cationic dye adsorption. The porous PMMA/$Na^+$–MMT cation-exchange membranes were successfully prepared by entrapment method. One approach (simple mixing) was to mix commercial PMMA polymer with $Na^+$–MMT clays in solvent for membrane preparation (Membrane A). The other approach (emulsion polymerization) was to synthesize the PMMA/$Na^+$–MMT composite *via* emulsion polymerization first, followed by membrane casting. Membrane B is for Kunipia F clays and Membrane C is for PK-802 clays. Membrane morphology and properties were characterized. The thermo-

gravimetric analysis (TGA) verified the near complete incorporation of feed $Na^+$–MMT clays in the PMMA/$Na^+$–MMT composite membranes, while X-ray diffractograms (WXRD) exhibited the slightly enlarged interlayer spacing of $Na^+$–MMT. The range of cation-exchange capacity (CEC) was 9–32 μequiv./47mm disc. For batch cationic dye adsorption, the best performance was achieved by Membrane B with feed $Na^+$–MMT/MMA (M/P) ratio (w/w) = 0.5 and Membrane C with feed M/P = 0.6, where about 95% methyl violet adsorption was attained in 2 h. The optimum desorption solution was 1M KSCN in 80% methanol and its related dye desorption efficiency was 92%. In the flow process using one piece of 47mm disc of Membrane B (M/P = 0.5), dye solution was recirculated for 6 h and ≥ 85% of dye could be removed. Higher than 94% of dye was desorbed at 1 or 4 mL/min, and the membrane regenerability was proved by successfully performing three consecutive cycles.

Kung-Chin Chang *et al.* [41] studied on the effect of clay on the corrosion protection efficiency of PMMA/Na+-MMT clay nanocomposite coatings evaluated by electrochemical measurements. The preparation of PMMA–clay nanocomposites was investigated by using sodium dodecylbenzenesulfonate (SDS) and potassium peroxodisulfate (KPS) as a surfactant and chain initiator for an in situ emulsion polymerization reaction, respectively. The as-prepared nanocomposites were then characterized by Fourier transformation infrared spectroscopy (FTIR), wide-angle X-ray diffraction (WAXRD) patterns and transmission electron microscopy (TEM). It should be noted that the nanocomposite coating containing 1 wt% of clay loading was found to exhibit an observable enhanced corrosion protection on cold-rolled steel (CRS) electrode at higher operational temperature of 50 °C, which was even better than that of uncoated and electrode-coated with PMMA alone at room temperature of 30 °C based on the electrochemical parameter evaluations (e.g., Ecorr, Rp, Icorr, Rcorr and impedance). In this work, all electrochemical measurements were performed at a double-wall jacketed cell, covered with a glass plate, through which water was circulated from a thermostat to maintain a constant operational temperature of 30, 40 and 50 ± 0.5 °C. Moreover, a series of electrochemical parameters shown in Tafel, Nyquist and Bode plots were all used to evaluate PCN coatings at three different operational temperatures in 5 wt% aqueous NaCl electrolyte. The molecular barrier properties at three different operational temperatures of PMMA and PCN membranes

were investigated by gas permeability analyzer (GPA) and vapor permeability analyzer (VPA). For example, they found that the CLMA1 membrane exhibited lower oxygen and water vapor permeability than neat PMMA. Moreover, they also found that the oxygen and water vapor permeability of PMMA and CLMA1 membranes increased as the operational temperature increase from 30 °C to 50 °C. This result indicates that the CLMA1 membrane provide an enhanced molecular barrier property because of the incorporation of clay platelets into the PMMA matrix, which led to a longer tortuosity of the diffusion pathway of oxygen and water vapor. Effect of material composition on the molecular weight and optical properties of neat PMMA and PCN materials, in the form of solution and membrane, were also studied by gel permeation chromatography (GPC) and UV–vis transmission spectra. Typically, the incorporation of clay platelets into PMMA matrix led to an observable decrease in Mw of polymeric chains. The UV/vis transmission spectra of PCN membranes showed that the visible region (400–700 nm) was almost completely unaffected by the presence of the clay and retained high transparency of PMMA.

Prafulla K. Sahoo *et al.* [42] concerned about the synthesis of poly(butyl acrylate)/sodium silicate nanocomposite (PBA/SS) fire retardant. The PBA/SS nanocomposites were prepared *via* emulsifier-free emulsion technique in presence of Cu(II)/glycine chelate complex and ammonium persulfate (APS) as an initiator. The strongly hydrophobic PBA was intercalated into the hydrophilic SS layer. Since the interlayers of silicate were filled with sodium cations, the hydrophilic properties were enhanced and lead to high degree of swelling. The formation of the PBA/SS nanocomposite was confirmed by infrared spectra (IR). Furthermore, as evidenced by transmission electron microscopy (TEM), the composite so obtained was found to have nanoscale structure. X-ray diffraction (XRD) was used to characterize the nanoscale dispersion of the layer silicate and useful for measurement of d-spacing in interlayer system. It was found from thermogravimetric analysis that PBA/SS nanocomposites had more thermal stability as compared to raw PBA due to intercalation. Burning test of the nanocomposites performance exhibited a flame retardant property, which was also verified from cone calorimeter analysis. For its commercialization, the ecological friendly nature was studied *via* biodegradation and was found to have better biodegradability than the raw PBA.

Hanying Zhao *et al.* [43] reported a study of poly(styrene-*block*-butyl acrylate) (PSBA) block copolymer brushes on the surfaces of intercalated and exfoliated silicate (clay) layers. The PSBA/clay nanocomposite was synthesized by in situ atom transfer radical polymerization (ATRP) from initiator moieties immobilized within the silicate galleries of the clay particles. Transmission electron microscopy (TEM) analysis showed the existence of both intercalated and exfoliated nanocomposites. Block copolymer brushes on the surface of exfoliated or intercalated clay layers were found to create the nanopatterns after treatment in different solvents. For the block copolymer brushes after treatment in THF, uniform collapsed brush layers are observed. After treatment in acetone, a selective solvent for PBA, wormlike surface aggregates are observed. After treatment in methanol, a precipitant for both of the blocks, micelles as well as wormlike aggregates can be observed. Furthermore, the polymer brushes tend to aggregate together and change their nanopatterns at an elevated temperature.

Inigo Gonzalez *et al.* [44] investigated in the role of methyl methacrylate on branching and gel formation in the emulsion copolymerization of BA/MMA monomers. Monomer ratios were spanned from pure BA used for adhesives to 50/50 wt/wt of BA/MMA copolymers used for coatings. The gel content varied from 55% for pure BA to nil for the 50/50 copolymer. The branching level was reduced from 2.6% for pure BA to 0.3% for a 75/25 BA/MMA copolymer. The mechanisms responsible for the reduction of gel content can be found in the lower reactivity of the MMA terminated chains for hydrogen abstraction, the absence of abstractable hydrogens in the MMA units and the fact that MMA radicals terminate predominantly by disproportionation. The reduction of the level of branches is mainly due to the lower reactivity of MMA for intramolecular transfer and the lower instantaneous conversions that favored propagation over backbiting.

Gabriela Diaconu *et al.* [45] studied on the synthesis of high solids content waterborne poly(MMA-*co*-BA)/montmorillonite nanocomposites. Small angle X-ray scattering of Na-montmorillonite (Na-MMT) aqueous dispersions showed that at concentrations below 1.5 wt%, clay platelets were fully dispersed with an average distance between platelets higher than 16 nm. At higher concentrations (3 wt%) platelet–platelet interaction was not negligible and SAXS measurements detected stack-ordered structures composed of 2–3 platelets with an average distance of around 14–16

nm. Thus, an emulsion polymerization of methyl methacrylate and butyl acrylate in an aqueous phase containing Na-MMT at concentrations below 1.5 wt% allowed the production of stable and coagulum free waterborne nanocomposites having 30 wt% solids content, with exfoliated structure. The in situ produced poly(methyl methacrylate-*co*-butyl acrylate)/Na-MMT nanocomposite latexes provided better mechanical, thermal and permeability properties than composites prepared by blending pristine latex with Na-MMT or the pristine copolymer synthesized in the same conditions. Furthermore, for the first time nanocomposite latexes with 45 wt% solids content and intercalated morphologies having enhanced mechanical properties were also produced by seeded semibatch emulsion polymerization. The intercalated structure was likely due to the higher clay concentration in the aqueous phase that favored platelet–platelet interaction increased the viscosity of the polymeric dispersion and prevented a complete exfoliation.

# Chapter 3

# Experimental Details

## *3.1 Materials*

1. Mac-gel Montmorillonite (Na-MMT), Thai Nippon Chemical Industry Co., Ltd.
2. Tetrabutylphosphonium bromide ($C_{16}H_{36}PBr$, TBPB), Fluka, Analytical grade
3. Methyl methacrylate monomer ($C_5H_8O_2$, MMA, Density = 0.963 g/cm$^3$), Thai Mitsui Specialty Chemicals Co., Ltd.
4. Butyl acrylate monomer ($C_7H_{12}O_2$, BA, Density = 0.899 g/cm$^3$), Thai Mitsui Specialty Chemicals Co., Ltd.
5. Benzoyl peroxide (BPO), CARLO ERBA, Analytical grade
6. Methanol ($CH_3OH$), Fisher, Commercial grade
7. Toluene ($C_7H_8$), LAB SCAN, Analytical grade
8. Silver nitrate ($AgNO_3$) 0.1 M
9. Nitrogen gas ($N_2$)
10. Deionized water

## *3.2 Apparatus*

1. X-ray diffractometer (XRD), D8 Advance, Bruker AG

| | |
|---|---|
| Wavelength ($\lambda$) | : 1.540562 Å (Cu $K_\alpha$ radiation) |
| Voltage | : 30 kV |
| Current | : 30 mA |
| Scanning range ($2\theta$) | : 1-25 ° |
| Step size | : 0.04 ° |
| Time/step | : 5 sec |

2. X-ray fluorescence spectrometer (XRF), SRS 3400, Bruker AG
3. Thermogravimetric analyzer (TGA), Pyris 1 TGA, Perkin Elmer

| | |
|---|---|
| Temperature range | : 50 – 800 °C |
| Heating rate | : 5 °C/min |
| Flow rate | : 40 ml/min |

4. UV-Visible Spectrometer (UV-vis), Helios, Thermo Electron Corporation
5. Gel permeation chromatography (GPC), Waters e2695, Milipore

| | |
|---|---|
| Column set | : PL GEL 10 µm Mixed B 2 columns |
| | Size 7.8 x 300.0 µm |
| | (MW resolving range = 500-10,000,000) |
| Eluent | : Tetrahydrofuran (THF) |
| Polymer standard | : Polystyrene (PS) |
| Column temperature | : 30 °C |
| Injector temperature | : 30 °C |
| Solvent/pump temperature | : 30 °C |
| Flow rate | : 1.0 ml/min |
| Injection volume | : 100.00 µl |
| Detector | : Refractive index |
| Sample preparation | : Dissolved with THF |
| Calibration method | : Polystyrene standard calibration |
| | (MW 4,490-1,112,000) |

6. Universal testing machine, LR5K, LLOYD Instrument
7. Transmission electron microscope (TEM), JEM-2100, JEOL
8. Differential scanning calorimeter (DSC), Pyris Diamond DSC, Perkin Elmer

| | |
|---|---|
| Temperature range | : -50 – 120 °C |
| Heating rate | : 10 °C/min |
| Flow rate | : 20 ml/min |

9. Balance, TC-254, Denver Instrument
10. Peristaltic pump, V 77120-52, Cole Parmer
11. Ultrasonic bath, ULTRAsonik, Fisher Scientific Worldwide
12. Mechanical stirrer, EURO-ST B, IKA LABORTECHNIK STAUFEN
13. Water bath
14. Desiccator
15. Oven
16. Vacuum filter
17. Magnetic bar
18. Doctor blade
19. Micrometer

20. Mortar and pestle
21. 400-mesh sieve
22. Glass substrate
23. Glasswares

## *3.3 Experimental Procedures*

### *3.3.1 Preparation of tetrabutylphosphonium intercalated MMT (P-MMT)*

➢ *Preparation of swelled-MMT (S-MMT)*

1. 25.0 g of sodium montmorillonite (Na-MMT) was added into 3000 ml of distilled water, after that, sonicated for 2 hrs in order to separate the montmorillonite tactoids.
2. The swelled montmorillonite (S-MMT) was dried in the oven at 105 °C for 48 hrs, then, ground with mortar.

➢ *Preparation of P-MMT*

1. 2.0 g of Na-MMT was dispersed into 600 ml of distilled water, and then, sonicated for 1 hr.
2. 20 ml of 0.36 M of tetrabutylphosphonium bromide (TBPB) solution was slowly dropped by using peristaltic pump into the S-MMT suspension with vigorous stirring by mechanical stirrer at 600 rpm. The mixture was then stirred and aged for 2 hrs.
3. The mixture was filtered to obtain the phosphonium modified MMT (P-MMT). After that, the P-MMT was washed several times with distilled water until the testing of the mother liquor with 0.1 M of $AgNO_3$ shown the clear solution, having no white precipitate formation.
4. The P-MMT was dried in an oven at 105 °C, ground with mortar, and sieved to pass a 400-mesh sieve.
5. The P-MMT was characterized by XRD, XRF and TGA techniques.

### *3.3.2 Synthesis of P(MMA-co-BA) via solution polymerization*

1. Each formula of P(MMA-*co*-BA) in Table 3.1 was prepared by dissolving MMA, BA, and BPO in 40 ml of toluene.
2. The monomer solution was purged with nitrogen gas for 15 min, and then, polymerized in water bath at 85 °C for 24 hrs.
3. The white precipitate of P(MMA-*co*-BA) was obtained by dropping the polymerized solution into methanol with well stirring. The precipitate was dried in an oven at 60 °C.
4. Molecular weight of P(MMA-*co*-BA) was analyzed by GPC technique.
5. Glass transition temperature ($T_g$) of P(MMA-*co*-BA) was determined by DSC technique.

**Table 3.1** Composition of copolymer formulas

| Formula name | Composition | | |
|---|---|---|---|
| | MMA (g) | BA (g) | BPO (g) |
| M10B0 | 10 | 0 | 0.01 |
| M9B1 | 9 | 1 | |
| M8B2 | 8 | 2 | |
| M7B3 | 7 | 3 | |
| M6B4 | 6 | 4 | |

### *3.3.3 Solvent Screening of P(MMA-co-BA) and P-MMT*

➢ *Solubility of P(MMA-co-BA)*

1. P(MMA-*co*-BA) was dissolved in a set of solvents, i.e., dichloromethane, xylene, and toluene, at the concentration of 10 wt%.
2. The mixtures were sonicated for 45 min.
3. The solubility of P(MMA-*co*-BA) mixtures was observed. If it is necessary, the mixtures might be further sonicated at 60 °C for 30 min to increase the solubility of the copolymers.
4. The good solvent for P(MMA-*co*-BA) was chosen.

➢ *Swelling of P-MMT*

1. P-MMT was dispersed and swelled in a set of solvents, i.e., xylene, dichloromethane, and toluene, at the concentration of 1 wt%.
2. The suspension was sonicated for 30 min. After that the suspension was allowed to sit for 24 hrs to look for settling.
3. The solvent providing the best P-MMT dispersion and swelling was chosen.

### *3.3.4 Preparation of P(MMA-co-BA)/P-MMT nanocomposite films by solvent casting using doctor blade technique*

1. P-MMT was dispersed in 10 ml of toluene by using sonication technique for 1 hr. The concentration of P-MMT was varied as 0.1, 0.2, 0.3 and 0.6 g, respectively. _____ [*Mixture no.1*]
2. 10.0 g of P(MMA-*co*-BA) was well dissolved in 30 ml of toluene by using magnetic stirrer. _____ [*Mixture no.2*]
3. Mixture no.1 was slowly added into mixture no.2 with continuously stirring until homogeneous mixture was obtained.
4. The P(MMA-*co*-BA)/P-MMT mixture was cast by using doctor blade technique to get nanocomposite film.
5. Repeat the $1^{st} - 4^{th}$ step for all formulas of the synthesized P(MMA-*co*-BA).
6. The nanocomposite films were characterized by XRD, XRF, TGA and DSC techniques.
7. Morphology of the nanocomposite films were investigated by transmission electron microscopy (TEM).

### *3.3.5 Properties testing of P(MMA-co-BA)/P-MMT nanocomposite films*

➢ *Optical property*

Percentage of the UV-vis transmission (%T) through the P(MMA-*co*-BA)/P-MMT nanocomposite films (0.1 ± 0.02 mm) were determined by UV-vis spectrometer with scanning wavelength between 200 - 800 nm.

➢ *Mechanical properties*

Following the ASTM D 882; tensile strength, % elongation at break, and Young's modulus values of P(MMA-*co*-BA) and P(MMA-*co*-BA)/P-MMT nanocomposite films were determined by universal testing machine. The nanocomposite films were cut to have a rectangular shape (5.0 x 60.0 mm with 0.1 ± 0.02 mm of thickness), and then, tested under 100 N loading with speed of 100 mm/min at 20 mm of gauge length.

# Chapter 4

# Results and Discussion

P-MMT was prepared *via* cation exchange reaction before being used for preparation of P(MMA-*co*-BA)/P-MMT composite films. The composite films were fabricated by using solution casting technique. The variations in compositions of P(MMA-*co*-BA) formulas and concentration of loaded P-MMT were assigned to study their effects on properties of the P(MMA-*co*-BA)/P-MMT composite films.

## *4.1 Characterization of MMTs*

### *4.1.1 X-ray Diffractometer (XRD)*

The XRD patterns of raw sodium montmorillonite (Na-MMT), swelled montmorillonite (S-MMT), and tetrabutylphosphonium modified montmorillonite (P-MMT) are shown in Fig. 4.1. When clay was swelled with deionized water, the characteristic peak of Na-MMT shifted from $2\Theta = 6.2°$ ($d_{001} = 14.2$ Å) to be the peak of S-MMT at $2\Theta = 7.15°$ ($d_{001} = 12.3$ Å). The smaller basal spacing of S-MMT indicated the cation exchange occurred between proton ($H^+$) of deionized water and exchangeable ions, mainly $Na^+$ ions. Then, after modification, the XRD pattern of P-MMT shows the shifting of $d_{001}$ peak from the peak of S-MMT ($d_{001} = 12.3$ Å) to $2\Theta = 5.64°$ ($d_{001} = 15.6$ Å), corresponding to the work of Patel *et al.* [23]. The d-spacing of P-MMT was wider than that of S-MMT, indicating the intercalation of phosphonium ions into the interlayers of montmorillonite, as illustrated the schematic in Fig. 4.2.

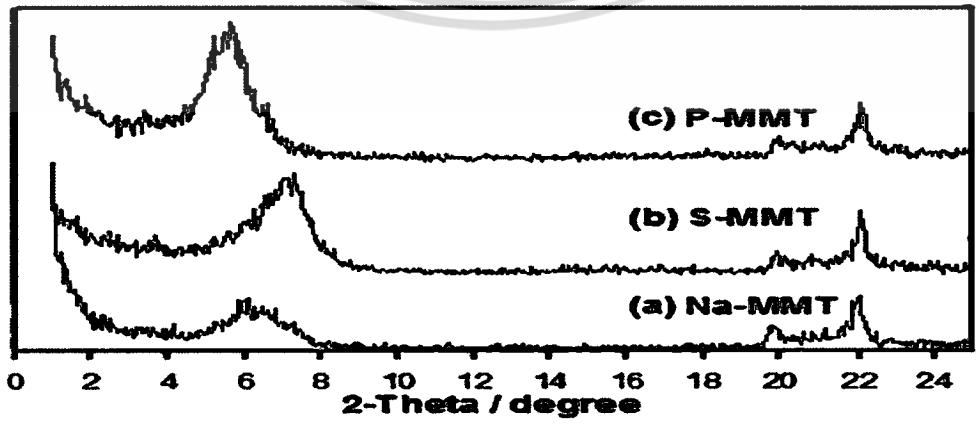


**Fig. 4.1** XRD patterns of (a) Na-MMT, (b) S-MMT, and (c) P-MMT

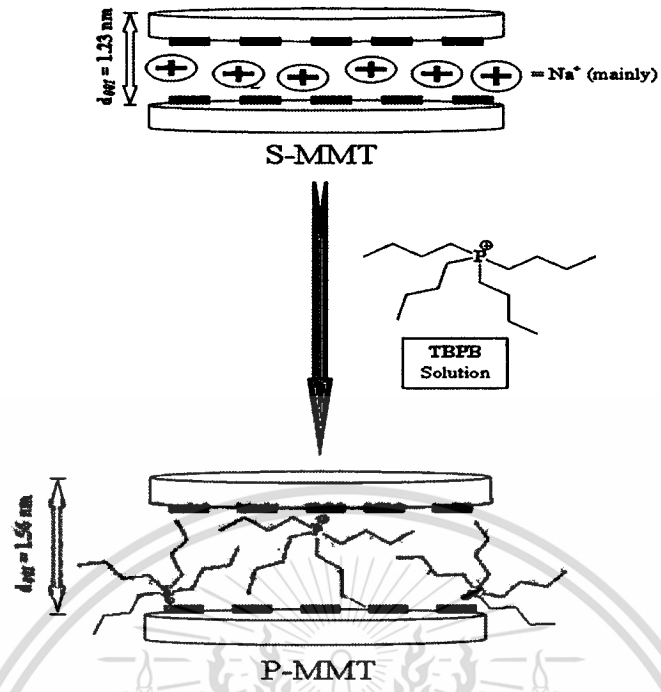


**Fig. 4.2** Schematic shows intercalation of TBPB modifier into the layers of S-MMT

### *4.1.2 X-ray Fluorescence (XRF)*

The chemical compositions of Na-MMT, S-MMT and P-MMT were shown in Appendix B. The molar ratios of Na:Al, Si:Al and P:Al are calculated and concluded in Table 4.1. The exchangeable sodium (Na) ions in *001* plane could be detected in the Na-MMT and S-MMT. When Na-MMT was swelled, the lower content of Na in S-MMT was observed comparing with that in Na-MMT. This might indicate the partial cation exchange between $H^+$ of deionized water and $Na^+$ ions of Na-MMT. After intercalation with TBPB, the presence of phosphorus (P) concomitant with the absence of Na was observed in P-MMT. This result would confirm the presence of the intercalated TBPB ions in the layers of P-MMT.

**Table 4.1** The molar ratios of Na:Al, Si:Al, and P:Al of MMTs

| Sample | Na:Al | Si:Al | P:Al |
|---|---|---|---|
| Na-MMT | 1.1 | 3.90 | - |
| S-MMT | 0.9 | 4.13 | - |
| P-MMT | - | 3.95 | 0.17 |

### *4.1.3 Thermogravimetric Analysis (TGA)*

The degradation temperature and percentage of weight loss of the Na-MMT, TBPB and P-MMT were investigated by TGA under oxygen atmosphere as shown their thermogram in Fig. 4.3. From the thermogram of Na-MMT, it shows a long range of degradation period (60 – 655 °C) with the weight loss about 11.0 wt% which could be divided into 2 main regions. The first degradation region (60 – 100 °C) was due to the moisture content with the weight of about 6.7 wt%. The second degradation region (587 – 655 °C) was a result of the organic impurities in natural clay with the weight about 4.3 wt%.

For the degradation of TBPB, its thermogram shows the main degradation period between 320 – 345 °C, owing to the degradation of hydrocarbon-part (91.9 wt%) in TBPB. However, there was some ash of TBPB was leftover, which must be mostly the oxides of phosphorus, with the weight of about 5 wt%.

After modification, the degradation of P-MMT was observed in the temperature range of 60 – 630 °C, which could be separated into 3 ranges with the total weight loss about 14.5 wt%. The first degradation region (60 – 100 °C) corresponded to the moisture content with the weight of about 4.5 wt%. The second range (284 – 385 °C) was due to the degradation of hydrocarbon-part possessed in the intercalated TBPB with the weight of about 5.4 wt%. And for the last one (516 – 630 °C), it was the degradation of organic matter within the MMT with the weight of about 4.6 wt%. Moreover, percentage of TBPB addition into MMT could be determined, as shown the calculation in the Appendix C, which came out as about 9.3 wt%.

Besides, from the Table 4.2, it was noticed at the 1$^{st}$-step of organic-phase degradation that the onset temperature of intercalated TBPB (P-MMT) was lower than that of raw TBPB for 36 °C. This might be due to less interaction force between phosphonium ions and MMT surfaces than that of its parent phosphonium salt form [23]. Meanwhile the endset temperature of intercalated TBPB was prolonged for 40 °C, which was higher than that of the raw TBPB. This effect should be counted as a merit of enormous MMT surface area which could retain the degradation of the intercalated TPBP not only by interfering in the diffusion of oxygen molecules, but also absorbing the heat from the surrounding at the same time.

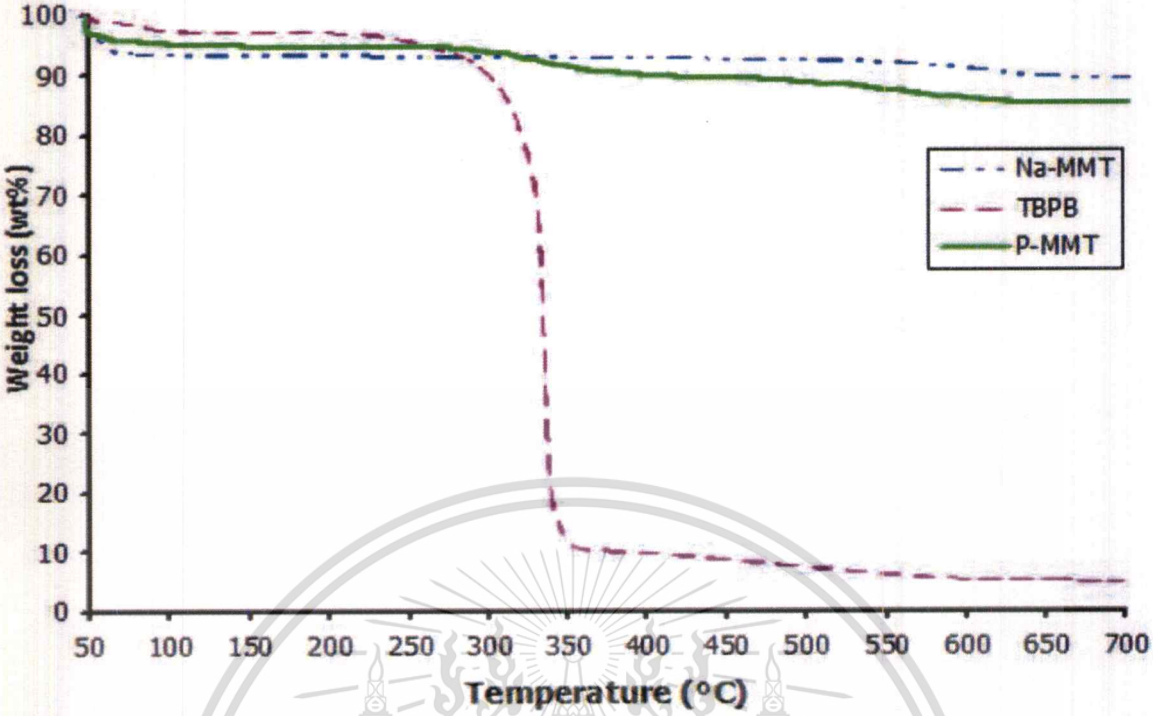


**Fig. 4.3** TGA thermograms of Na-MMT, TBPB, and P-MMT under $O_2$ atmosphere

**Table 4.2** Degradation temperature of organic phase in Na-MMT, TBPB and P-MMT

| Sample | Degradation temperature of organic phase | | | | | |
|---|---|---|---|---|---|---|
| | 1st-step of degradation | | | 2nd-step of degradation | | |
| | Onset (°C) | Endset (°C) | Weight loss (%) | Onset (°C) | Endset (°C) | Weight loss (%) |
| Na-MMT | 587 | 655 | 4.3 | - | - | - |
| TBPB | 320 | 345 | 91.9 | - | - | - |
| P-MMT | 284 | 385 | 5.4 | 516 | 630 | 4.6 |

## *4.2 Molecular weight of P(MMA-co-BA)*

A series of P(MMA-*co*-BA) were synthesized *via* solution polymerization method. These systems have the yield in the range of 45-60 wt%. To predict the copolymer-type for a pair of monomers, it has to consider about the monomer reactivity ratio [46], i.e. $r_A$ and $r_B$, as shown in Eq. 4.5. This is the ratio of the homo-propagation (Eq. 4.1 and 4.4) to the cross-propagation (Eq. 4.2. and 4.3) rate constants for the active centers derived from each respective monomer. The propagating reactions of monomer A ($M_A$) and monomer B ($M_B$) and their monomer reactivity ratios of $M_A$ ($r_A$) and $M_B$ ($r_B$) are shown below;

$$M_A^* + M_A \xrightarrow{k_{AA}} M_A^* \quad \text{... (Eq. 4.1)}$$

$$M_A^* + M_B \xrightarrow{k_{AB}} M_B^* \quad \text{... (Eq. 4.2)}$$

$$M_B^* + M_A \xrightarrow{k_{BA}} M_A^* \quad \text{... (Eq. 4.3)}$$

$$M_B^* + M_B \xrightarrow{k_{BB}} M_B^* \quad \text{... (Eq. 4.4)}$$

$$r_A = \frac{k_{AA}}{k_{AB}} \quad and \quad r_B = \frac{k_{BB}}{k_{BA}} \quad \text{... (Eq. 4.5)}$$

Thus, if $r_A > 1$ then the propagating reaction prefers to add monomer A (i.e. it prefers to homopolymerize), whereas if $r_A < 1$ the propagating reaction prefers to add monomer B and hence copolymerize. Similarly, $r_B$ describes the behaviour of monomer B. For this copolymer system, $r_A$ and $r_B$ are the monomer reactivity ratios of MMA ($r_M$) and BA ($r_{BA}$), respectively. Referring to data from a textbook [46], the monomer reactivity ratios for free-radical copolymerization of MMA and BA are $r_M$ = 1.8, $r_{BA}$ = 0.37, and $r_M r_{BA}$ = 0.67. At this point, it could be assumed that the structural type of P(MMA-*co*-BA) was a random structure which had longer homo-part of MMA than that of BA.

Weight average molecular weight ($\overline{M}_w$), number average molecular weight ($\overline{M}_n$), and molecular weight distribution ($MWD$) of the copolymers were determined by GPC technique as shown the chromatograms in the Appendix D. The results for all of the copolymer formulas show the narrow range of the molecular weight as summarized in Table 4.3. This insignificant difference in the molecular weight of all

copolymer formulas was actually expected, not only because they were synthesized under the same condition, but, MMA and BA monomers have a quite similarity in both of their molecular weight and molecular structure as well.

Therefore, in this work, the effect of the variety in molecular weight of the copolymer matrices on the mechanical properties of the nanocomposite films could be remained inactive.

**Table 4.3** Molecular weight of P(MMA-*co*-BA) formulas with varying weight ratios of MMA:BA monomer

| Co-polymer formula | Molecular weight (g/mole) | | Molecular weight distribution (*MWD*) |
|---|---|---|---|
| | Weight average ($\overline{M}_w$) | Number average ($\overline{M}_n$) | |
| M10B0 | $1.00 \times 10^5$ | $5.3 \times 10^4$ | 1.9 |
| M9B1 | $1.40 \times 10^5$ | $7.2 \times 10^4$ | 1.9 |
| M8B2 | $1.20 \times 10^5$ | $6.6 \times 10^4$ | 1.8 |
| M7B3 | $1.30 \times 10^5$ | $6.9 \times 10^4$ | 1.9 |
| M6B4 | $1.08 \times 10^5$ | $5.7 \times 10^4$ | 1.9 |

## *4.3 Solvent Screening of P(MMA-co-BA) and P-MMT*

To fabricate the polymer/organoclay composites by undergoing solvent casting technique, solvent screening is one of the most crucial preparation steps. This step is in order to search for the most suitable solvent, which has the polarity close to that of the organoclay and the polymer in the system. Therefore, this solvent should give the good swelling of dispersed phase, i.e., organoclay, and dissolve the polymer matrix as well. On the side, not only clay can be dispersed thoroughly in the polymer matrix with the help of the solvent, but also the solvent can be regarded as a medium which assist polymer chains to penetrate into the *001* plane of the organoclay.

The solvent screening test for P(MMA-*co*-BA) and P-MMT had been run with a set of the solvents, i.e., dichloromethane, xylene, and toluene. The outcome showed that P(MMA-*co*-BA) copolymers could be dissolved in all of those solvents while P-MMT could show the better swelling in xylene and toluene than in dichloromethane (Fig. 4.4). At this point, both of xylene and toluene were worth considering, but in this experiment, the nanocomposite films would be left to dry the solvent out at room temperature. Therefore, toluene which has lower boiling point was more suitable, and thus, it was selected as the solvent to use for preparation of P(MMA-*co*-BA)/P-MMT nanocomposite films.

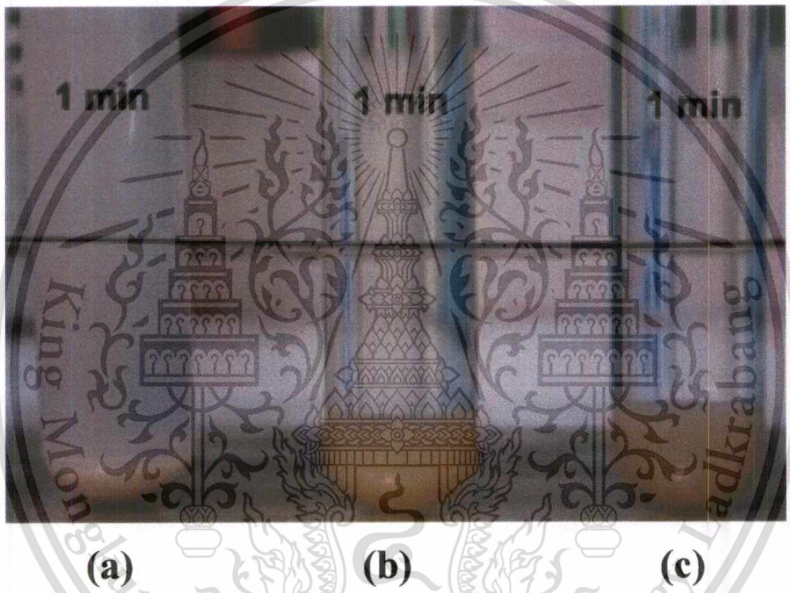


**Fig. 4.4** Swelling of P-MMT in some selected solvents after sonication and shaken then left for 1 minute; (a) Dichloromethane, (b) Xylene, and (c) Toluene

## *4.4 Characterization of P(MMA-co-BA)/P-MMT films*

P(MMA-*co*-BA)/P-MMT composite films had been fabricated by doctor blade technique and the obtained composite films were highly transparent. Therefore, to confirm the presence of P-MMT within the fabricated films, the films were characterized by using XRF technique. The results ensured that the composite films contained the compositions of silicon (Si), aluminium (Al), and phosphorous (P), which are the components of the P-MMT, as shown in the Appendix B.

The XRD was used to characterize the interlayer distances and structure of the P-MMT within the composite films. The XRD patterns of P(MMA-*co*-BA)/P-MMT composite films with both varying of copolymer formula and concentrations of P-MMT loading are shown in Fig. 4.5. They were seen that all of the copolymer formula variations showed the same patterns of the diffraction spectra. For the P(MMA-*co*-BA)/P-MMT containing 1 and 2 wt% of P-MMT, the crystalline peak of *001* plane was observed at $2\Theta \sim 4\text{-}6^\circ$ with very low intensity, implying that the intercalation of the P(MMA-*co*-BA) into the P-MMT layers caused the expansion of the *001* plane. The higher amount of P-MMT content (3 and 6 wt%), the stronger intensity of the $d_{001}$ peak was observed without significant change of its peak position, indicating that the intercalated nanostructure was mainly occurred with almost the same basal spacing as 1 and 2 wt% of P-MMT loading. These results indicate the penetration of the copolymer chains into the *001* plane of the P-MMT, forming the intercalated nanostructure. However, the penetration of the copolymer chains was cumbersome due to their relatively high molecular weight which containing steric butyl side-chain, thus, the exfoliated nanostructure might not occur.

Besides, TEM micrograph of P(MMA-*co*-BA)/P-MMT composite film, which has MMA:BA ratio as 9:1 and contains 2 wt% of P-MMT (M9B1-P2), is demonstrated in Fig. 4.6. From the TEM micrograph, the dispersion of P-MMT tactoids in the P(MMA-*co*-BA) matrix can be seen. The loosely packed structure of P-MMT tactoids in the composites was observed. This morphology represented the intercalated nanostructure of the P(MMA-*co*-BA)/P-MMT nanocomposite films, supporting the previous XRD analysis.

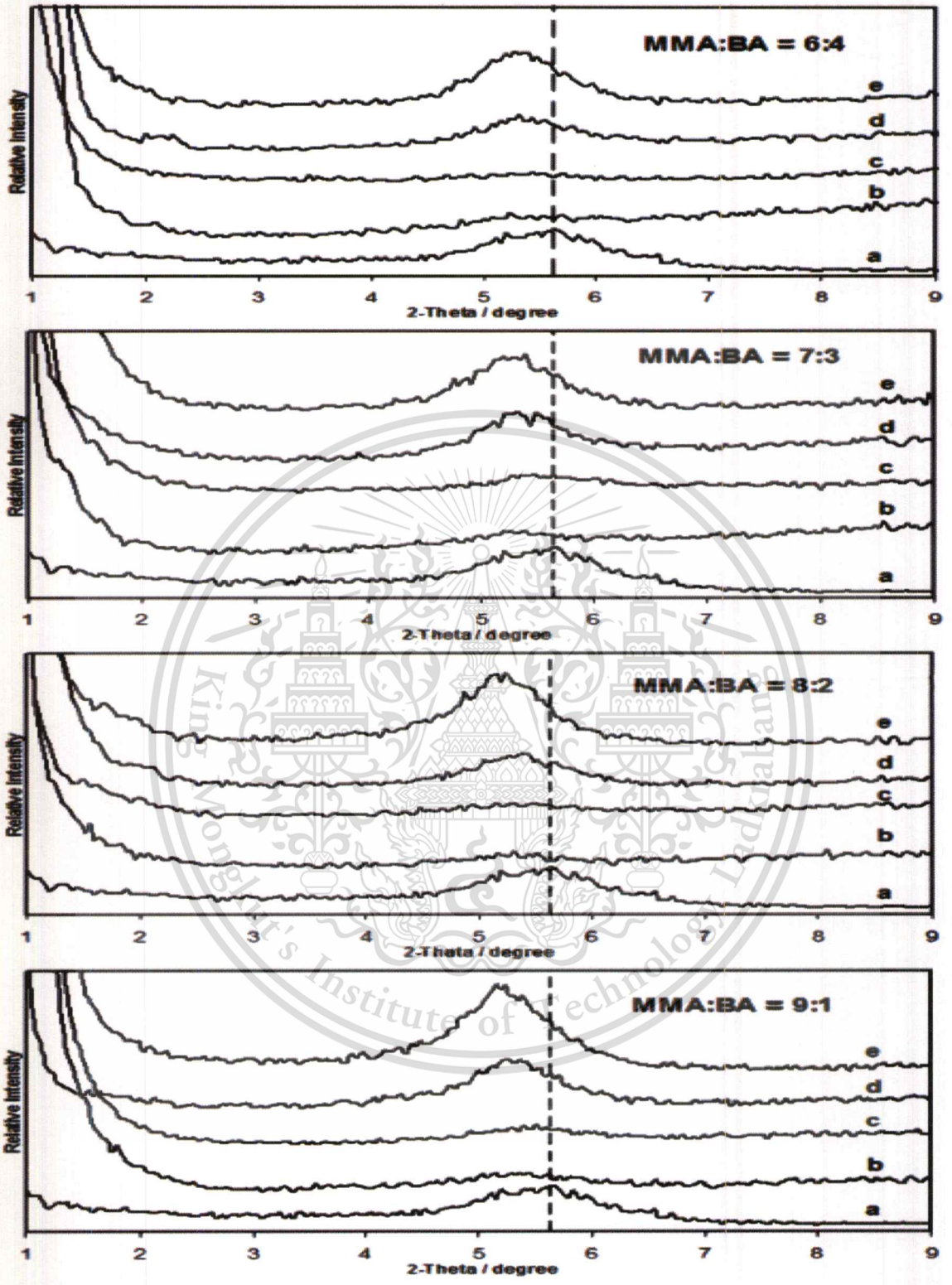


**Fig. 4.5** XRD patterns of P-MMT, and P(MMA-*co*-BA)/P-MMT composite films; (a) pristine P-MMT, (b) 1wt% P-MMT, (c) 2wt% P-MMT, (d) 3wt% P-MMT, and (e) 6wt% P-MMT, shown with varying MMA:BA ratios in the composite formulas

**Table 4.4** Interlayer $d_{001}$-spaces of P-MMT and P(MMA-*co*-BA)/P-MMT films

| Sample | | $d_{001}$ peak position (2Θ, degree) | d-spacing (nm) |
|---|---|---|---|
| P-MMT | | 5.64 | 1.56 |
| M6B4 | P1 | Broad peak with very low intensity around 4-6 | *N/A* |
| | P2 | Broad peak with very low intensity around 4-6 | *N/A* |
| | P3 | 5.32 | 1.66 |
| | P6 | 5.28 | 1.67 |
| M7B3 | P1 | Broad peak with very low intensity around 4-6 | *N/A* |
| | P2 | Broad peak with very low intensity around 4-6 | *N/A* |
| | P3 | 5.32 | 1.66 |
| | P6 | 5.40 | 1.64 |
| M8B2 | P1 | Broad peak with very low intensity around 4-6 | *N/A* |
| | P2 | Broad peak with very low intensity around 4-6 | *N/A* |
| | P3 | 5.36 | 1.65 |
| | P6 | 5.24 | 1.69 |
| M9B1 | P1 | Broad peak with very low intensity around 4-6 | *N/A* |
| | P2 | Broad peak with very low intensity around 4-6 | *N/A* |
| | P3 | 5.24 | 1.69 |
| | P6 | 5.16 | 1.71 |

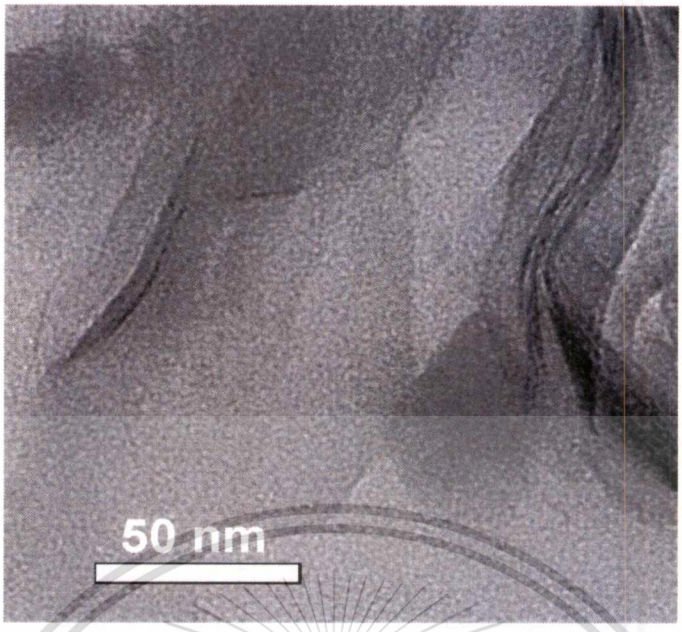


**Fig. 4.6** TEM micrograph of M9B1-P2 nanocomposite film

## *4.5 Thermal properties of P(MMA-co-BA)/P-MMT films*

### *4.5.1 Thermogravimatric analyst (TGA)*

Thermal stability of the PMMA, P(MMA-*co*-BA), and nanocomposites of P(MMA-*co*-BA) containing P-MMT and unmodified-MMT (uMMT) were evaluated by TGA under nitrogen atmosphere and shown thermograms in Fig. 4.8 – 4.12. The decomposition temperature at 10% ($T_{d\text{-}10\%}$) weight loss data for the neat copolymers and the nanocomposites are summarized in Table 4.5.

From Fig. 4.8 and $T_{d\text{-}10\%}$ values in Table 4.5, they were clearly seen that the decomposition temperature of neat P(MMA-*co*-BA) copolymers increased with the increment of the BA contents. Therefore, the P(MMA-*co*-BA) with higher portion of BA is more stable than the less ones. This could be regarded as the stabilizing effect of BA units in the copolymer structure as reported by Leskovac *et al.* [47]. Moreover, the P(MMA-*co*-BA) copolymers also showed less steps in the degradation than that of PMMA. There is a report of Kashiwagi *et al.* [48] identifies three steps in the thermal degradation of radically-prepared PMMA, which are assigned as; the first and easiest step (Fig. 4.7(1)) is initiated by the scissions of head-to-head linkages at about 160 °C, representing one type of defect at the polymer backbone; the second step (Fig. 4.7(2)) is the scissions at the chain-end initiated from vinylidene ends at around 270 °C; and the last step (Fig. 4.7(3)) is the random scissions within the polymer chain (at the

weakest bonds) at about 355 ºC. Therefore, in this work, it would be suggested that the presence of the more thermal stable part of the BA units in the P(MMA-*co*-BA) copolymers might compensate the scissions of the weak linkages in the polymer structure, and thus, the copolymers could show less steps in the degradation and better thermal stability.

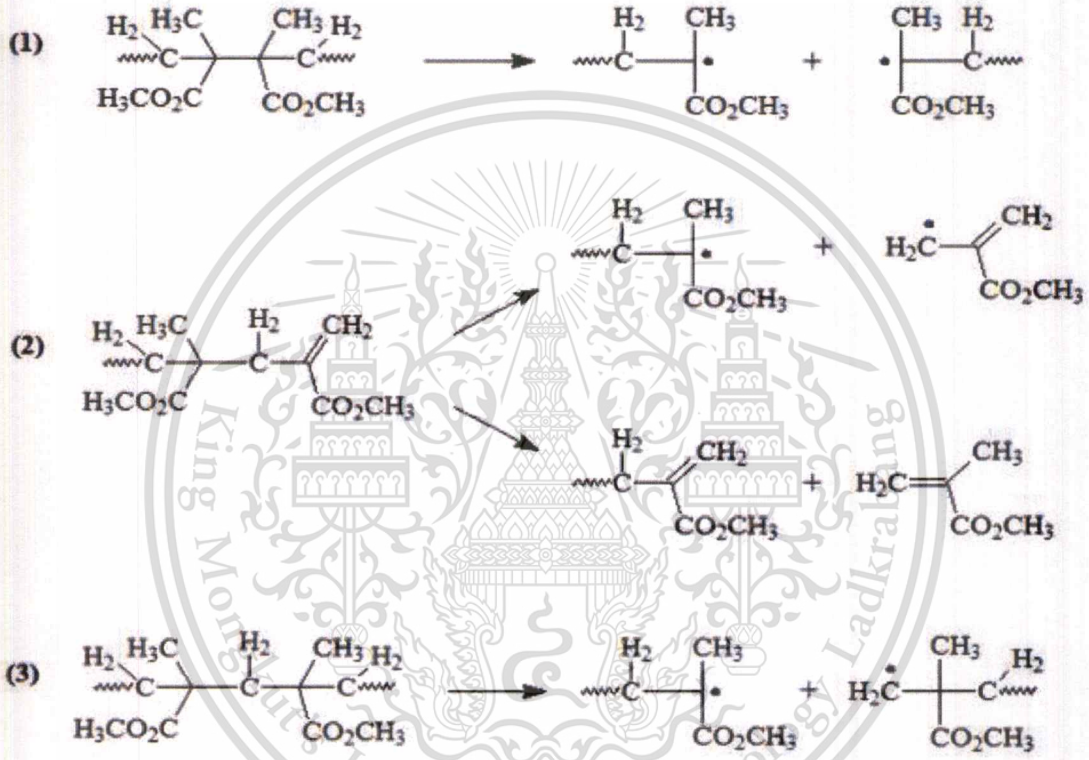


**Fig. 4.7** Schematic of three chain-scission steps leading to thermal degradation behavior in acrylic polymers. *(This figure was modified from [48] and [49].)*

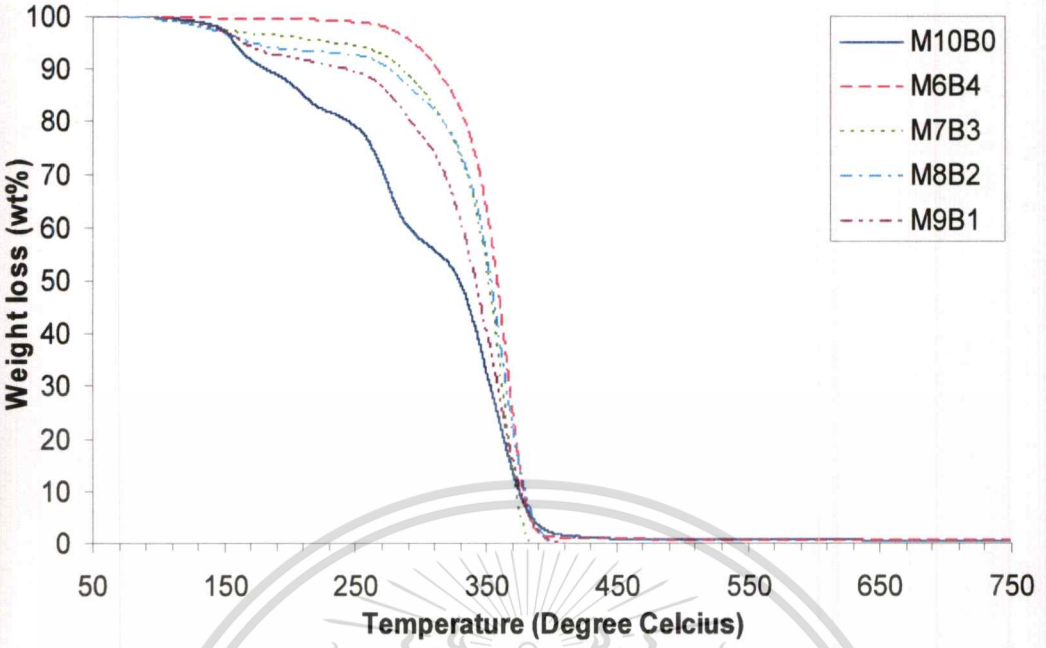


**Fig. 4.8** TGA thermograms of P(MMA-*co*-BA) copolymers with varying MMA:BA ratios under nitrogen atmosphere

For the nanocomposites, the effects of P-MMT addition and the different formula of copolymer matrices on their thermal stability were investigated. From Table 4.5, the nanocomposites showed the higher $T_d$ than those of their neat copolymers, indicating the enhancement of thermal stability of the nanocomposite films. This phenomenon can be attributed to the presence of P-MMT, which is a high thermal stability and high aspect ratio inorganic nanoscale-substance, thus, it can act not only as a thermal barrier but also preventing and delaying out-diffusion of the volatile decomposition products, resulting in the higher thermal stability of the P(MMA-*co*-BA)/P-MMT nanocomposites compared to their neat copolymers.

Moreover, as seen in Table 4.5, it was noticed that the nanocomposites of M9B1 showed the highest $T_{d\text{-}10\%}$ value at 1 wt% of P-MMT loading (273 °C) whereas those of M6B4 had the highest $T_{d\text{-}10\%}$ value at 3 wt% of P-MMT loading (322 °C). In addition, it could be observed that the shifting of those highest $T_{d\text{-}10\%}$ values from $T_{d\text{-}10\%}$ of their neat copolymers of the M9B1 (32 °C) was higher than that of the M6B4 (10 °C). The explanation for those effects was based on the dispersion of P-MMT in the copolymer matrices and the penetrating possibility of copolymer chains into *001* plane of P-MMT with the different formulas of the copolymer matrices.

Generally, the mechanism to delay the decomposition temperature for the polymer/clay composites system is holding heat flux by absorbing and spreading the heat throughly on the organoclay surfaces. Hence, it could be said that the better dispersion of P-MMT, the higher surface area and heat absorption rate could be obtained. Practically, in this work, the fabricated nanocomposites came out with mainly intercalated nanostructure, hence, the dispersion of P-MMT was quite limited comparing to that of the exfoliated nanocomposites. Then, the dispersion of P-MMT was mainly affected by the formula of the copolymer matrices. When the portion of BA in the copolymer formula was higher, the polarity of the copolymer system was relatively lower. Thus, P-MMT might be better dispersed with less aggregation in the M6B4-copolymer matrix than in the M9B1 system, resulting in the higher compatible point of P-MMT addition for the M6B4 formula than that for the M9B1 system. As seen in Table 4.5, the highest $T_{d\text{-}10\%}$ of the M6B4 system was at 3 wt% addition of P-MMT (M6B4-P3) whereas the highest $T_{d\text{-}10\%}$ of the M9B1 system was at 1 wt% addition of P-MMT (M9B1-P1).

Furthermore, in the lower-BA-system, it would cause some more aggregation of the P-MMT particles due to the difference in the compatibility between P-MMT and different copolymer matrices. As the previous mentioned, the organoclay can absorb heat from the surrounding, hence, it can be regarded as not only a heat barrier but also as heat storage. The more agglomeration of P-MMT particles, the larger heat sink would be occurred, resulting in the faster thermal decomposition of the copolymer matrix at lowering $T_{d\text{-}10\%}$ value. As noticed in the Table 4.5 for the $T_{d\text{-}10\%}$ values of M7B3, M8B2, and M9B1 systems, their highest $T_{d\text{-}10\%}$ values were at 1 wt% loading of P-MMT and the values were lowering with the increment of P-MMT contents. However, all of the nanocomposites were still more stable than their neat copolymers. This can be suggested that the addition of P-MMT could give the better thermal stability of the P(MMA-*co*-BA)/P-MMT nanocomposites, nevertheless, the excess concentration of P-MMT beyond thermal compatible point would cause the descending of thermal stability of the nanocomposites.

Besides, the degradation mechanism of acrylate polymers is proposed to the unzipping of their monomers at the weakest bonds within the polymer backbone [47-49]. Thus, the more possibility to penetrate into the interlayers of P-MMT of the copolymer main-chains, the better protection by the P-MMT layers would be obtained. Thereby, higher $T_d$ value could be acquired. Based on structure of the copolymers, the

M9B1 could have more possibility for the penetration of the copolymer main-chains into the interlayer spaces of P-MMT than the higher-BA-content copolymer formulas. Therefore, the shifting of the highest $T_{d\text{-}10\%}$ values from $T_{d\text{-}10\%}$ of their neat copolymers of M9B1 series (32 ºC) was higher than that of M8B2 (25 ºC), M7B3 (22 ºC), and M6B4 series (10 ºC), respectively.

The comparison between the thermal stability of P(MMA-*co*-BA)/P-MMT and P(MMA-*co*-BA)/unmodified MMT (uMMT) was investigated at 2% addition. The composites with uMMT exhibited lower $T_{d\text{-}10\%}$ than those of the nanocomposites with P-MMT. For instance, $T_{d\text{-}10\%}$ of M9B1-P2 was 253 ºC which was 17 ºC higher than that of M9B1-2%uMMT (236 ºC). This indicated the higher thermal stability of the P(MMA-*co*-BA)/P-MMT than the P(MMA-*co*-BA)/uMMT. This effect was due to the incompatible between the uMMT and P(MMA-*co*-BA) matrix leading to more agglomerate of the uMMT, implying the less possibility for the intercalation of copolymer chains into the interlayer space of the uMMT layers.

In addition, as seen in Fig. 4.12, the presence of the uMMT could slightly enhance the thermal stability of the neat M9B1 copolymer at the earlier of decomposition until about 5% weight loss where $T_{d\text{-}5\%}$ of M9B1 and M9B1-2% uMMT were 163 ºC and 166 ºC, respectively. This could be attributed to the presence of clay, which is a high thermal stability inorganic substance. However, the MMT is not only act as a thermal barrier but also as heat storage. Hence, the agglomeration of the uMMT caused the larger heat sink in the copolymer matrix. Besides, the agglomeration of the uMMT particles could also increase the continuity of the copolymer matrix in the nanocomposites. Since more continuity of the copolymer matrix, faster thermal decomposition of the copolymer matrix would be observed with less interference by the MMT particles. Therefore, the presence of the larger heat sink and the higher continuity of the copolymer matrix could accelerate the thermal decomposition of the P(MMA-*co*-BA) as seen more decomposition beyond 5% weight loss, consequently, the decomposition temperature of the P(MMA-*co*-BA)/MMT 2% composite could be lower than that of the neat copolymer.

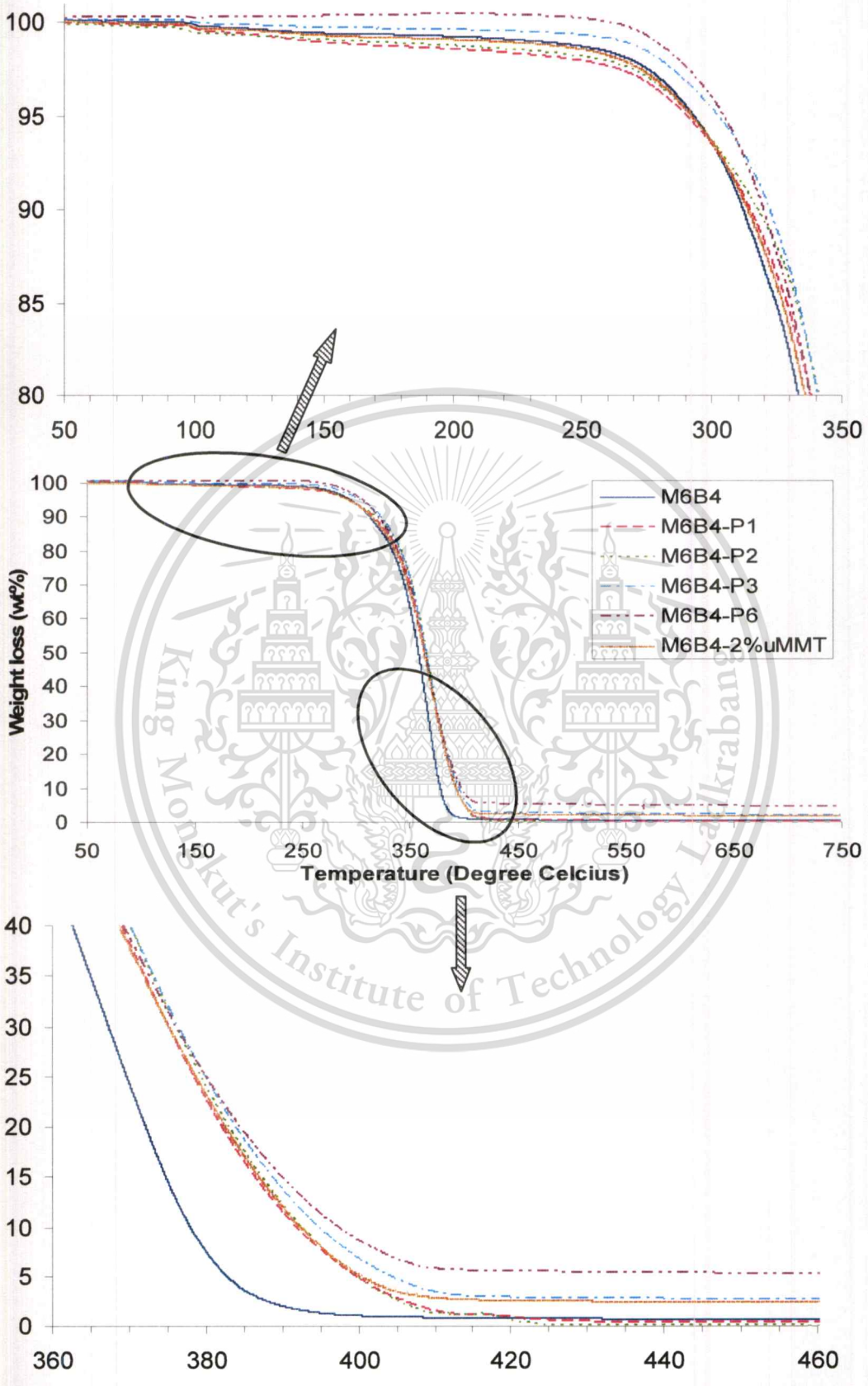


**Fig. 4.9** TGA thermograms of copolymer at ratio of MMA:BA = 6:4 (M6B4) and its nanocomposites with P-MMT and uMMT loading under $N_2$ atmosphere

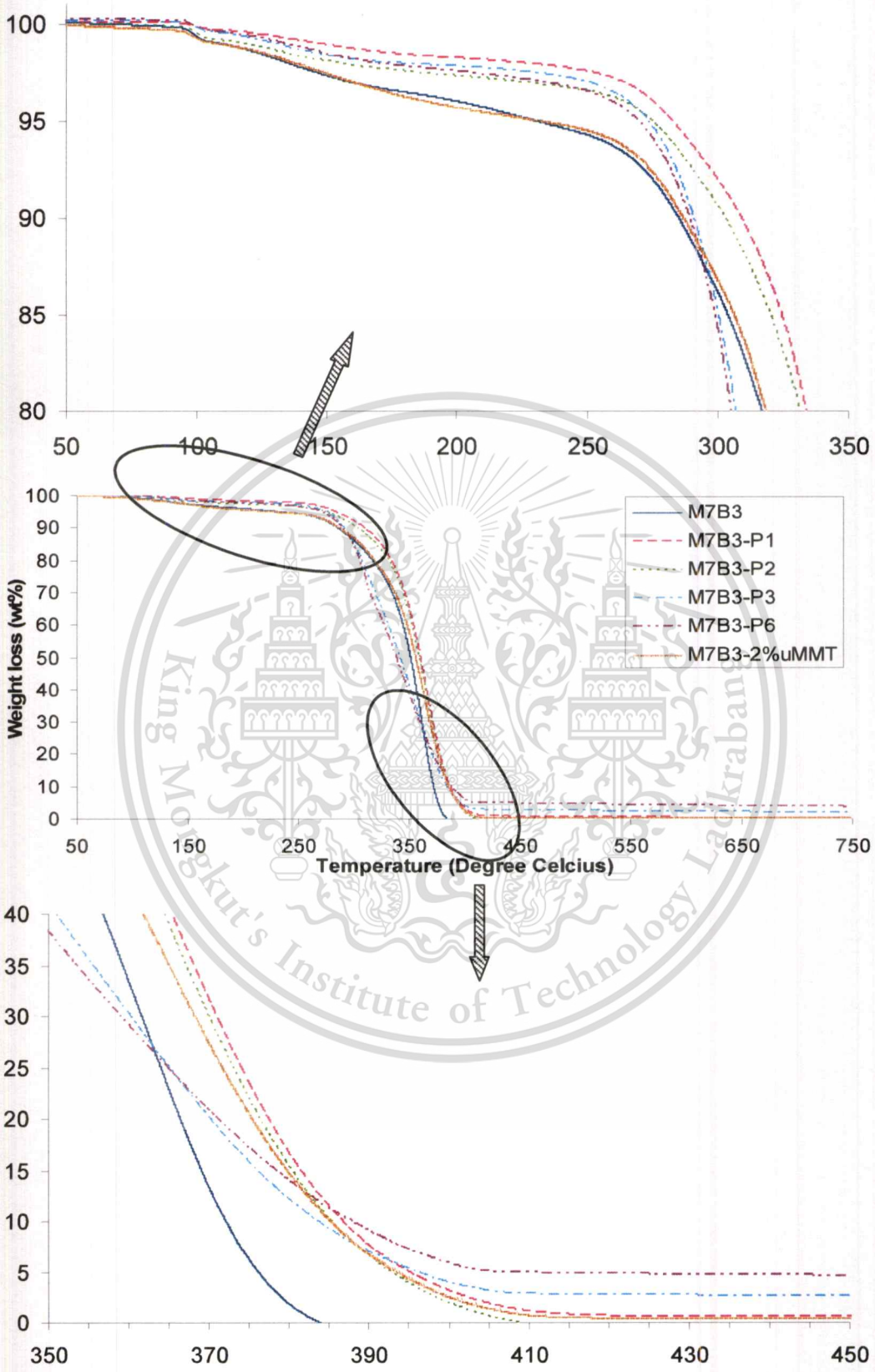


**Fig. 4.10** TGA thermograms of copolymer at ratio of MMA:BA = 7:3 (M7B3) and its nanocomposites with P-MMT and uMMT loading under $N_2$ atmosphere

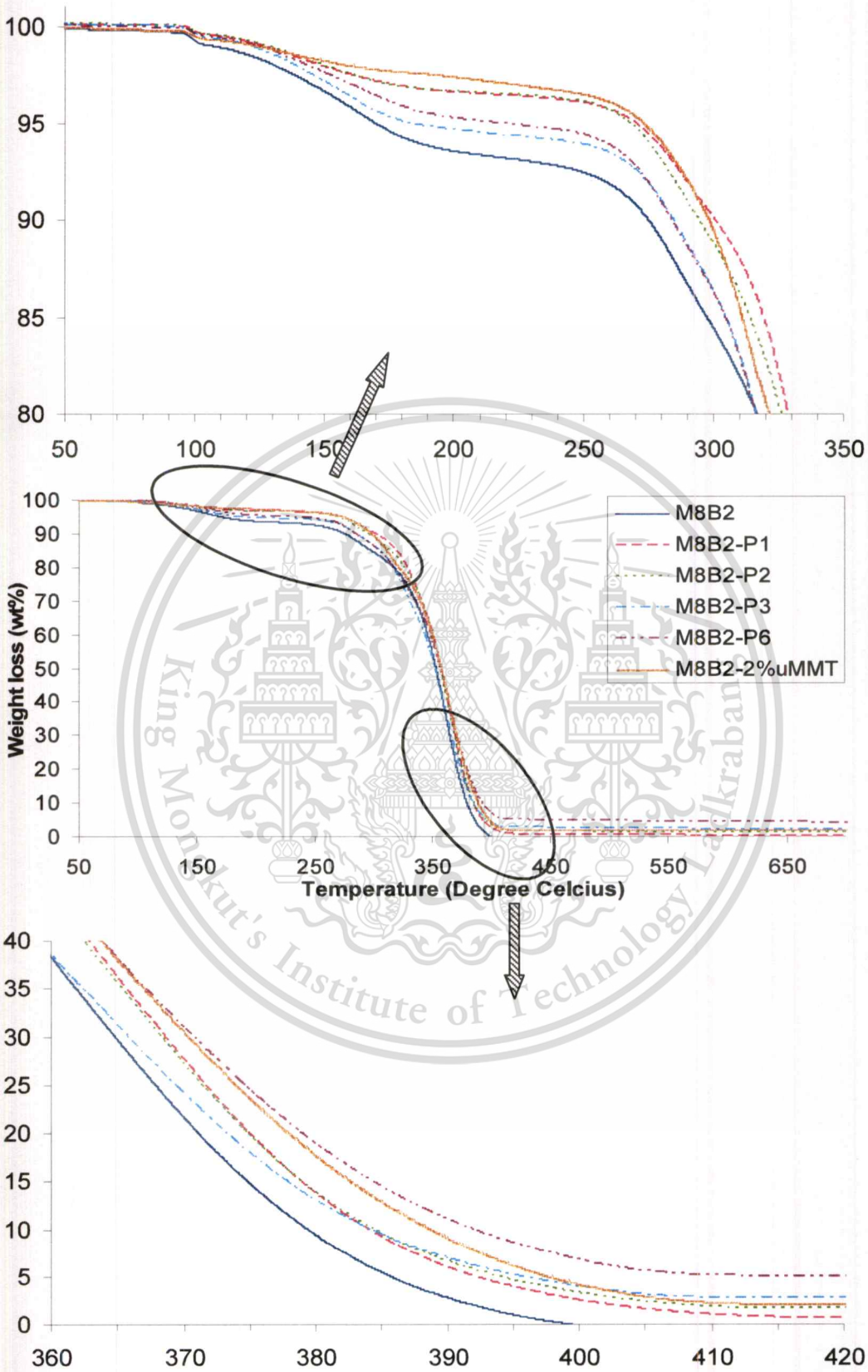


**Fig. 4.11** TGA thermograms of copolymer at ratio of MMA:BA = 8:2 (M8B2) and its nanocomposites with P-MMT and uMMT loading under $N_2$ atmosphere

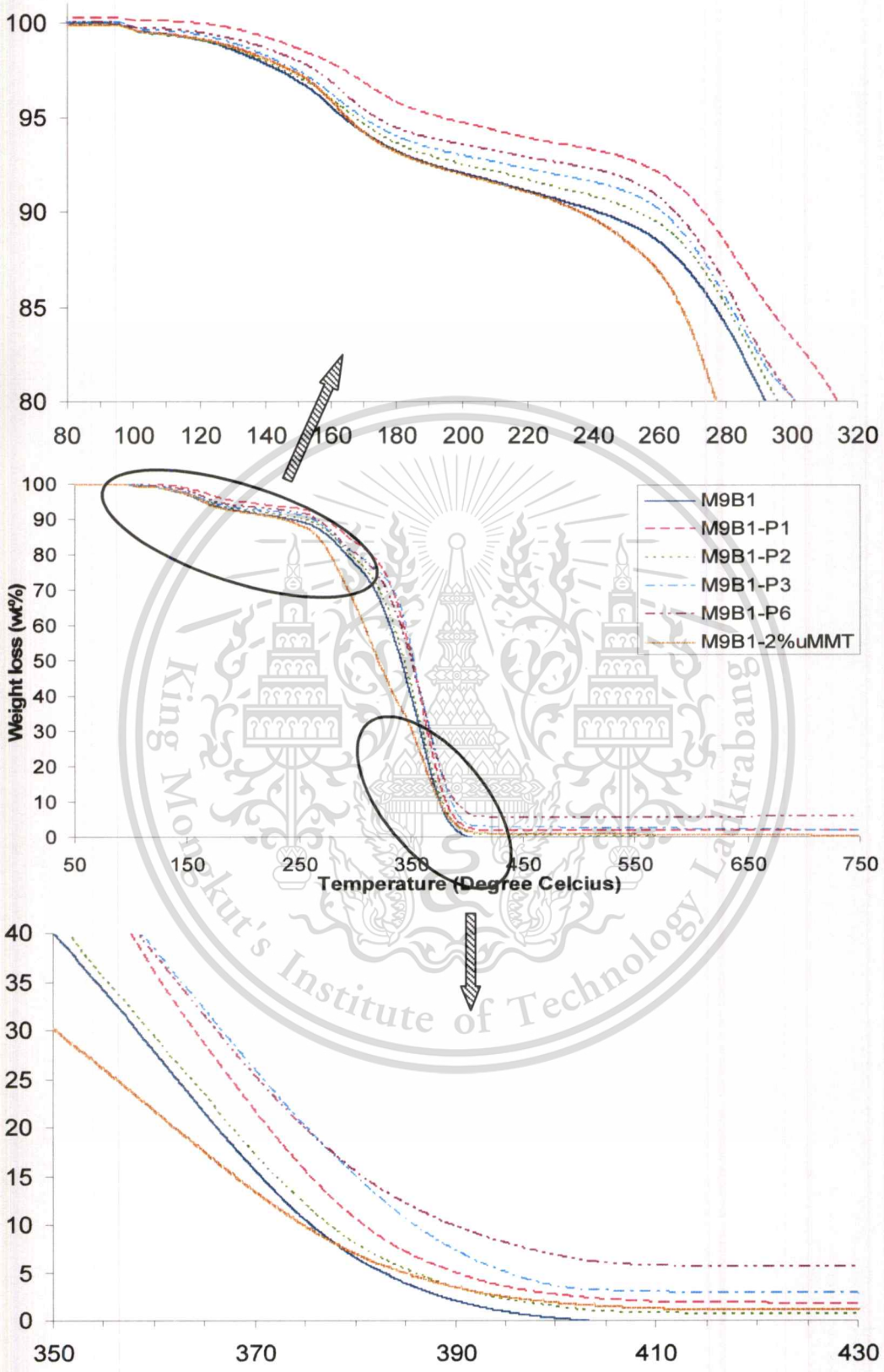


**Fig. 4.12** TGA thermograms of copolymer at ratio of MMA:BA = 9:1 (M9B1) and its nanocomposites with P-MMT and uMMT loading under $N_2$ atmosphere

**Table 4.5** Decomposition temperature ($T_d$) and glass transition temperature ($T_g$) of copolymers and P(MMA-*co*-BA)/P-MMT nanocomposite films

| Sample | | Thermal properties | |
|---|---|---|---|
| | | $T_{d\text{-}10\%}$ (°C)[a] | $T_g$ (°C)[b] |
| M6B4 | P0 | 312 | 27 |
| | P1 | 314 | *N/D*[c] |
| | P2 | 317 | *N/D* |
| | P3 | 322 | 26 |
| | P6 | 319 | 25 |
| | 2%uMMT | 313 | *N/D* |
| M7B3 | P0 | 286 | 40 |
| | P1 | 308 | *N/D* |
| | P2 | 302 | *N/D* |
| | P3 | 290 | 45 |
| | P6 | 289 | *N/D* |
| | 2%uMMT | 286 | *N/D* |
| M8B2 | P0 | 275 | 49 |
| | P1 | 300 | *N/D* |
| | P2 | 294 | *N/D* |
| | P3 | 285 | 48 |
| | P6 | 284 | *N/D* |
| | 2%uMMT | 286 | *N/D* |
| M9B1 | P0 | 241 | 62 |
| | P1 | 273 | *N/D* |
| | P2 | 253 | *N/D* |
| | P3 | 260 | 59 |
| | P6 | 264 | 59 |
| | 2%uMMT | 236 | *N/D* |

[a] As measured by TGA under $N_2$ atmosphere, $T_{d\text{-}10\%}$ was the decomposition temperature value at 10% weight loss.

[b] As measured by DSC, $T_g$ was the onset glass transition temperature.

[c] As short for "Not determined"

### *4.5.2 Differential scanning calorimeter (DSC)*

Effect of P-MMT content in the P(MMA-*co*-BA)/P-MMT nanocomposite films on the glass transition temperature ($T_g$) was examined by differential scanning calorimeter (DSC) as illustrated in Fig. 4.13 and summarized the onset $T_g$ values in Table 4.5. Generally, the $T_g$ can imply to how easy of the polymer chains can move with the change of temperature. The polymer system, which has longer branched chain – more free volume, is able to move more easily, thus it can provide lower $T_g$ than that of the short one. From Table 4, it can be seen that $T_g$ of M6B4 was about 27 ºC that is lower than that of M7B3 (40 ºC), M8B2 (49 ºC), and M9B1 (62 ºC), respectively, indicating the reduction of $T_g$ value with the increment of BA portion in the P(MMA-*co*-BA) formula.

Furthermore, when P-MMT was added in the copolymer matrices, $T_g$ values of the nanocomposites were not significantly changed comparing to those of their neat copolymers as noticed in Table 4.5. These results might because the nanofiller is not only ranged in nano-size but also added in a small amount, hence, the movement of copolymer chains during the change of temperature would not be effectively interfered by the P-MMT nanofiller.

Besides, referring to the discussion in the previous techniques, the higher BA content in copolymer matrices, the more compatible with the P-MMT could be obtained, resulting in better properties due to the less aggregation of P-MMT dispersed phase. Theoretically, the more compatibility, the greater interaction should be acquired, bringing about the higher of $T_g$ value. But, in this work, the $T_g$ values of the nanocomposites were observed insignificant change comparing to those of their neat copolymers. This was because the fabricated nanocomposites were not fully intercalation. Thus, BA-side-chain could not perfectly penetrate into the interlayer spaces of P-MMT, leading to the lower interaction force, and consequently, a small changing in those $T_g$ values. In addition, if the nanocomposites were fully intercalation, not only the interlayer space of P-MMT would be wider, but the come out properties, i.e. $T_d$ and $T_g$ values, would increase as well.

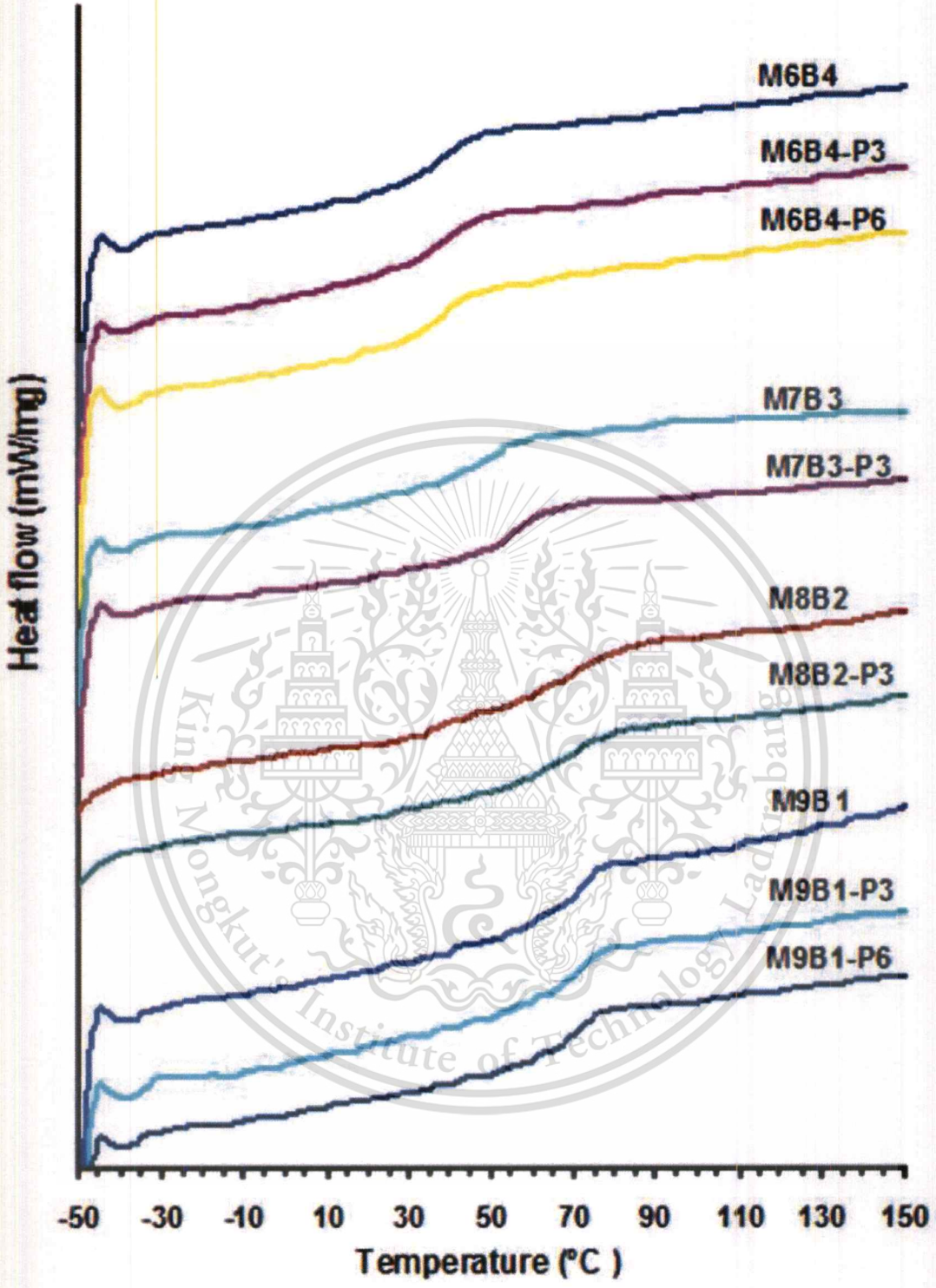


**Fig. 4.13** DSC curves of P(MMA-*co*-BA) and P(MMA-*co*-BA)/P-MMT with varying copolymer formula and amount of P-MMT addition at 3 and 6 wt%

## *4.6 Mechanical properties of P(MMA-co-BA)/P-MMT films*

The mechanical properties, i.e., tensile strength, Young's modulus, and % elongation at break of neat P(MMA-*co*-BA) and nanocomposite films prepared by varying MMA:BA ratios in the copolymer formula and P-MMT contents are illustrated in Fig. 4.14 - 4.18. The influences of the different copolymer formula on mechanical properties were observed in Fig. 4.14. It could be seen that the tensile strength and the Young's modulus of M9B1 were higher than those of M8B2, M7B3, and M6B4, whereas their elongation at break showed conversely tendency. These effects will be actually observed when the content of the BA portion – the rubbery phase – in copolymer matrix is increased. Therefore, the higher concentration of the BA portion in the copolymer formula, the lower tensile strength and the Young's modulus, but the higher % elongation at break, were obtained.

Effects of P-MMT content in the nanocomposites on the tensile strength and Young's modulus were shown in Fig. 4.15 and 4.16, respectively. They can be seen that the tensile strength and Young's modulus of the P(MMA-*co*-BA)/P-MMT were superior to their neat copolymers. In addition, the tensile strength and Young's modulus were also increased with the P-MMT contents. For instance, the M6B4 series, its tensile strength was increased from 9 (M6B4-P0) to 52.7 (M6B4-P3) MPa and its Young's modulus was increased from 197 (M6B4-P0) to 1728 (M6B4-P3) MPa, comparatively increased up to about 6 and 9 times, respectively. Due to the rigidity of the P-MMT nanoparticles, they could tolerate external stress better than the polymer matrix without distortion during deformation process. Hence, P-MMT nanoparticles could receive and absorb the incoming stress from the copolymer matrix, acting as stress concentrators in nano-scale dispersing in the polymer matrix, then, the applied stress was distributed to be smaller than the critical stress concentration. The P-MMT could, therefore, delay the fracture of the nanocomposites, resulting in an increase of tensile strength and Young's modulus of the nanocomposite films. Besides, the tensile strength and Young's modulus of the nanocomposites were found to be dropped when higher loading amount of P-MMT, as observed at 3 wt% (M7B3 and M8B2 series) or 6 wt% (M6B4 and M9B1 series) addition. This could be suggested that the concentration at 3 or 6 wt% loading would be excess for those systems. The excess concentration of P-MMT loading, the more agglomeration was obtained, resulting in the larger stress concentrators. When the nanocomposites had

larger stress concentrators – the bigger defect points – this could bring about the reduction of tensile strength and Young's modulus of those nanocomposites. However, those lowering mechanical properties of the nanocomposites were still greater than those of their original copolymers.

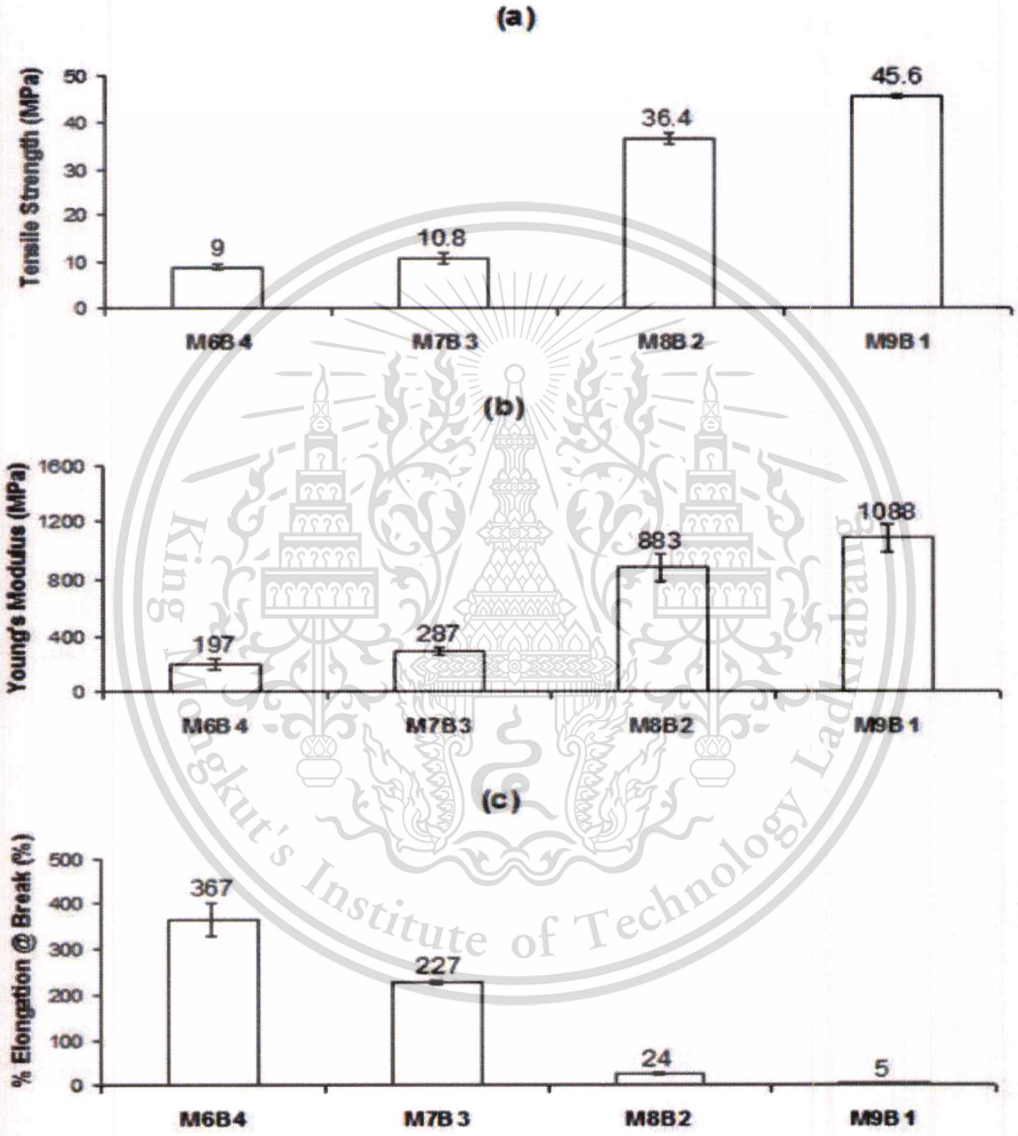


**Fig. 4.14** Effect of copolymer formula on mechanical properties of P(MMA-*co*-BA): (a) Tensile strength, (b) Young's modulus, and (c) % Elongation at break

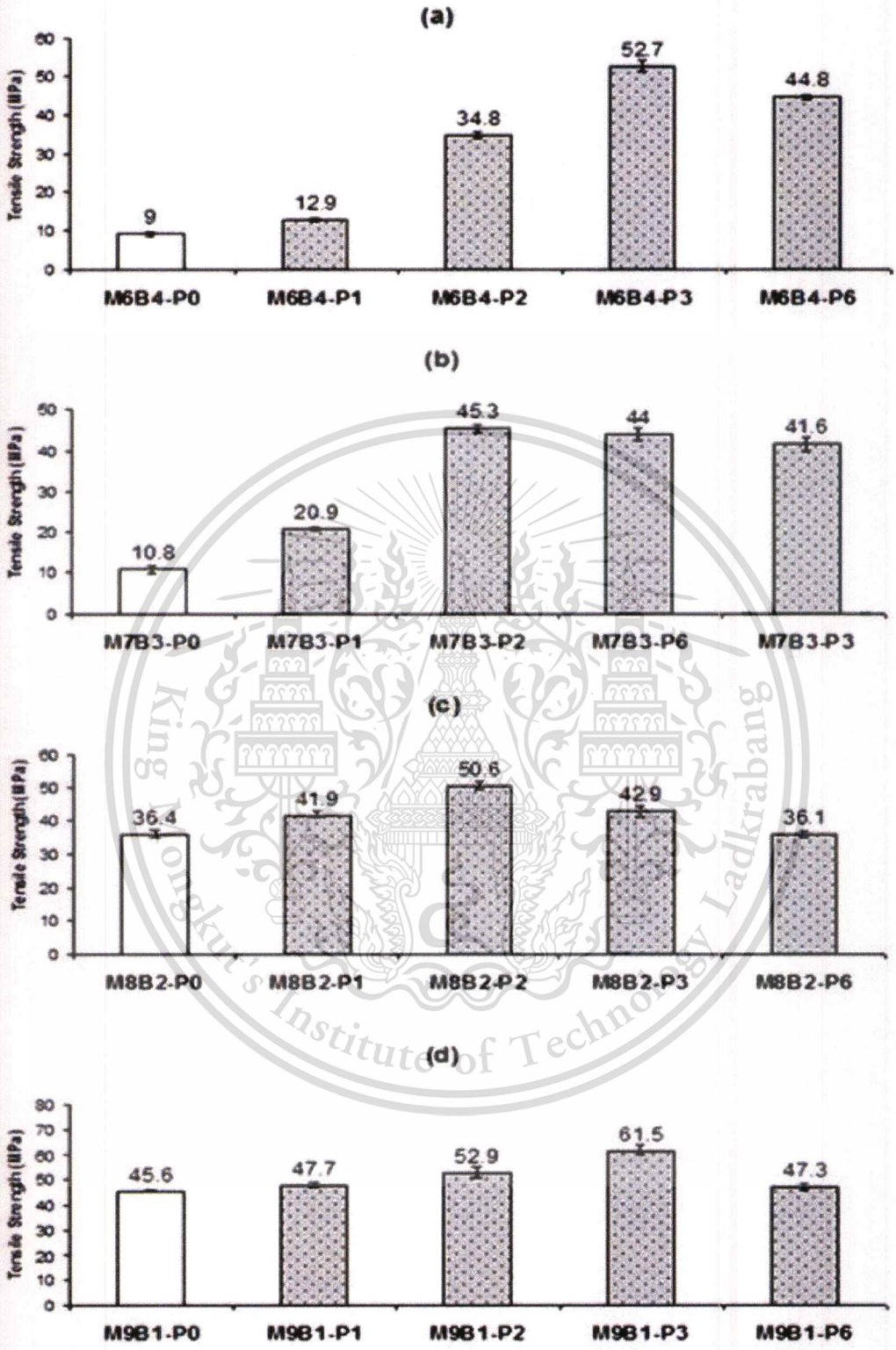


**Fig. 4.15** Effect of P-MMT contents on tensile strength of P(MMA-*co*-BA)/P-MMT nanocomposite films with varying copolymer formula:
(a) M6B4, (b) M7B3, (c) M8B2, and (d) M9B1

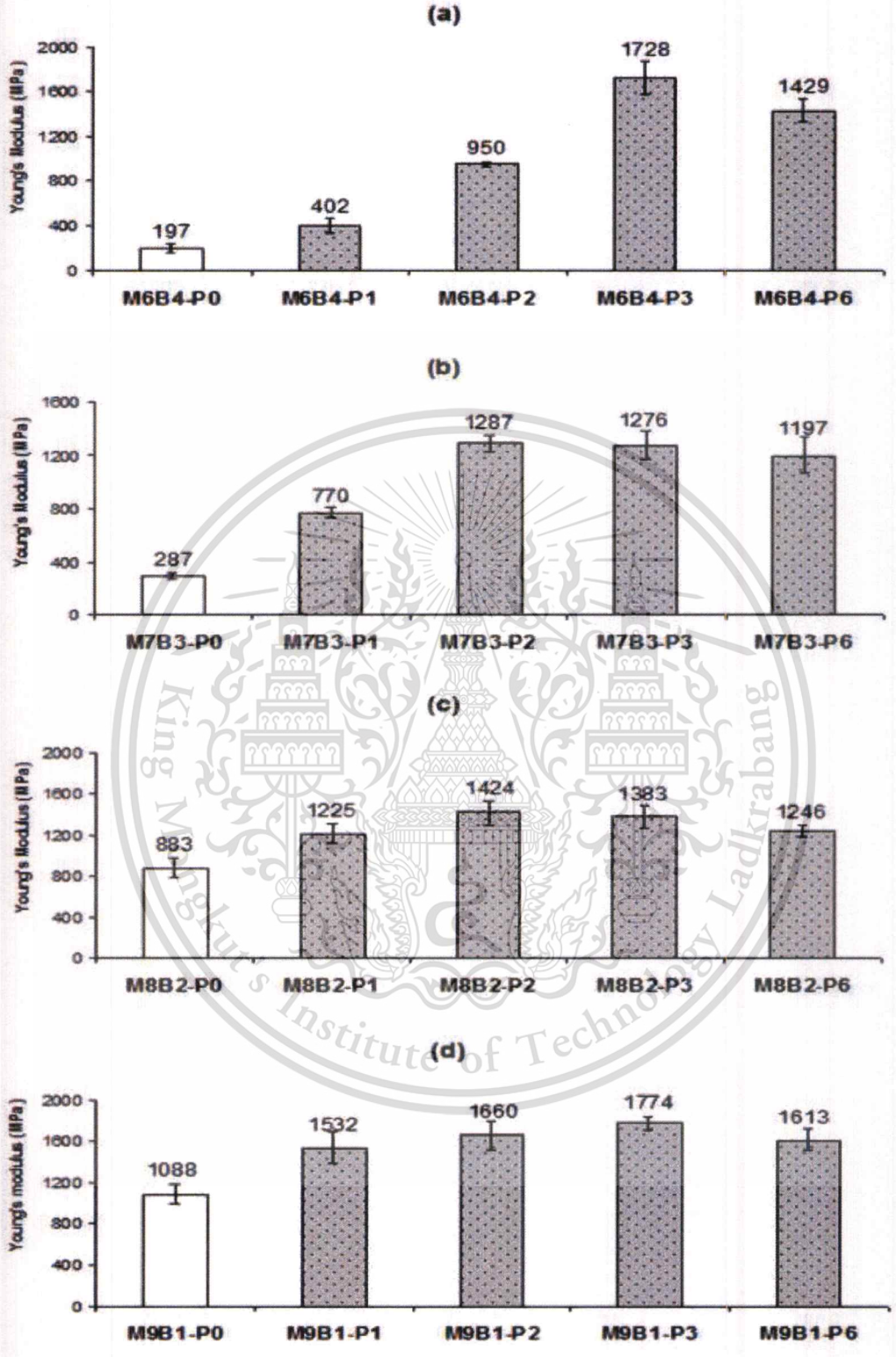


**Fig. 4.16** Effect of P-MMT contents on Young's modulus of P(MMA-*co*-BA)/ P-MMT nanocomposite films with varying copolymer formula: (a) M6B4, (b) M7B3, (c) M8B2, and (d) M9B1

In addition, it was noticed the differences in the increment of tensile strength and Young's modulus of the nanocomposites for each formula of copolymer series at the same loading content of P-MMT. These were mainly due to the dispersion behaviour of P-MMT in the copolymer matrices. As previous mentioned, the better dispersion of P-MMT, the better dissipation and diminishing of external stress was obtained. Moreover, the intercalation between copolymer chains and P-MMT layers could promote the better transference of the external force as well. Therefore, from Fig. 4.15 and 4.16, tensile strength and Young's modulus of the M6B4 series were increase greater with the higher concentration of P-MMT than those of the lower-BA-content series, e.g. M8B2 series. For the M6B4 system, there was high content of BA part then the P-MMT in this system had the better dispersion, but, the penetration of the copolymer chains into the interlayer spaces of P-MMT was slightly more difficult due to the higher steric branched chains of BA units. This resulted the great increase of their mechanical properties, however, this increment might not be as high as the case of fully-intercalation of the polymer chains. While, for the lower-BA-content series, the dispersion of P-MMT was worse and the aggregation was presumably higher, but the penetration of the copolymer chains into the interlayer spaces of P-MMT was possibly easier, resulting in the gradual increase of those properties.

The influence of P-MMT concentration on the ductility of the nanocomposite films was studied. As seen in Fig. 4.17, % elongation at break of all formula, but M9B1 series, decreased when P-MMT was incorporated, e.g., M6B4 series, their % elongation reduced from 336 % (M6B4-P0) to 34 % (M6B4-P2), 7% (M6B4-P3), and 7 % (M6B4-P6). Whereas, in the case of M9B1 series, the presence of P-MMT in the composites did not show the significantly change on their % elongation. The % elongation values both of the neat M9B1 and its nanocomposites were around 5 %. This reduction of the % elongation at break could be supposed as a result of the presence of P-MMT nanoparticles which cannot be distorted during deformation process, causing defect points in the films. In addition, even if the higher BA content in copolymer matrix could probably provide better dispersion of P-MMT, some agglomeration still occurred along with the intercalated structure of P-MMT. Therefore, the presence of P-MMT particles could cause the reduction of % elongation at break as well as the enhancement of tensile strength and Young's modulus of the P(MMA-*co*-BA)/P-MMT nanocomposites. However, the indifference in ductility of M9B1-nanocomposites might be a result of the predominant property of MMA parts in

those polymer matrices, which its polymer has normally low % elongation at break. Hence, the decrease of their % elongation might not clearly observe.

Figure 4.18 shows the mechanical properties in comparison at 2 wt% addition between the nanocomposite films loaded with P-MMT and unmodified-MMT (uMMT). It can be observed that the tensile strength and Young's modulus of the nanocomposites loaded with P-MMT were higher than those loaded with uMMT. This was due to the incompatibility between the uMMT and P(MMA-*co*-BA) that caused the less possibility for the polymer chains to intercalate into the interlayer spaces of uMMT, and also, lead to the bad dispersion and high agglomeration of uMMT in the copolymer matrices. Therefore, the stress concentrator size would be larger, causing higher stress concentration – bigger defect point in the polymer matrix. In addition, more agglomeration of uMMT particles in the copolymer matrices would cause more continuity of the matrix matter. Since the higher continuity of the matrix, the less consistency of stress transmission from the copolymer matrix to the dispersed-inorganic-phase would be occurred. Consequently, the uMMT composite films were probably easier to be deformed than the intercalated P-MMT nanocomposite films. However, the tensile strength and Young's modulus of the composites containing uMMT were still higher than those of the neat copolymer. This might be attributed to the effect of the inorganic addition as previous described.

Nevertheless, tensile strength and Young's modulus of the nanocomposites loaded with P-MMT were observed being slightly higher than those loaded with uMMT. This indicated that P(MMA-*co*-BA)/P-MMT nanocomposites also had some aggregate parts of P-MMT particles, leading to restricted improvement for the properties of the P(MMA-*co*-BA)/P-MMT nanocomposites and supporting the results from the previous analysis.

For the ductility comparing between the composite films containing P-MMT and uMMT, M6B4 and M7B3 with uMMT-filling composites exhibited higher value of the % elongation at break than those of the P-MMT-filling nanocomposites, but there were no significantly differences between two of those M8B2 and M9B1 formulas. The phenomena for the M6B4 and M7B3 series might be supposed to the incompatibility – less intercalation – between dispersed phase and copolymer chains in the high-BA-copolymer/uMMT system, leading to high agglomeration of the uMMT. Hence, the phase separation in the high-BA-copolymer/uMMT system would be quite predominant comparing to the low-BA-copolymer/uMMT system, along with just

small amount of uMMT filling, thus, the deformation of high-BA-copolymer/uMMT system could happen with infrequent obstruction by uMMT particles during applying the external stress. For this reason, the higher % elongation at break value of M6B4 and M7B3 with uMMT-filling composites than those with the P-MMT-filling nanocomposites was observed. Besides, in case of the lower-BA-copolymer/uMMT composites (M8B2 and M9B1 series), their % elongation was decrease to the values similarly to those added with P-MMT-filling nanocomposites. This might be a result of the predominant property of the MMA parts in those formulas, causing more brittle manner of the uMMT-filling films with the higher contents of MMA in the system.

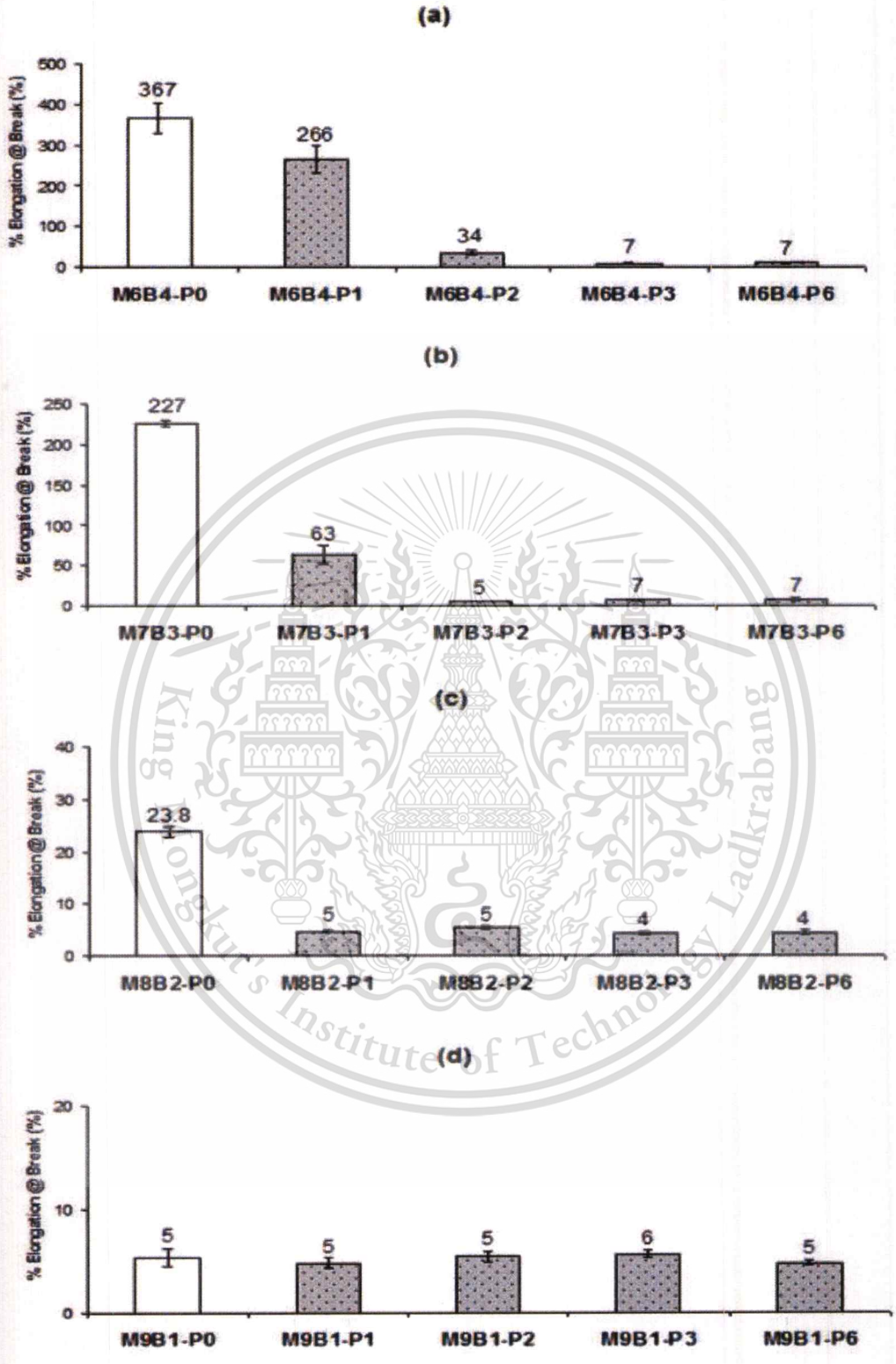


**Fig. 4.17** Effect of P-MMT contents on % elongation at break of P(MMA-*co*-BA)/P-MMT nanocomposite films with varying copolymer formula:
(a) M6B4, (b) M7B3, (c) M8B2, and (d) M9B1

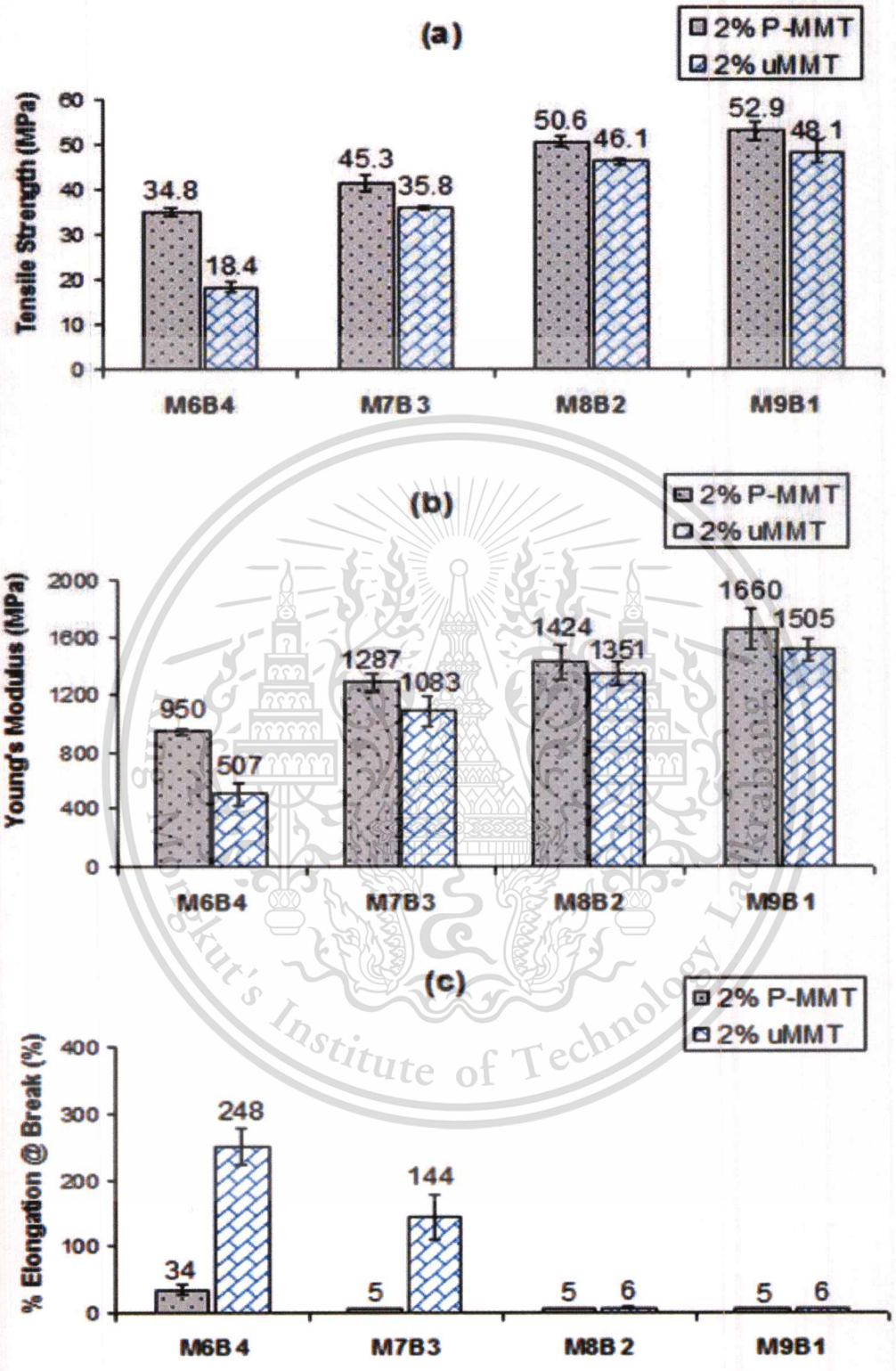


**Fig. 4.18** Comparison of mechanical properties between those of P(MMA-*co*-BA)/P-MMT and P(MMA-*co*-BA)/uMMT films at 2 wt% addition; (a) Tensile strength, (b) Young's modulus, and (c) % Elongation at break

## *4.7 Optical property of P(MMA-co-BA)/P-MMT films*

The transmittance spectra of the neat P(MMA-*co*-BA) and P(MMA-*co*-BA)/P-MMT nanocomposite films measured by UV-vis spectrophotometer are demonstrated in Fig. 4.19. These nanocomposite films were highly transparent in the visible range and they showed intense energy absorption for wavelengths lower than 320 nm (UV-B region). Besides, it could be also noticed that the higher concentration of BA in the formula, the higher transmission for wavelengths of 230 - 260 nm (UV-C region) would be observed.

In addition, it was found that the higher P-MMT content in the nanocomposites, the lower transmittances of UV and visible light were obtained, pointing to the UV shielding ability of P-MMT layers. Although the presence of P-MMT in the nanocomposites resulted in the decreases of both UV and visible light transmittances, the reduction of UV transmittance was relatively quite higher than that of the visible light transmittance. This was due to the dimensions of the P-MMT nanoparticles have the range close to the wavelength-magnitude of UV, thus, they were more capable of screening the UV.

However, the decreasing proportion of %T in those UV regions was observed some differences for each formula of the copolymer matrices. It might be suggested that this difference of %T reduction was affected by the dispersion behaviour of P-MMT in those copolymer matrices. For instance, in UV-A range seen in Fig. 4.19, %T of the M6B4-series nanocomposites was more decrease than that of M8B2 system. As mentioned in the previous analysis, P-MMT was likely to have better dispersion in higher-BA-content copolymer, therefore, in the system of M8B2 – lower BA portion, the P-MMT might have higher possibility to agglomerate, resulting in lower transmittance in the UV regions.

Moreover, thickness of the nanocomposite films also affected on %T of both UV and visible light. The thicker of the films, the higher amount of P-MMT would be presented. Hence, both UV ray and visible light could be more screened by the thicker film, resulting in the lower of %T in those regions. For example, i.e. M7B3-P3 and M7B3-P6 films, transmittances of these films were quite low in both UV and visible light ranges, especially in the visible light region. This could be not only the effect of more thickness of those nanocomposite films but also worse dispersion of P-MMT, as previous discussed.

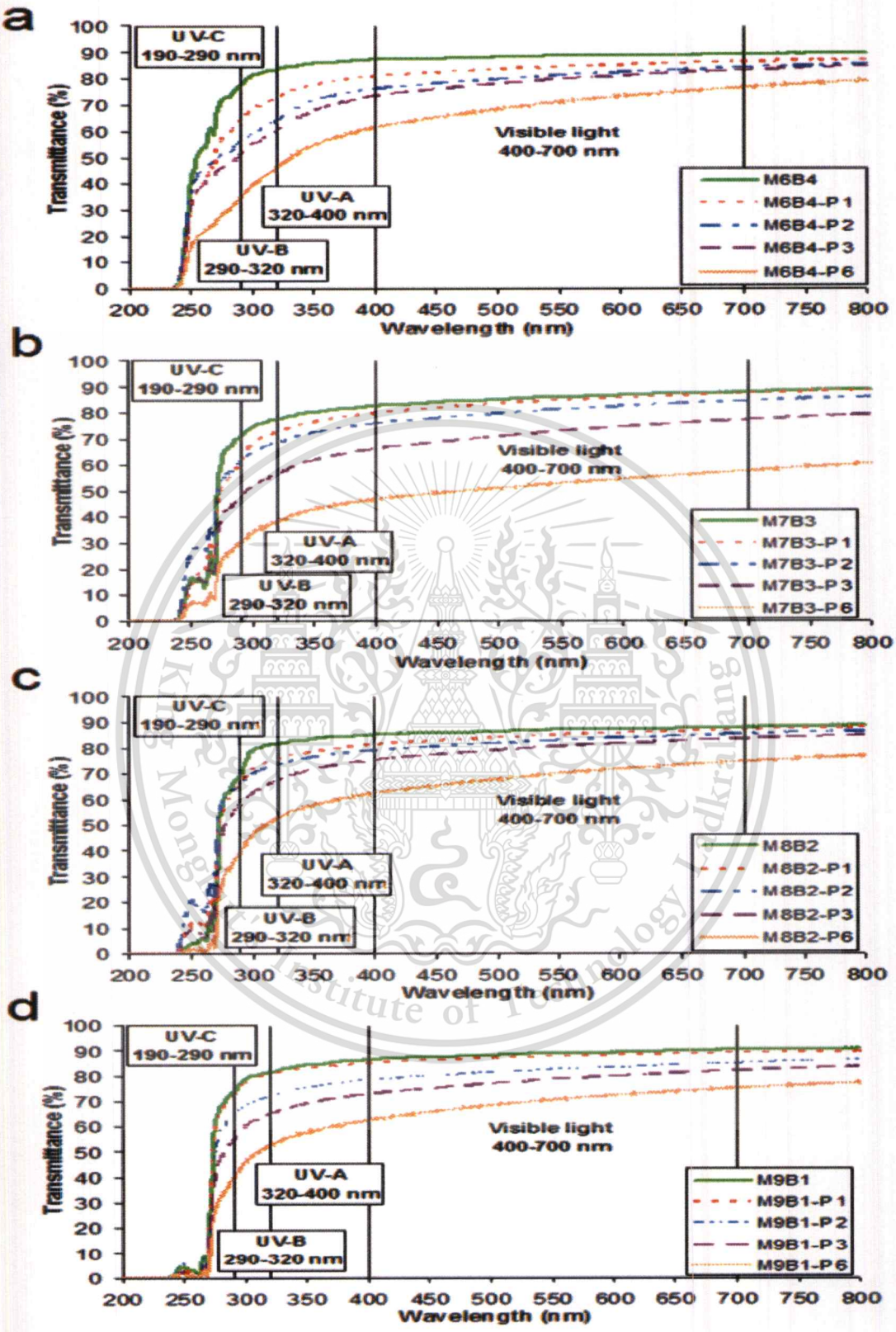


**Fig. 4.19** UV-vis transmittance spectra of P(MMA-*co*-BA)/P-MMT nanocomposite films (thickness = 0.1 ± 0.02 mm) with different copolymer formulas and varying P-MMT contents; (a) M6B4, (b) M7B3, (c) M8B2, and (d) M9B1 series

# Chapter 5
# Conclusion and Recommendations

## *5.1 Conclusion*

- Montmorillonite was modified by intercalation with tetrabutylphosphonium bromide. The amount of intercalated TBPB in the P-MMT was about 9.3 wt%. The onset degradation temperature of P-MMT was at 284 °C.

- The P(MMA-*co*-BA)/P-MMT nanocomposite films containing 1, 2, 3 and 6 wt% P-MMT could be prepared by simple solvent casting technique. The films containing 1 and 2 wt% of P-MMT showed intercalated nanocomposite structure with some agglomerate particles. The higher content of P-MMT (3 and 6 wt%) in the composites still had intercalated nanostructure along with more agglomeration of P-MMT.

- Thermal stability of PMMA was improved with the presence of BA part in P(MMA-*co*-BA) copolymers. Moreover, thermal stability of P(MMA-*co*-BA) copolymers was enhanced with the presence of P-MMT. The highest $T_{d\text{-}10\%}$ of M6B4 series was at 3 wt% addition of P-MMT while the highest $T_{d\text{-}10\%}$ of M7B3, M8B2, and M9B1 series were at 1 wt% addition of P-MMT. However, all formulas of the nanocomposites showed better thermal stability than those of the neat P(MMA-*co*-BA) copolymers.

- For the P(MMA-*co*-BA)/P-MMT nanocomposite films containing 1, 2, and/or 3 wt% P-MMT, it was seen that the higher of P-MMT loading, the higher tensile strength and Young's modulus of the nanocomposites were obtained. Beyond those contents the mentioned properties decreased due to the excess of stress concentration. Besides, ductility of the nanocomposite films decreased with the increment of P-MMT contents.

- P(MMA-*co*-BA)/P-MMT films were transparent and the absorbance of these nanocomposite films were high in the UV region, especially in UV-A and UV-B.

- P(MMA-*co*-BA)/P-MMT nanocomposites showed better thermal stability and mechanical properties than those of the P(MMA-*co*-BA)/unmodified-MMT composite films, indicating the more compatibility of P(MMA-*co*-BA) copolymers with P-MMT rather than uMMT.

## *5.2 Recommendations*

1. TBPB might be replaced by the other cationic salts, which could give the better and/or various properties of the nanocomposites.

2. The nanocomposite films containing P-MMT should be prepared from other kinds of polymer matrix structure, e.g., linear and/or high-branched structures. This is in order to study the effects on their mechanical properties, especially their elongation.

3. The preparation method of the P(MMA-*co*-BA)/P-MMT nanocomposites should be modified to obtain the exfoliated nanocomposites such as using *in situ* polymerization technique, i.e. mixing organoclay with MMA:BA monomers before polymerization.

# REFERENCES


[1] Alexandre M. and Dubois P. "Polymer-layered Silicate Nanocomposites: Preparation, Properties and Uses of a New Class of Materials." **Mater. Sci. Eng.,** vol.28, 2000. pp. 1-63.

[2] Tyan H.L., Leu C.M., and Wei K.H. "Effect of Reactivity of Organics-Modified Montmorillonite on the Thermal and Mechanical Properties of Montmorillonite/Polyimide Nanocomposites." **Chem. Mater.,** vol.13, no.1, 2001. pp. 222-226.

[3] Rui Z., Yuan H., Jiayan X., Weicheng F., and Zuyao C.. "Flammability and Thermal Stability Studies of Styrene-Butyl Acrylate Copolymer/Graphite Oxide Nanocomposite." **Polym. Deg. Stab,.** vol.85, 2004. pp. 583-588.

[4] Mathias L.J., and Michalovic M., et al. **"Poly(methyl methacrylate)."** [Online]. Available : http://pslc.ws/mactest/pmma.htm. 2004.

[5] Brandrup J., and Immergut E.H. (editors). **Polymer Handbook ; Poly(butyl acrylate).** 3rd ED. New York : John Wiley. 1989. pp. 428-429.

[6] Pinnavaia T.J. and Beall G.W. (editors). **Polymer–clay Nanocomposites.** Wiley series in polymer science. 2000.

[7] LeBron P.C., Wang Z., Pinnaviaia T.J. "Polymer-layered Silicate Nanocomposites : An Overview." **Appl. Clay Sci.,** vol.15, 1999. pp. 11-29.

[8] Bala P., Samantatay B.K., and Srivastava S.K. "Synthesis and Characterization of Na-montmorillonite-alkylammonium Intercalation Compounds." **Mater. Res. Bull.,** vol.35, 2000. pp. 1717-1724.

[9] Pospišil M., Capkova P., Merinska D., Malac Z., and Simonik J. "Structure Analysis of Montmorillonite Intercalated with Cetylpyridinium and Cetyltrimethylammonium: Molecular Simulations and XRD Analysis." **J. Colloid Interf. Sci.,** vol.236, 2001. pp. 127-131.

[10] Meier L.P., Nueesch R., and Madsent F.T. "Organic Pillared Clays." **J. Colloid Interf. Sci.,** vol.238, 2001. pp. 24–32.

[11] Sarmiento D.C.R. and Bello P.J.A. "Adsorption of Sodium Dodecylbenzene Sulfonate on Organophilic Bentonites." **Appl. Clay Sci.,** vol.18, 2001. pp. 173-181.

[12] Hedley C.B., Yuan G., and Theng B.K.G. "Thermal Analysis of Montmorillonites Modified with Quaternary Phosphonium and Ammonium Surfactants." **Appl. Clay Sci.,** vol.35, 2007. pp. 180-188.

[13] Takekoshi T., Khouri F., Campbell J.R., Jordan T.C., and Dai K.H. **"Layered Minerals and Compositions Comprising the Same."** U.S patent no. 5707439, 13 January 1998.

[14] Patel H.A., Somani R.S., Bajaj H.C., and Jasra R.V. "Preparation and Characterization of Phosphonium Montmorillonite with Enhanced Thermal Stability." **Appl. Clay Sci.,** vol.35, 2006. pp. 194-200.

[15] Calderon J.U., Lennox B., and Kamal M.R. "Thermally Stable Phosphonium-Montmorillonite Organoclays." **Appl. Clay Sci.,** vol.40, 2008. pp. 90-98.

[16] J.N. Hay and S.J. Shaw. **"Clay-Based Nanocomposites."** [Online]. Available : http://www.azom.com/details.asp?ArticleID=936. 2001.

[17] Amethyst Galleries, Inc. **"The clay mineral group."** [Online]. Available : http://mineral.galleries.com/minerals/silicate/clays.htm. 1995.

[18] Wikipedia, The Free Encyclopedia. **"Clay."** [Online]. Available : http://en.wikipedia.org/wiki/Clay. 2006.

[19] Wikipedia, The Free Encyclopedia. **"Montmorillonite."** [Online]. Available : http://en.wikipedia.org/wiki/Montmorillonite. 2006.

[20] Wyoming Inc. **"What is Wyoming Bentonite Clay?"** [Online]. Available : http://www.aquatechnologies.com/ info_bentonite_clay.htm. 2006.

[21] Benjamin K. and Galton-Fenzi. **"The clay mineral – Properties."** [Online]. Available : http://www.groundwaterresearch.com.au/reference/Hydrology%20and%20the%20Clay%20Minerals/Properties.htm. 2003.

[22] Wikipedia, The Free Encyclopedia. **"Organophosphorus."** [Online]. Available : http://en.wikipedia.org/wiki/Organophosphorus. 2006.

[23] Patel H.A., Somani R.S., Bajaj H.C., and Jasra R.V. "Preparation and Characterization of Phosphonium Montmorillonite with Enhanced Thermal Stability." **Appl. Clay Sci.,** vol.35, 2006. pp. 194-200.

[24] Kosolapoff G.M. and Maier L. **"Organic Phosphorus Compounds."** New York : John Wiley & Sons. 1972. p. 2.

[25] Sigma-Aldrich, Inc. **"Tetrabutylphosphonium bromide."** [Online]. Available : http://www.sigmaaldrich.com. 2006.

[26] Wei X., Rongcai X., Wei-Ping P., Doug H., Bryan K., Loon-Seng T., Richard V. "Thermal Stability of Quaternary Phosphonium Modified Montmorillonites." **Chem. Mater.,** vol.14 2002. pp. 4837–4845.

[27] Lee Y., Kim M.J., and Lee Y.B. "Preparation and Characterization of Epoxy/Clay Nanocomposites." **Solid State Phenom.,** vol.119, 2007. pp. 243-246.

[28] Hua R., Jianzhong S., Binjie W., and Qiyun Z. "Synthesis and Properties of a Phosphorous-containing Flame Retardant Epoxy Resin Based on Bis-phenoxy (3-hydroxy) Phenyl Phosphine Oxide." **Polym. Deg. Stab.,** vol.6, 2007. pp. 956-961.

[29] Wikipedia, The Free Encyclopedia. **"Composite material."** [Online]. Available : http://en.wikipedia.org/wiki/Composite_material. 2006.

[30] Quinzi M. and Francesco G.D. **"Clay/Polymer Nanocomposites: Brief Outline."** [Online]. Available : http://www.nanocompositech.com/review-nanocomposite.htm. 2006.

[31] Utracti L.A. "Clay-containing Polymeric Nanocomposites." **Rapra. Technol.,** vol.1, 2004. p. 8.

[32] Usuki A., Kawasumi M., Kojima Y., Okada A., Kurauchi T., and Kamigaito O. "Swelling Behavior of Montmorillonite Cation Exchanged for ω-amino Acids by ε-caprolactam." **Mater. Res.,** vol.8, no.5, 1993. p. 1174-1178.

[33] Usuki A., Kojima Y., Kawasumi M., Okada A., Fukushima Y., Kurauchi T., and Kamigaito O. "Synthesis of Nylon 6-Clay Hybrid." **J. Mater. Res.,** vol.8, 1993. pp. 1179-1184.

[34] Kojima Y., Usuki A., Kawasumi M., Okada A., Fukushima Y., Kurauchi T., and Kamigaito O. "Mechanical Properties of Nylon 6-Clay Hybrid." **J. Mater. Res.,** vol.8, 1993. pp. 1185-1189.

[35] Joseph H.K. **"Polymer Nanocomposite: Processing, Characterization, and Applications."** New York : McGraw-Hill. 2006. pp. 64-69.

[36] Yamaguchi T., and Yamada E. "Preparation and Properties of Clay/SEBS Intercalated Composites" **e-Journal of Soft Mater.,** vol.2, 2006. pp. 1–6.

[37] Marras S.I., Tsimpliaraki A., Zuburtikudis I., and Panayiotou C. "Surfactant-induced Morphology and Thermal Behavior of Polymer Layered Silicate Nanocomposites." **J. Phys: Conf. Ser.,** vol.61, 2007. pp. 1366–1370.

[38] Moore C.M., Hackman S., Brennan T., and Minteer S.D. **"Effect of Mixture Casting Phosphonium Salts with Nafion® on the Proton Exchange Capacity and Mass Transport Through the Membranes."** J. Membr. Sci., vol.254, no.1-2, 2005. pp. 63-70.

[39] Tsung-Yen T., Mei-Ju L., Ching-Wen C., and Chen-Chi L. "Morphology and Properties of Poly(Methyl Methacrylate)/Clay Nanocomposites by in-situ Solution Polymerization." **J. Phys. Chem. Solid.,** vol.71, 2010. pp. 590-594.

[40] Ray-Yi L., Bang-Shuo C., Guan-Liang C., Jeng-Yue W., Hsin-Cheng C., and Shing-Yi S. "Preparation of Porous PMMA/$Na^+$-montmorillonite Cation-exchange Membranes for Cation Dye Adsorption." **J. Membr. Sci.,** vol.326, 2009. pp. 117-129.

[41] Kung-Chin C., Shih-Ting C., Hui-Fen L., Chang-Yu L., Hsin-Hua H., Jui-Ming Y., and Yuan-Hsiang Y. "Effect of Clay on the Corrosion Protection Efficiency of PMMA/$Na^+$-MMT Clay Nanocomposite Coatings Evaluated by Electrochemical Measurements." **Euro. Polym. J.,** vol.44, 2008. pp. 13-23.

[42] Prafulla K.S., Ramakanta S., Sarat K.S., and Pradeep K.R. "Synthesis of Poly(butyl acrylate)/Sodium Silicate Nanocomposite Fire Retardant." **Euro. Polym. J.,** vol.44, 2008. pp. 3522-3528.

[43] Hanying Z., Brendan P.F., and Devon A.S. "Nanopatterns of Poly(styrene-block-butyl acrylate) Block Copolymer Brushes on the Surfaces of Exfoliated and Intercalated Clay Layers." **Polym.,** vol.45, 2004. pp. 4473-4481.

[44] Inigo G., Jose M.A., and Jose R.L. "The Role of Methyl Methacrylate on Branching and Gel Formation in the Emulsion Copolymerization of BA/MMA." **Polym.,** vol.48, 2007. pp. 2542-2547.

[45] Gabriela D., Maria P., and Jose R.L. "Towards the Synthesis of High Solids Content Waterborne Poly(Methyl Methacrylate-*co*-Butyl Acrylate)/Montmorillonite Nanocomposites." **Polym.,** vol.76, 2007. pp. 1746-1750.

[46] Young R.J., and Lovell P.A. **Introduction to Polymers ; Synthesis ; Chain copolymerization**. 2nd ED. London : Chapman & Hall. 1996.

[47] Leskovac M., Kovacevic V., Fles D., and Hace D. "Thermal Stability of Poly(Methyl Methacrylate-*co*-Butyl Acrylate) and Poly(Styrene-*co*-Butyl Acrylate) Polymers." **Polym. Eng. Sci.,** vol.39, no.3, 1999. pp. 600-608.

[48] Kashiwagi T., Inaba A., Brown J.E., Hatada K., Kitayama T., and Masuda E. "Effects of Weak Linkages on the Thermal and Oxidative Degradation of Poly(Methyl Methacrylates)." **Macromolecules.,** vol.19, no.8, 1986. pp. 2160-2168.

[49] Kashiwagi T. "Thermal and Oxidative Degradation of Polymers." **A Century of Excellence in Measurements, Standards, and Technology: A Chronicle of Selected NBS/NIST Publications, 1901-2000.,** vol.958, 2001. pp. 344-346. [Online]. Available : http://nistdigitalarchives.contentdm.oclc.org/cdm/compoundobject/collection/p15421coll5/id/1709/rec/18

# Appendices

# Appendix A

## XRD patterns of Na-MMT, S-MMT and P-MMT

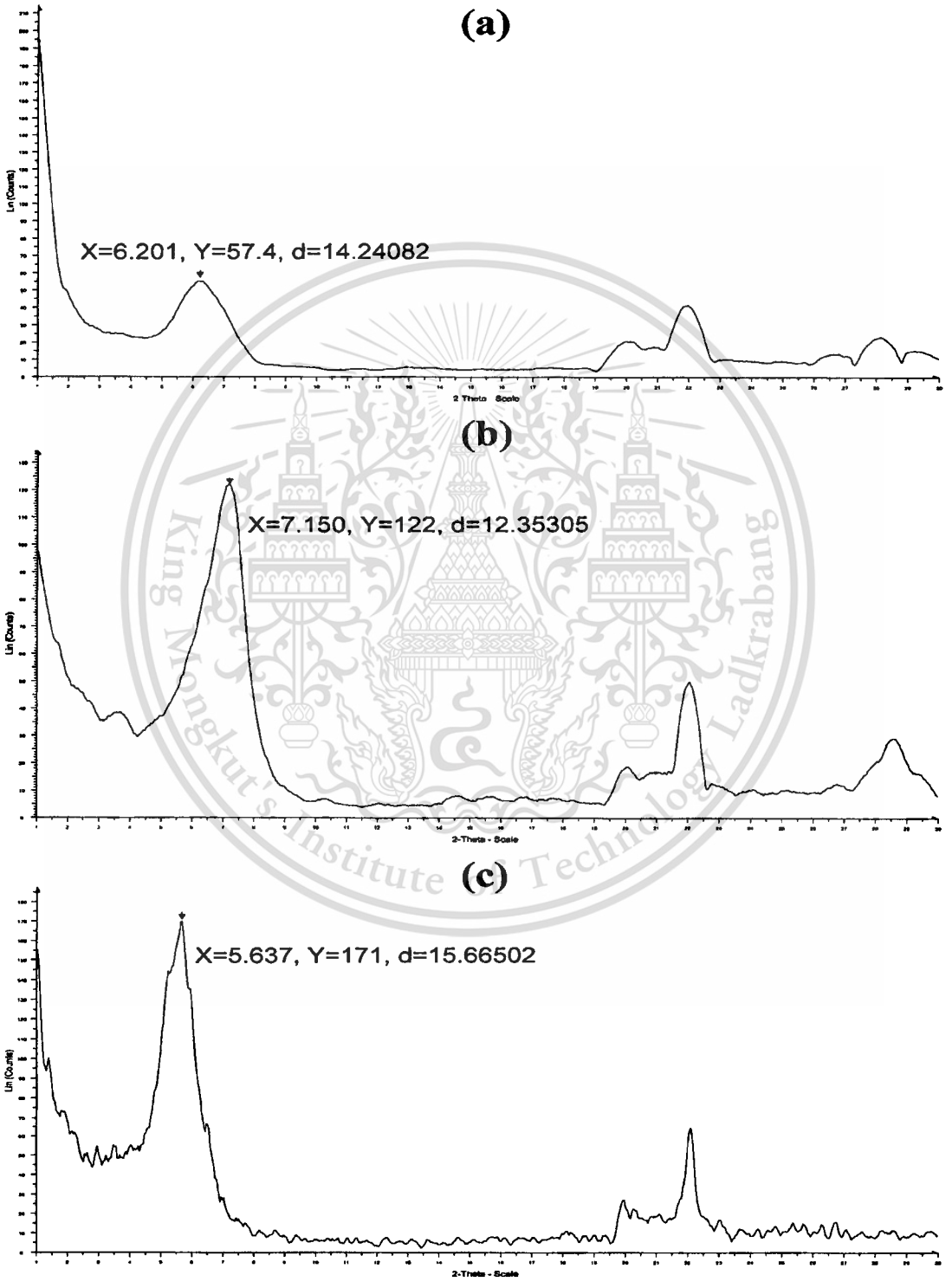


**Fig. A-1** XRD patterns of (a) Na-MMT, (b) S-MMT, and (c) P-MMT

# Appendix B

## Compositions of MMTs and P(MMA-*co*-BA)/P-MMT nanocomposites

**Table B-1** Composition of MMTs

| Samples | Composition (%Atom) | | | | | | | | |
|---|---|---|---|---|---|---|---|---|---|
| | Al | Si | P | Na | Mg | Ca | K | Fe | O |
| Na-MMT | 7.7 | 31.6 | - | 7.3 | 1.9 | 0.4 | 0.5 | 1.1 | 49.5 |
| S-MMT | 7.2 | 32.8 | - | 5.7 | 1.9 | 0.5 | - | 1.2 | 50.7 |
| P-MMT | 8.2 | 33.7 | 1.6 | - | 2.4 | 0.5 | 0.5 | 1.3 | 51.8 |

**Table B-2** Composition of nanocomposite films of M6B4 copolymer formula

| Samples | Composition (%Atom) | | | | | | | | |
|---|---|---|---|---|---|---|---|---|---|
| | Al | Si | P | Na | Mg | Ca | K | Fe | O |
| P(MMA-*co*-BA)/1%P-MMT | 4.2 | 30.6 | 2.6 | - | 1.5 | 1.1 | 1.3 | 2.7 | 56.0 |
| P(MMA-*co*-BA)/2%P-MMT | 4.8 | 34.2 | 2.9 | - | 2.4 | 1.2 | - | 1.2 | 53.3 |
| P(MMA-*co*-BA)/3%P-MMT | 5.3 | 33.9 | 3.2 | - | - | 1.2 | 1.2 | 1.3 | 53.9 |
| P(MMA-*co*-BA)/6%P-MMT | 5.6 | 33.7 | 2.9 | - | 1.8 | 1.2 | 1.2 | 1.1 | 52.5 |

**Table B-3** Composition of nanocomposite films of M7B3 copolymer formula

| Samples | Composition (%Atom) | | | | | | | | |
|---|---|---|---|---|---|---|---|---|---|
| | Al | Si | P | Na | Mg | Ca | K | Fe | O |
| P(MMA-*co*-BA)/1%P-MMT | 5.0 | 30.1 | 3.1 | - | 2.3 | 0.1 | 1.2 | 2.3 | 55.9 |
| P(MMA-*co*-BA)/2%P-MMT | 5.0 | 32.3 | 3.4 | - | 1.2 | - | 1.3 | 1.7 | 55.1 |
| P(MMA-*co*-BA)/3%P-MMT | 5.1 | 33.9 | 3.2 | - | - | 1.3 | 1.3 | 1.4 | 53.8 |
| P(MMA-*co*-BA)/6%P-MMT | 5.7 | 33.2 | 3.3 | - | 1.5 | 1.1 | 1.1 | 1.1 | 53.0 |

**Table B-4** Composition of nanocomposite films of M8B2 copolymer formula

| Samples | Composition (%Atom) | | | | | | | | |
|---|---|---|---|---|---|---|---|---|---|
| | Al | Si | P | Na | Mg | Ca | K | Fe | O |
| P(MMA-*co*-BA)/1%P-MMT | 4.3 | 27.4 | 2.7 | - | 2.3 | 1.2 | 1.2 | 2.5 | 58.4 |
| P(MMA-*co*-BA)/2%P-MMT | 4.5 | 28.8 | 2.8 | - | 2.2 | 1.3 | 1.5 | 2.3 | 56.6 |
| P(MMA-*co*-BA)/3%P-MMT | 5.2 | 34.4 | 3.1 | - | 1.3 | 1.4 | 1.2 | 1.6 | 51.8 |
| P(MMA-*co*-BA)/6%P-MMT | 5.4 | 33.4 | 3.0 | 2.4 | 1.4 | 1.2 | 1.3 | 1.2 | 50.7 |

**Table B-5** Composition of nanocomposite films of M9B1 copolymer formula

| Samples | Composition (%Atom) | | | | | | | | |
|---|---|---|---|---|---|---|---|---|---|
| | Al | Si | P | Na | Mg | Ca | K | Fe | O |
| P(MMA-*co*-BA)/1%P-MMT | 4.8 | 30.6 | 2.7 | 3.5 | 2.3 | 0.99 | 1.4 | 2.2 | 51.51 |
| P(MMA-*co*-BA)/2%P-MMT | 5.2 | 34.0 | 3.2 | - | 1.9 | 1.3 | - | 1.6 | 52.80 |
| P(MMA-*co*-BA)/3%P-MMT | 5.04 | 32.2 | 2.8 | 2.3 | 2.2 | 1.2 | 1.4 | 1.5 | 51.36 |
| P(MMA-*co*-BA)/6%P-MMT | 5.5 | 34.1 | 3.1 | 0.98 | 1.3 | 1.2 | 1.3 | 1.2 | 51.32 |

# Appendix C

## TGA thermograms of Na-MMT, TBPB, and P-MMT tested under oxygen atmosphere and Calculation of percentage of TBPB in P-MMT

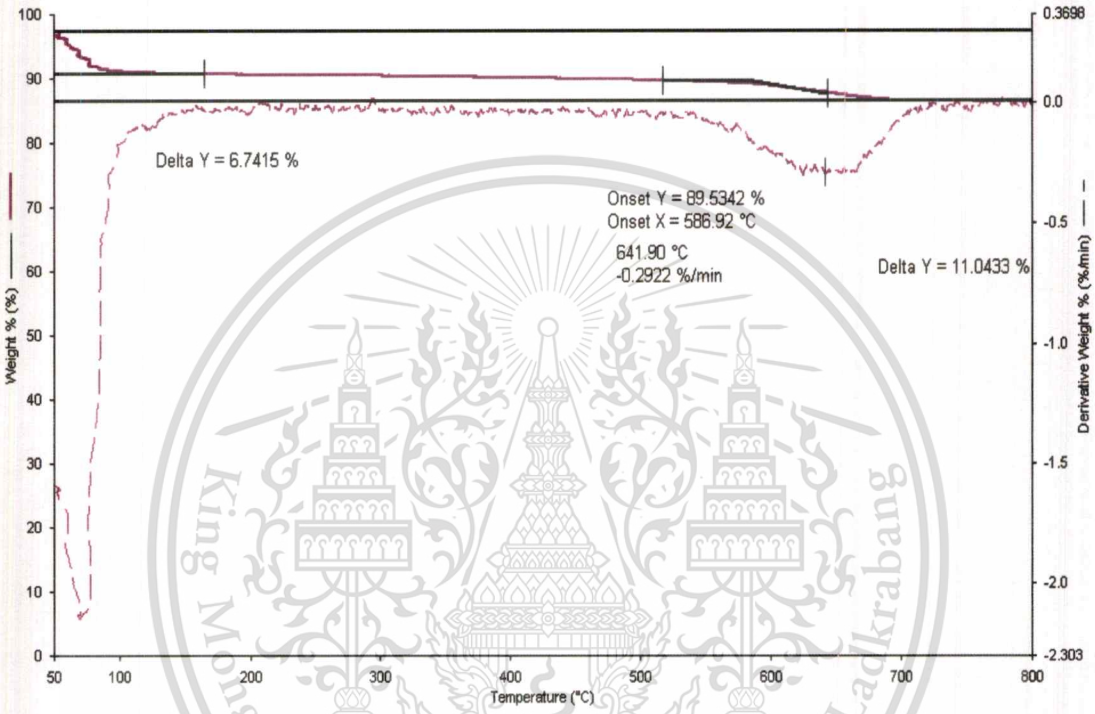


**Fig. C-1** TGA thermogram of Na-MMT

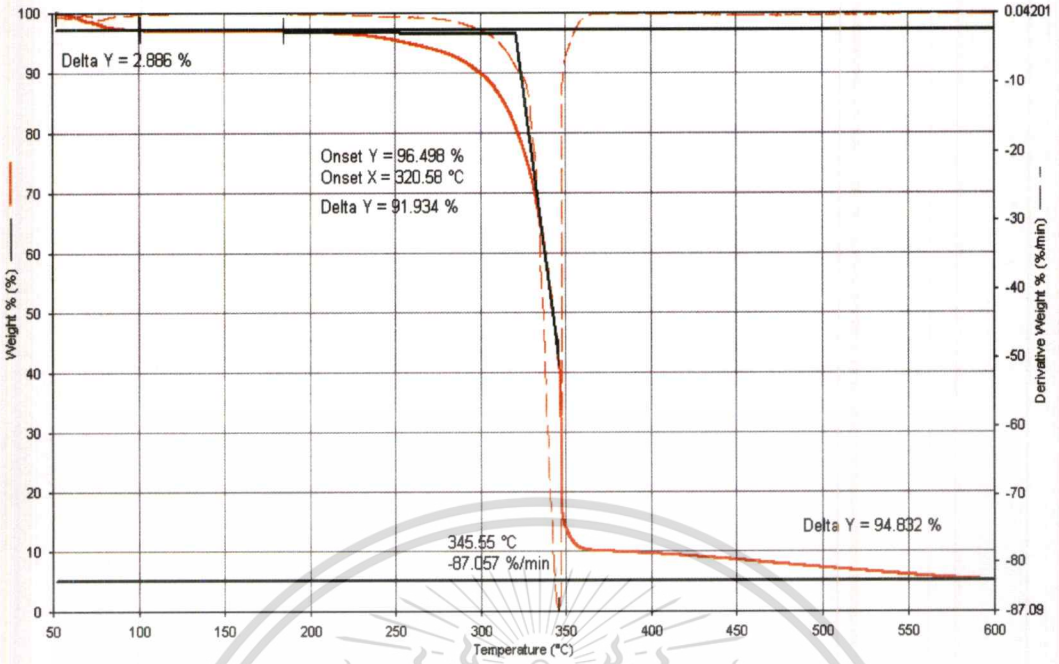


**Fig. C-2** TGA thermogram of tetrabutylphosphonium bromine (TBPB)

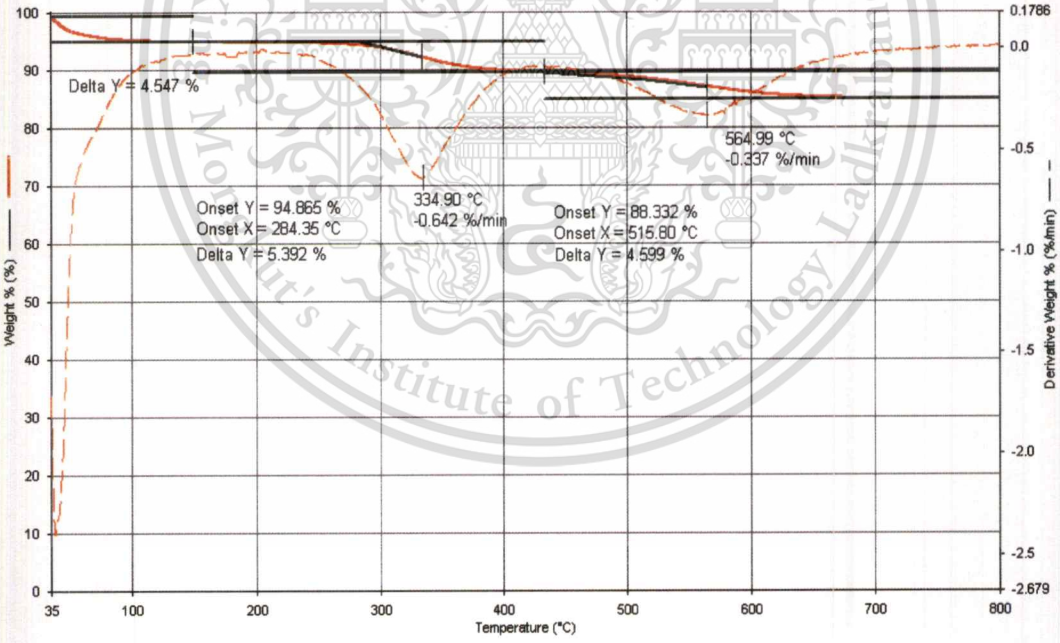


**Fig. C-3** TGA thermogram of P-MMT

## Calculation of percentage of TBPB addition into P-MMT

According to Fig. C-2 and C-3;

- ⇨ TBPB possesses 91.9 wt% of hydrocarbon parts (HC).
- ⇨ While, the P-MMT give out 5.4 wt% of HC which belong to the intercalated TBPB within the P-MMT.

Therefore, the calculation should be as following;

91.9 g of HC come from 100 g of TBPB

So, 5.4 g of HC should come from $\frac{5.4 \ x \ 100}{91.9} = 5.876$ g of TBPB

$\therefore$ 100 g of P-MMT come from 5.876 g of TBPB

But from chapter 3;

2.0 g of MMT was modified by 2.44 g of TBPB, so, total weight of P- MMT would be 4.44 g. However, the weight of P-MMT should decrease to be 3.86 g due to the dissociation of bromide during modification.

From this point, it can find that;

100 g of P-MMT will come from 5.876 g of TBPB

3.86 g of P-MMT will use TBPB as $\frac{3.86 \ x \ 5.876}{100} = 0.227 \ g$

Hence, % addition of TBPB = $\frac{0.227}{2.44} x \ 100 = 9.29$ wt% ***Ans.***

# Appendix D

## Molecular weight analysis of PMMA and P(MMA-*co*-BA) copolymers

| ID | PMMA | Flow | 1.0000 |
|---|---|---|---|
| Method | Conventional | Inj Vol | 100.0 |
| Acq. | Nov 25, 2010 - 10:30:06 | Col | 35.00 |
| Solvent | THF | Det | 35.00 |

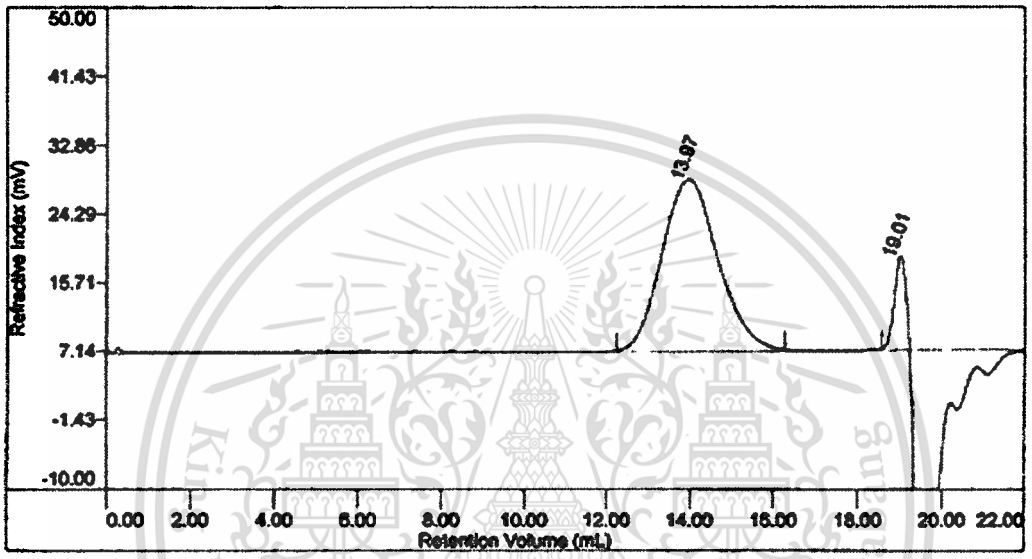


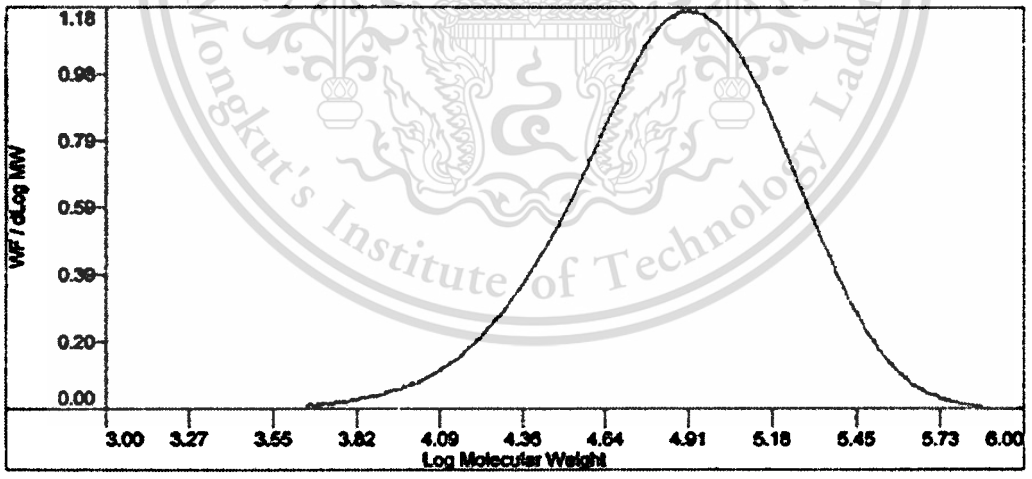


| Sample | Mn | Mw | Mz | Mw/Mn |
|---|---|---|---|---|
| 25-11-2010_10;30;06_PMMA_01.vdt | 53,087 | 100,094 | 165,414 | 1.885 |

**Fig. D-1** Chromatogram of PMMA

| ID | PMMA_BA_9_1 | Flow | 1.0000 |
|---|---|---|---|
| Method | Conventional | Inj Vol | 100.0 |
| Acq. | Nov 25, 2010 - 12:08:17 | Col | 35.00 |
| Solvent | THF | Det | 35.00 |

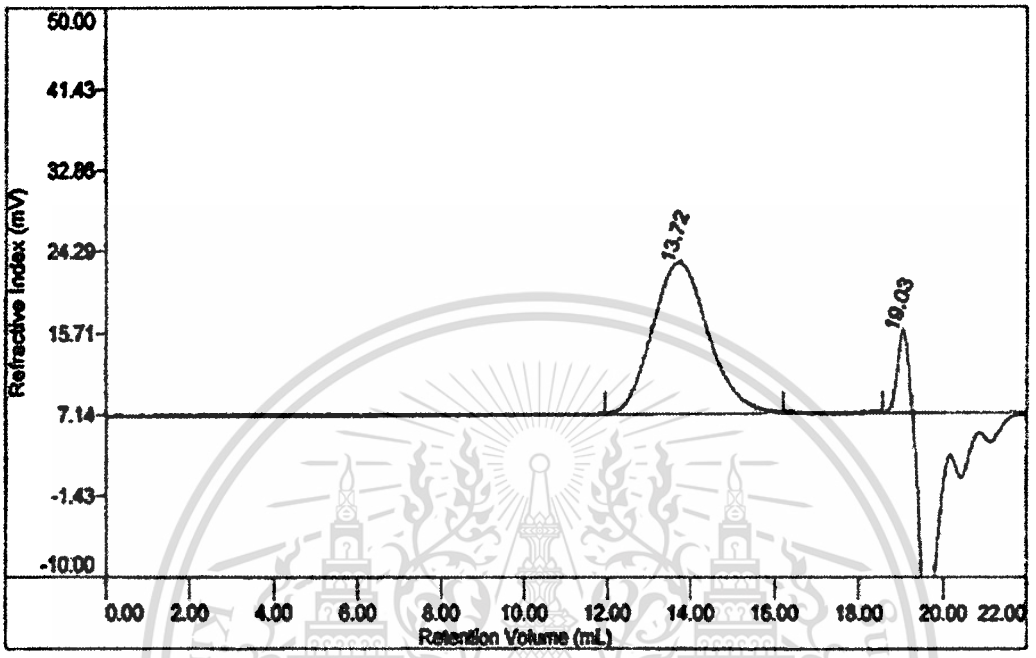


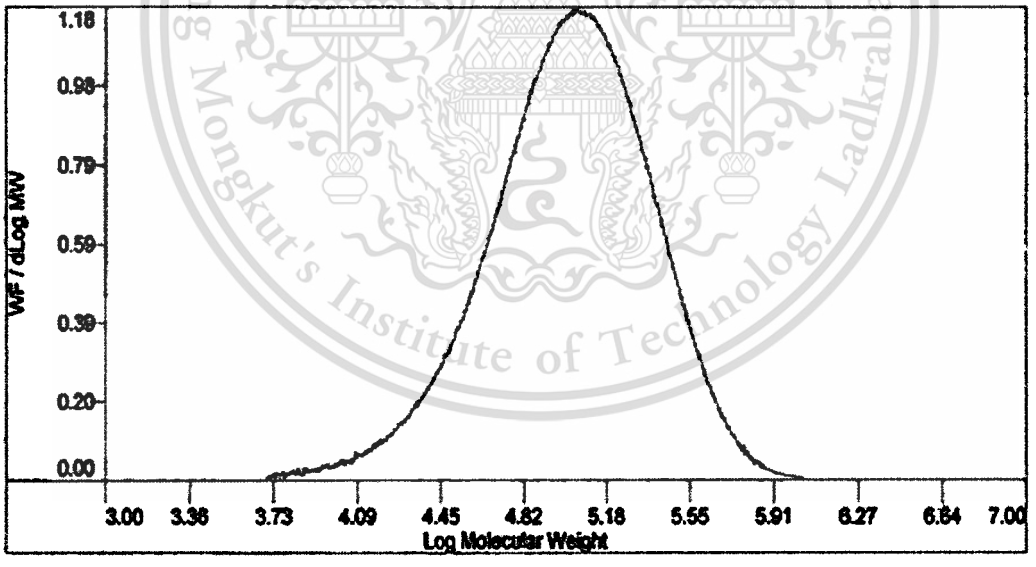


| Sample | Mn | Mw | Mz | Mw/Mn |
|---|---|---|---|---|
| 25-11-2010_12;08;17_PMMA_BA_9_1_01.vdt | 72,333 | 139,557 | 230,830 | 1.929 |

**Fig. D-2** Chromatogram of P(MMA-*co*-BA) for M9B1 formula

| | | | |
|---|---|---|---|
| ID | PMMA_BA_8_2 | Flow | 1.0000 |
| Method | Conventional | Inj Vol | 100.0 |
| Acq. | Nov 25, 2010 - 11:43:45 | Col | 35.00 |
| Solvent | THF | Det | 35.00 |

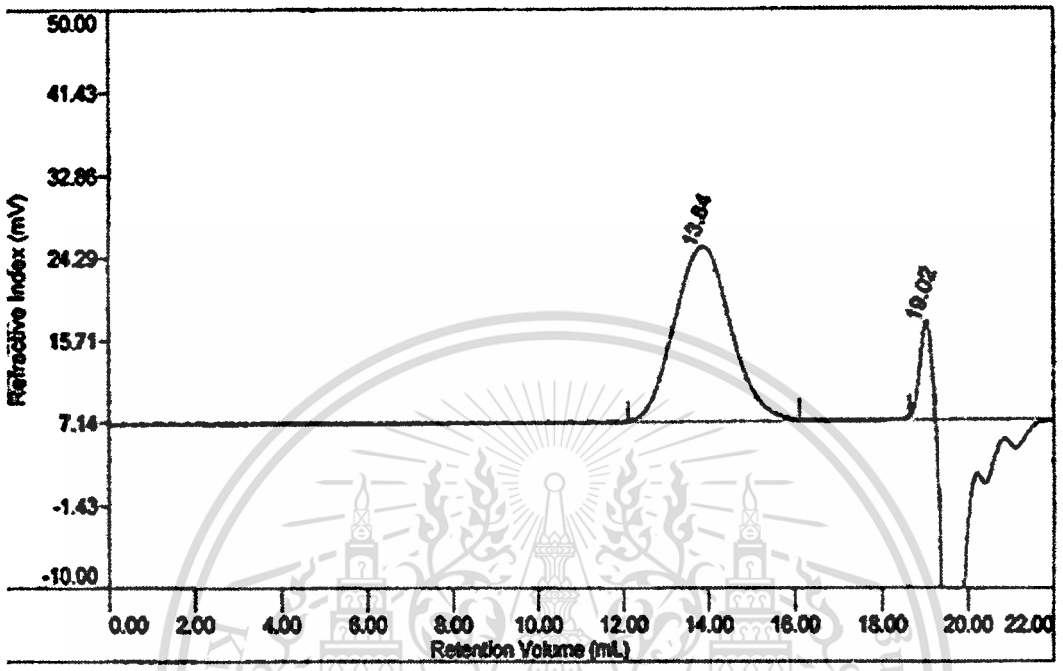


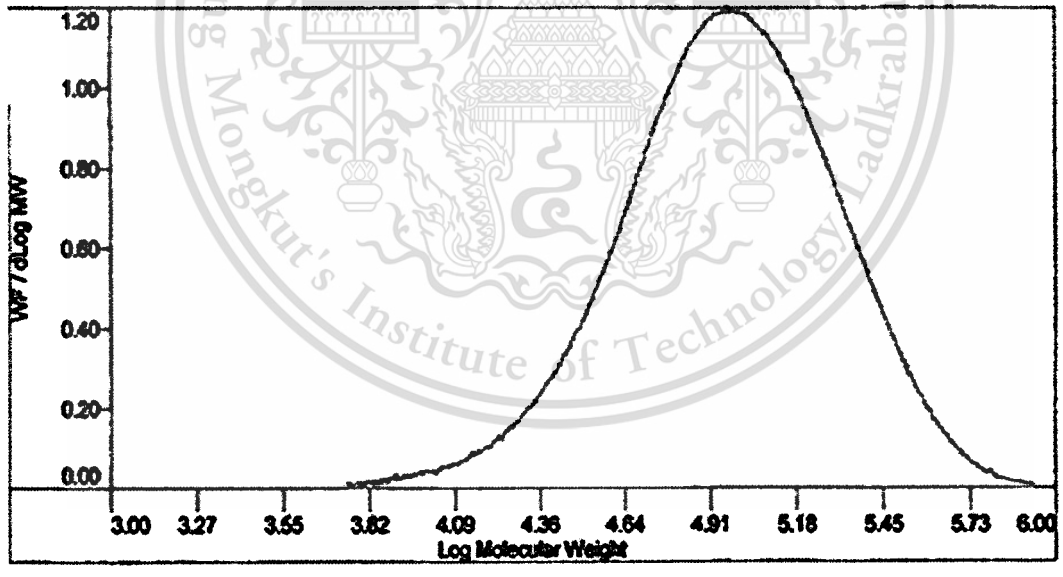


| Sample | Mn | Mw | Mz | Mw/Mn |
|---|---|---|---|---|
| 25-11-2010_11;43;45_PMMA_BA_8_2_01.vdt | 66,485 | 121,332 | 198,116 | 1.825 |

**Fig. D-3** Chromatogram of P(MMA-*co*-BA) for M8B2 formula

| ID | PMMA_BA_7_3 | Flow | 1.0000 |
|---|---|---|---|
| Method | Conventional | Inj Vol | 100.0 |
| Acq. | Nov 25, 2010 - 11:19:12 | Col | 35.00 |
| Solvent | THF | Det | 35.00 |

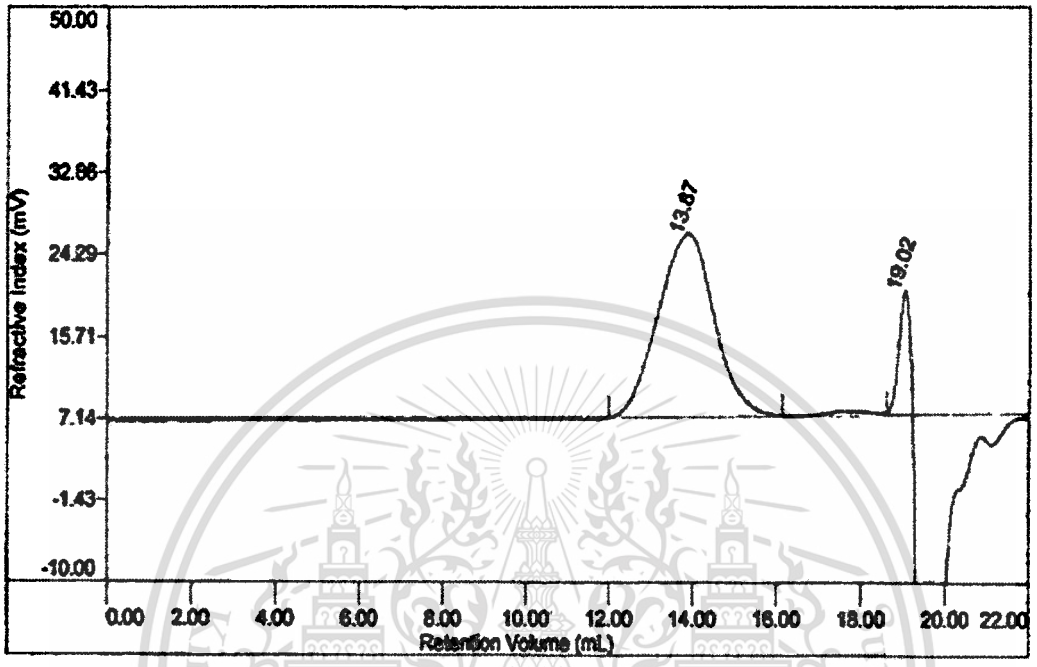


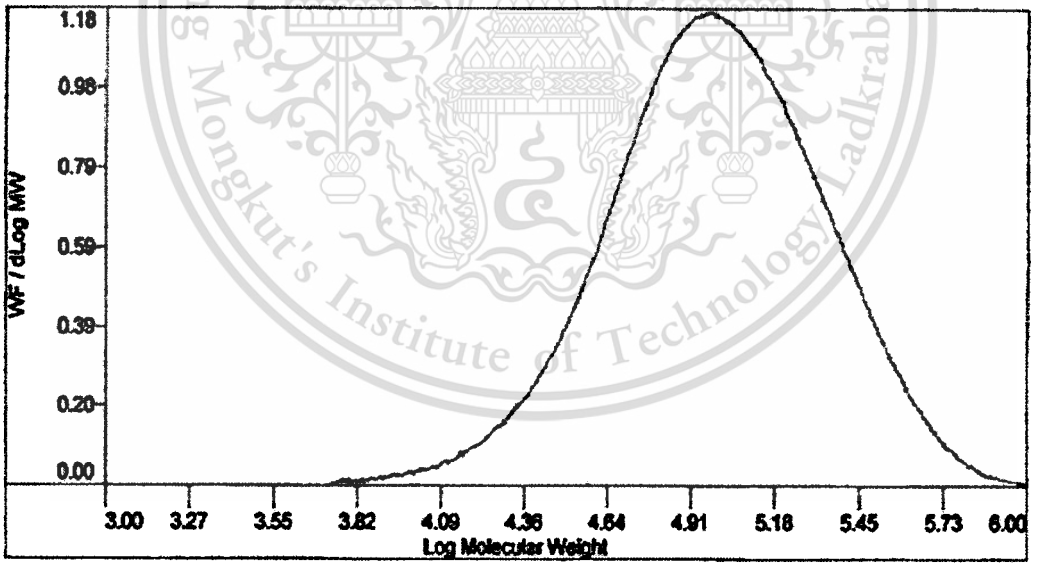


| Sample | Mn | Mw | Mz | Mw/Mn |
|---|---|---|---|---|
| 25-11-2010_11:19:12_PMMA_BA_7_3_01.vdt | 69,950 | 130,103 | 220,710 | 1.860 |

**Fig. D-4** Chromatogram of P(MMA-*co*-BA) for M7B3 formula

| ID | PMMA_BA_6_4 | Flow | 1.0000 |
|---|---|---|---|
| Method | Conventional | Inj Vol | 100.0 |
| Acq. | Nov 25, 2010 - 10:54:39 | Col | 35.00 |
| Solvent | THF | Det | 35.00 |

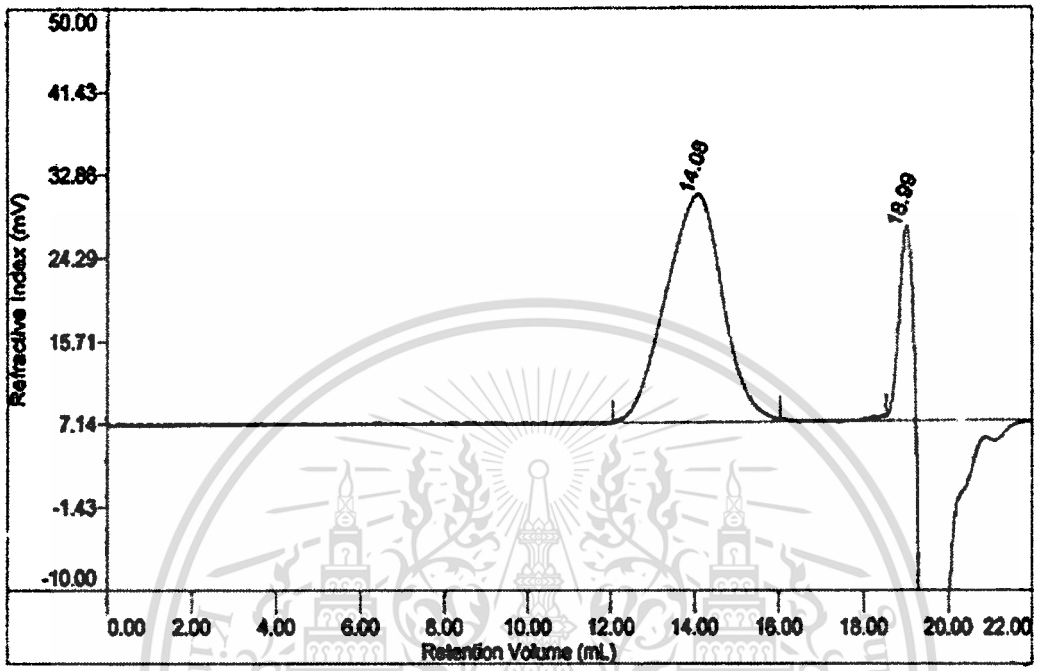


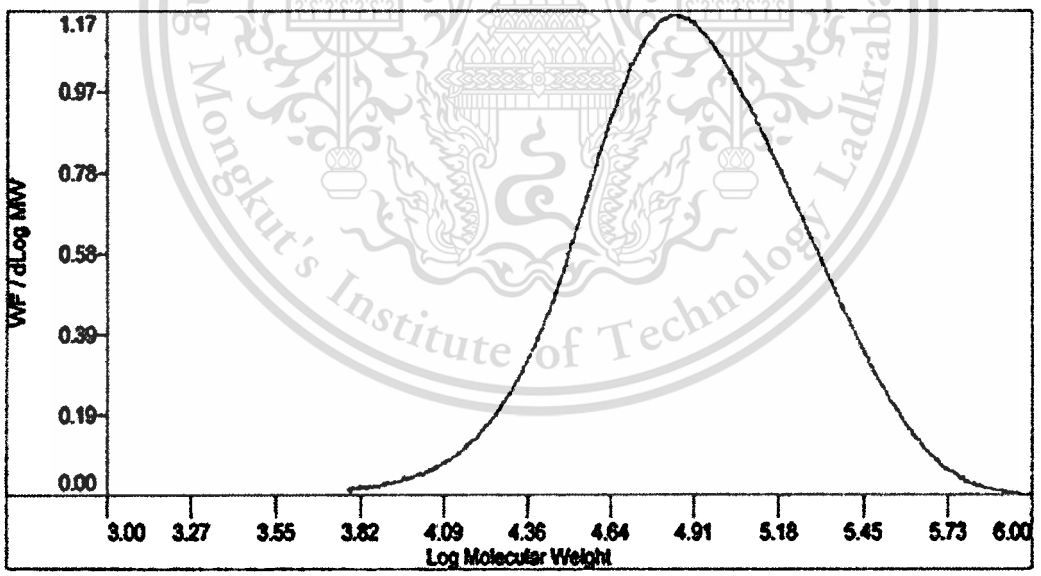


| Sample | Mn | Mw | Mz | Mw/Mn |
|---|---|---|---|---|
| 25-11-2010_10;54;39_PMMA_BA_6_4_01.vdt | 57,705 | 108,064 | 190,680 | 1.873 |

**Fig. D-5** Chromatogram of P(MMA-*co*-BA) for M6B4 formula

# Appendix E

## XRD patterns of PMMA, PBA, P(MMA-*co*-BA), and P(MMA-*co*-BA)/P-MMT nanocomposite films

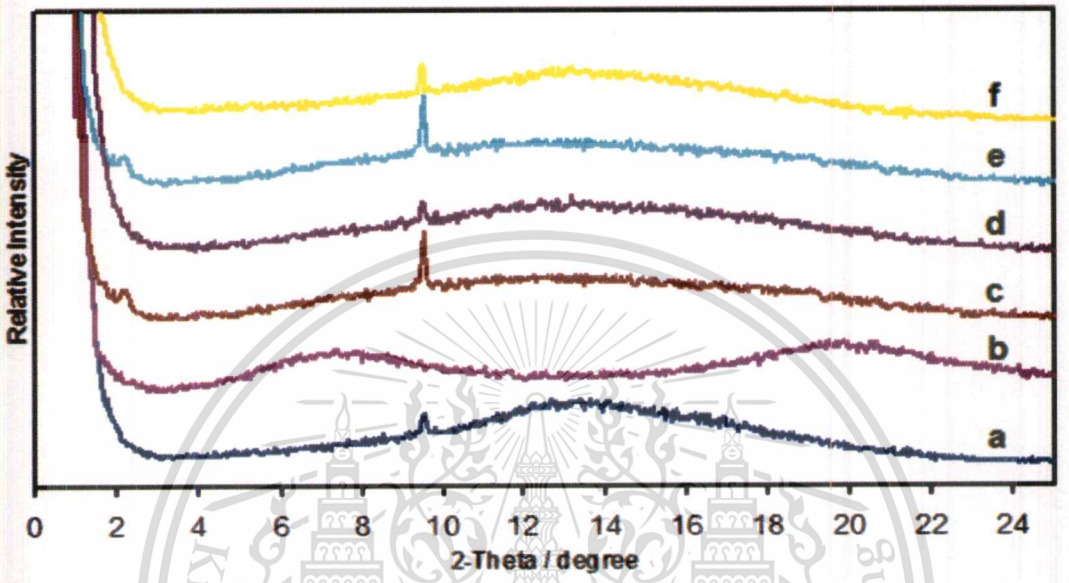


**Fig. E-1** XRD spectra of PMMA, PBA, and different formulas of P(MMA-*co*-BA); (a) PMMA, (b) PBA, (c) M9B1, (d) M8B2, (e) M7B3, and (f) M6B4

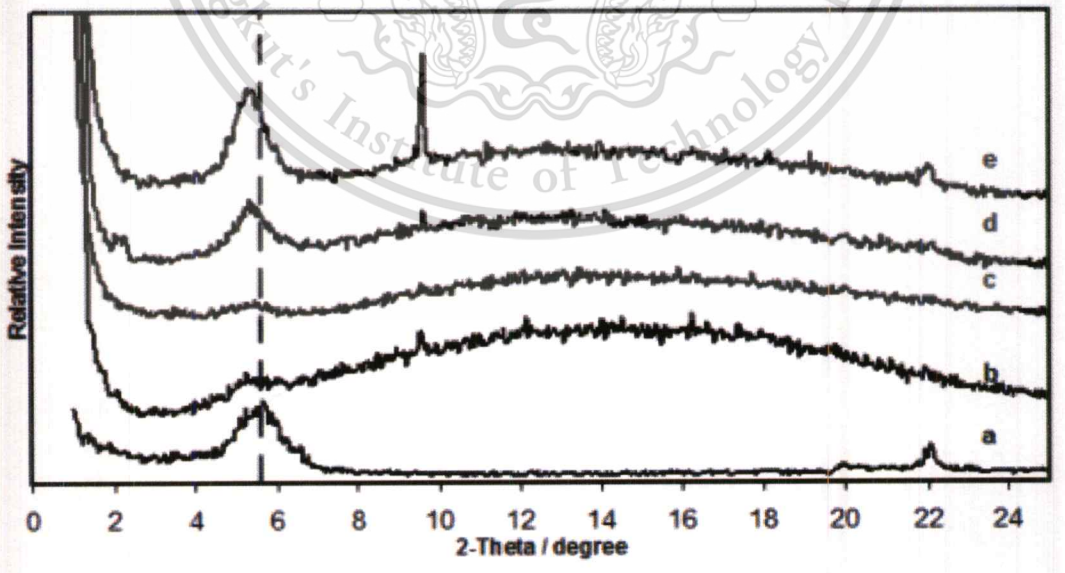


**Fig. E-2** XRD spectra of P(MMA-*co*-BA)/P-MMT nanocomposite films for M6B4 formula with varying P-MMT contents of the films; (a) lean P-MMT, (b) 1% P-MMT, (c) 2% P-MMT, (d) 3% P-MMT, and (e) 6% P-MMT

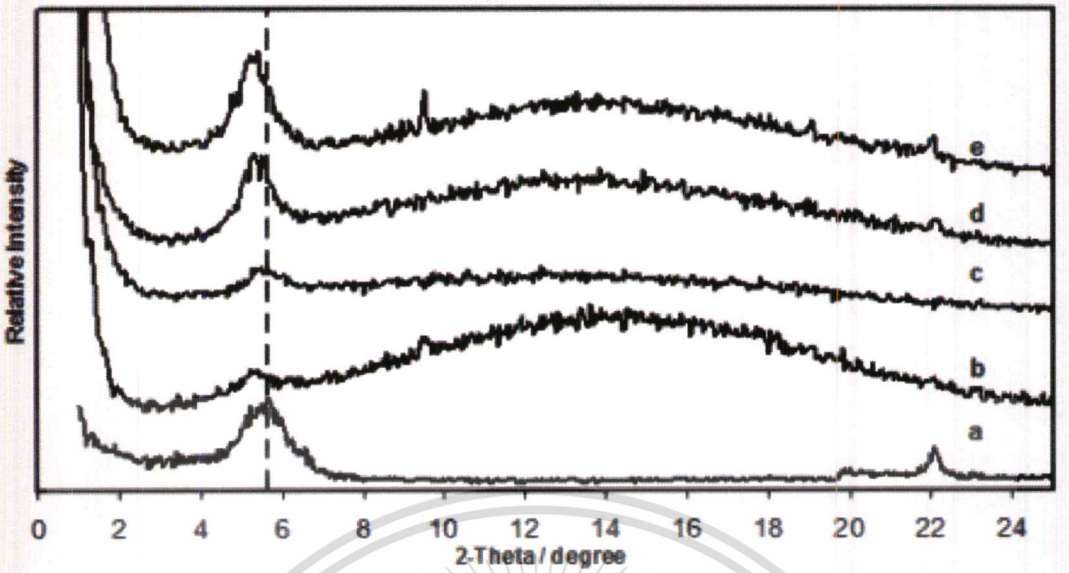


**Fig. E-3** XRD spectra of P(MMA-*co*-BA)/P-MMT nanocomposite films for M7B3 formula with varying P-MMT contents of the films; (a) lean P-MMT, (b) 1% P-MMT, (c) 2% P-MMT, (d) 3% P-MMT, and (e) 6% P-MMT

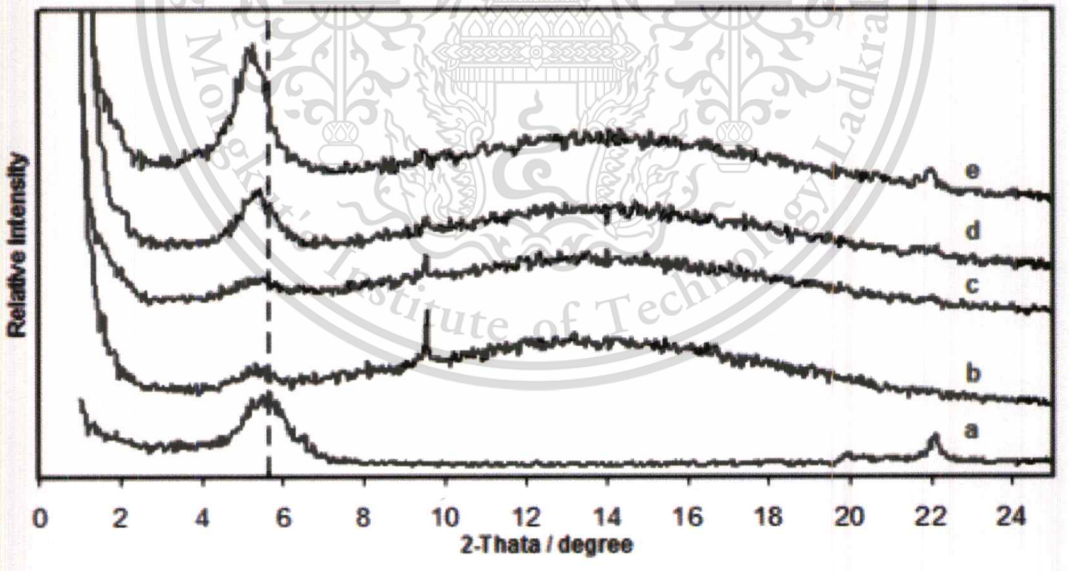


**Fig. E-4** XRD spectra of P(MMA-*co*-BA)/P-MMT nanocomposite films for M8B2 formula with varying P-MMT contents of the films; (a) lean P-MMT, (b) 1% P-MMT, (c) 2% P-MMT, (d) 3% P-MMT, and (e) 6% P-MMT

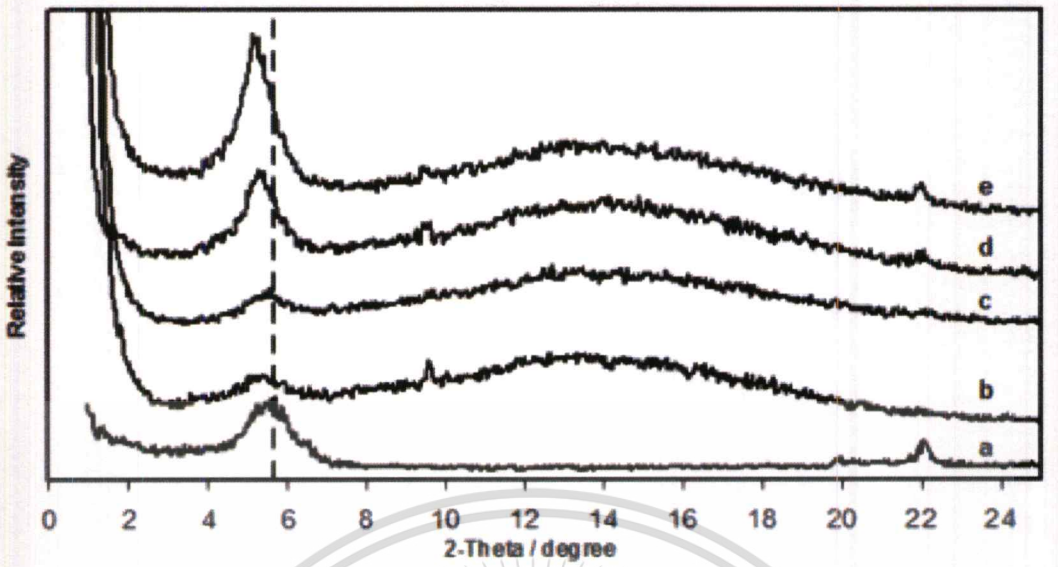


**Fig. E-5** XRD spectra of P(MMA-*co*-BA)/P-MMT nanocomposite films for M9B1 formula with varying P-MMT contents of the films; (a) lean P-MMT, (b) 1% P-MMT, (c) 2% P-MMT, (d) 3% P-MMT, and (e) 6% P-MMT

# Appendix F

## TGA thermograms of PMMA, P(MMA-*co*-BA), and P(MMA-*co*-BA)/ P-MMT nanocomposites tested under nitrogen atmosphere

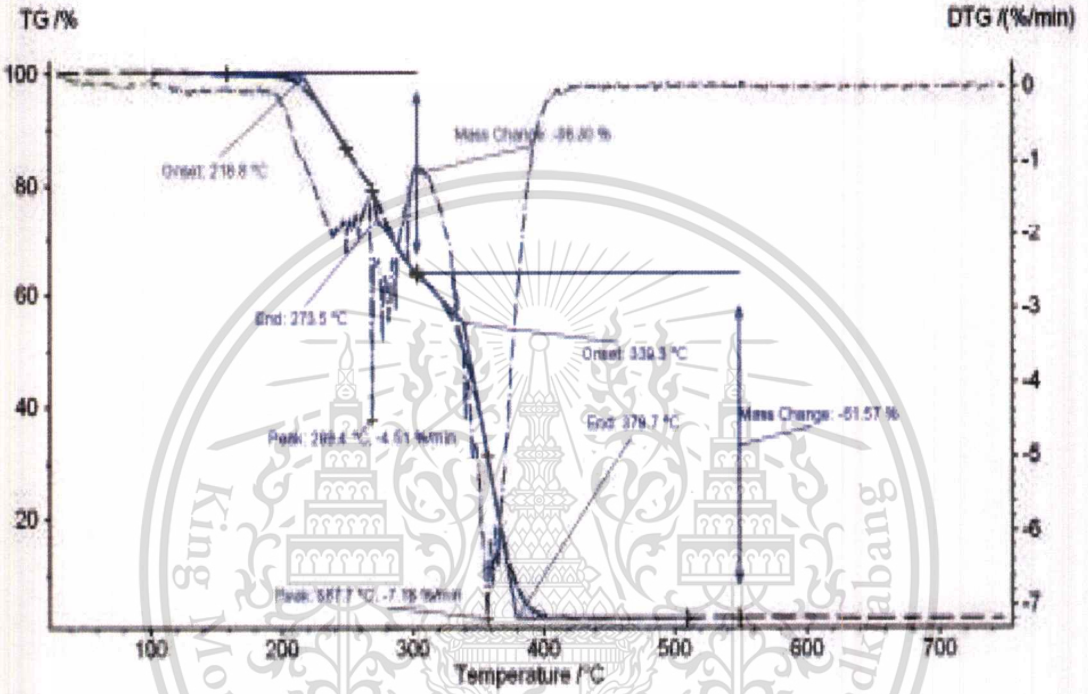


**Fig. F-1** TGA thermogram of PMMA

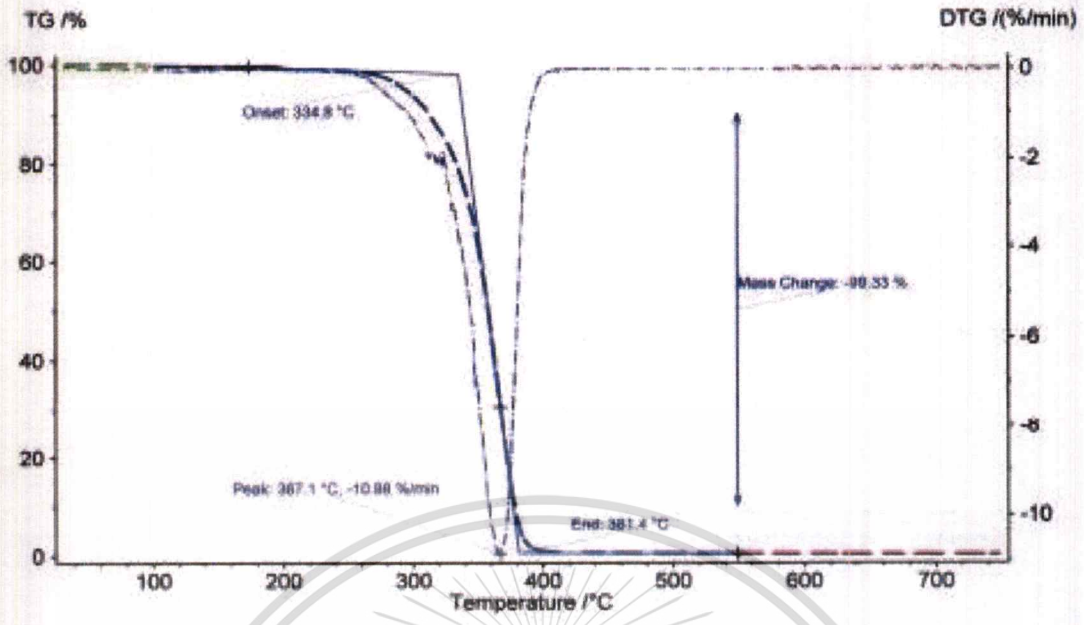


**Fig. F-2** TGA thermogram of M6B4 copolymer

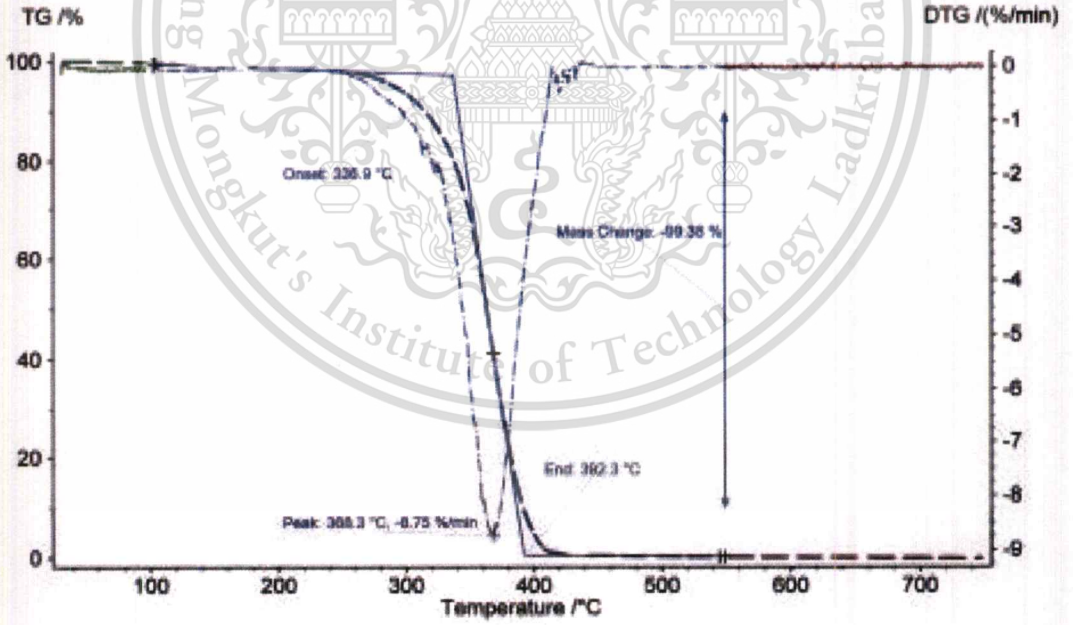


**Fig. F-3** TGA thermogram of M6B4-P1 nanocomposite film

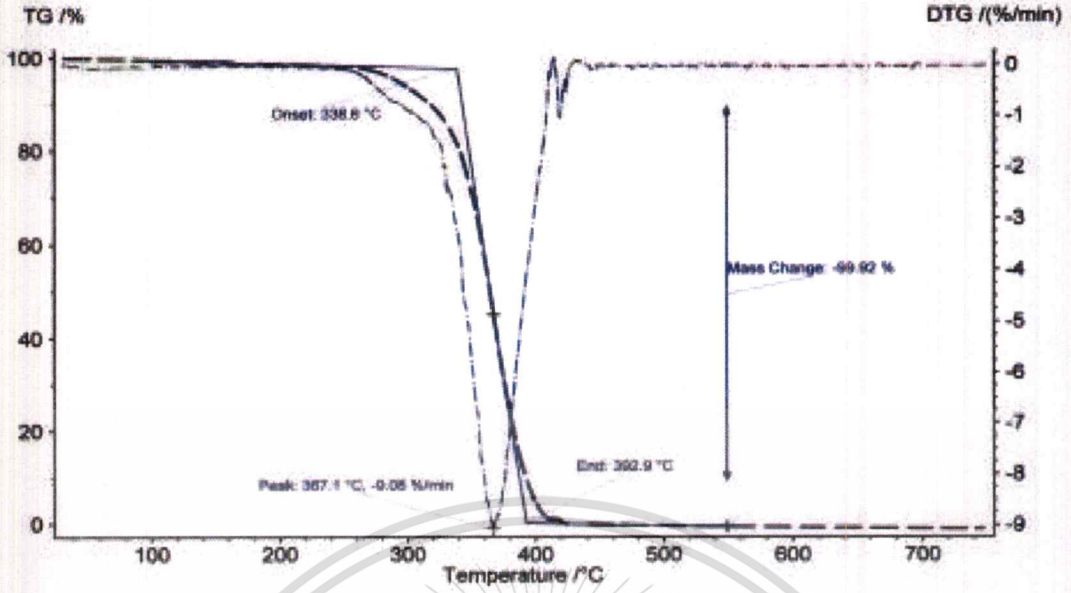


**Fig. F-4** TGA thermogram of M6B4-P2 nanocomposite film

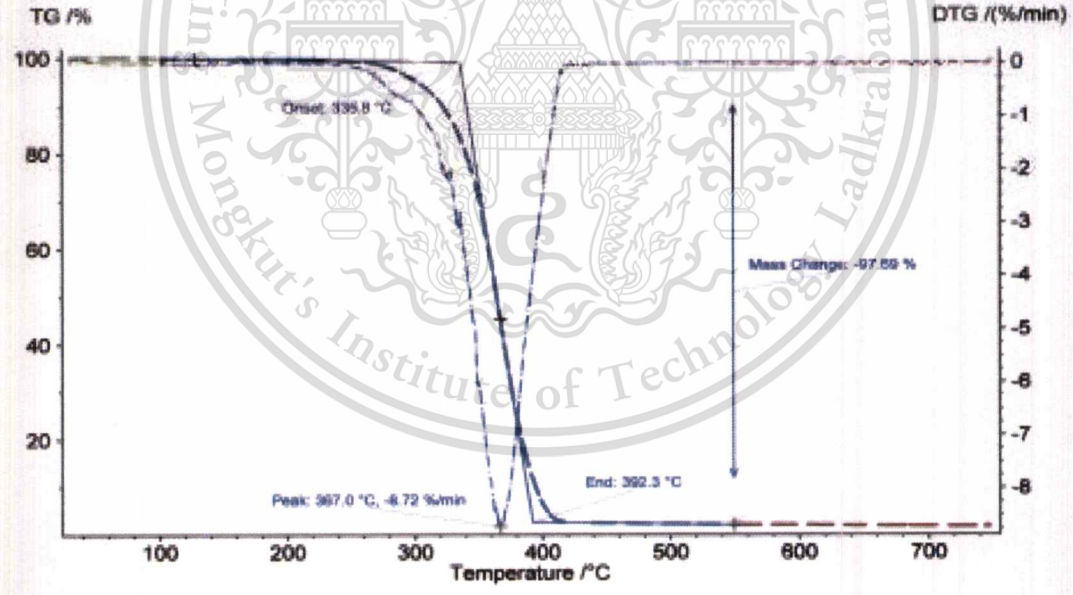


**Fig. F-5** TGA thermogram of M6B4-P3 nanocomposite film

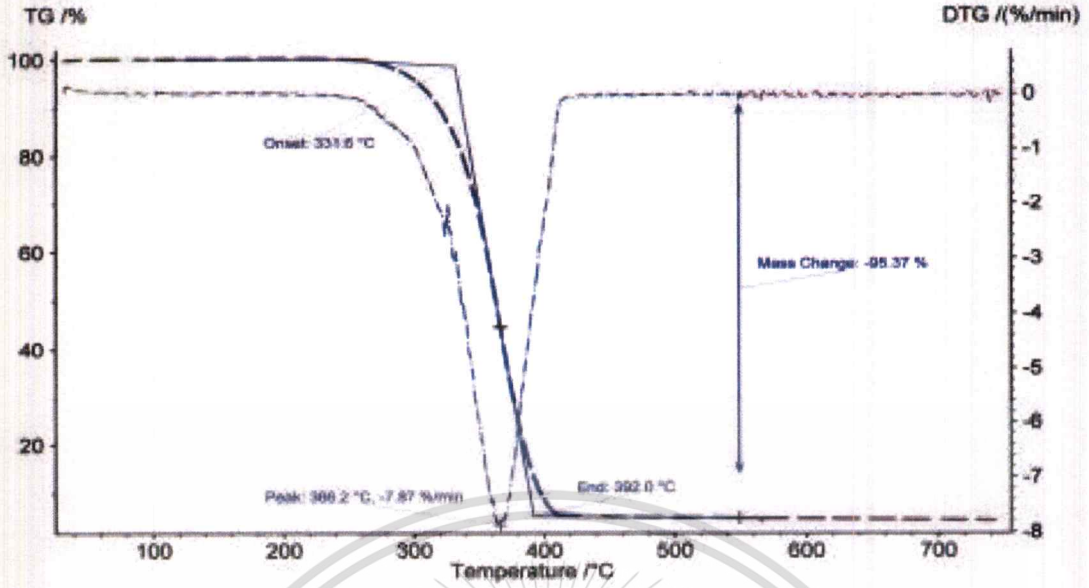


**Fig. F-6** TGA thermogram of M6B4-P6 nanocomposite film

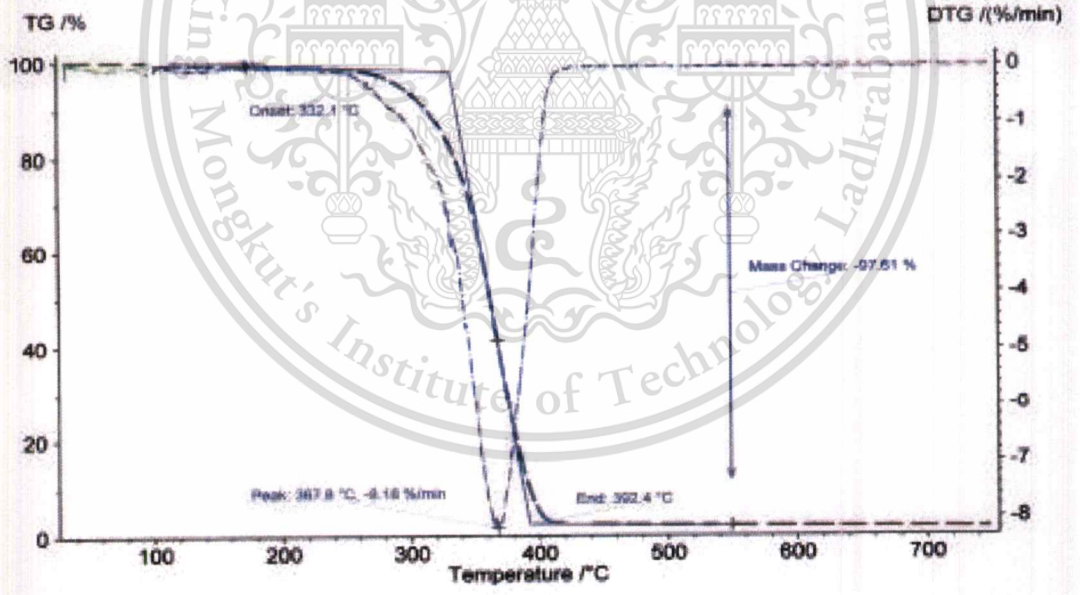


**Fig. F-7** TGA thermogram of M6B4-U2 nanocomposite film

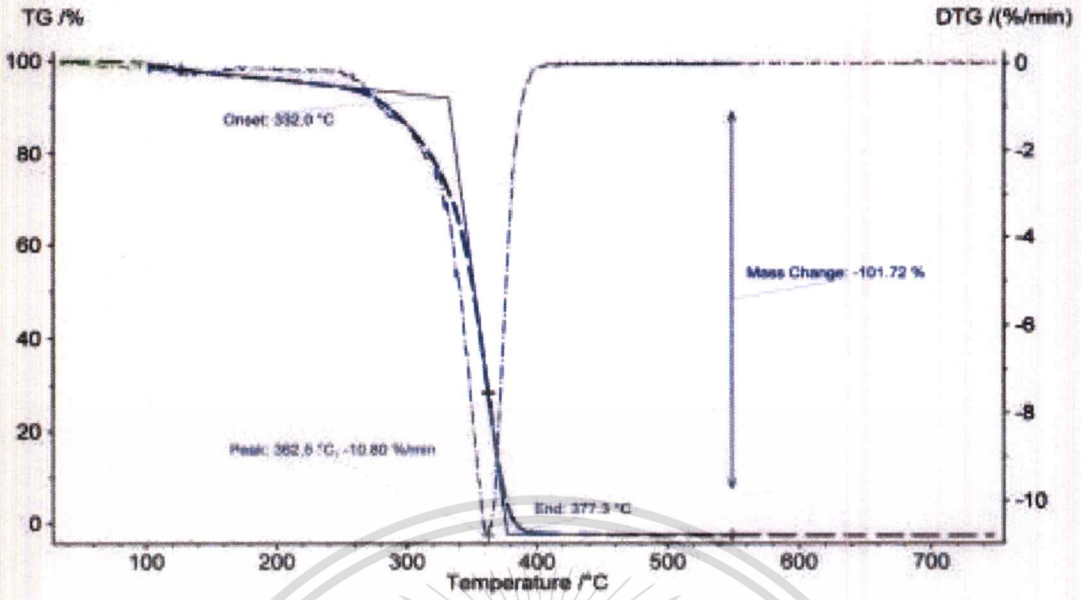


**Fig. F-8** TGA thermogram of M7B3 copolymer

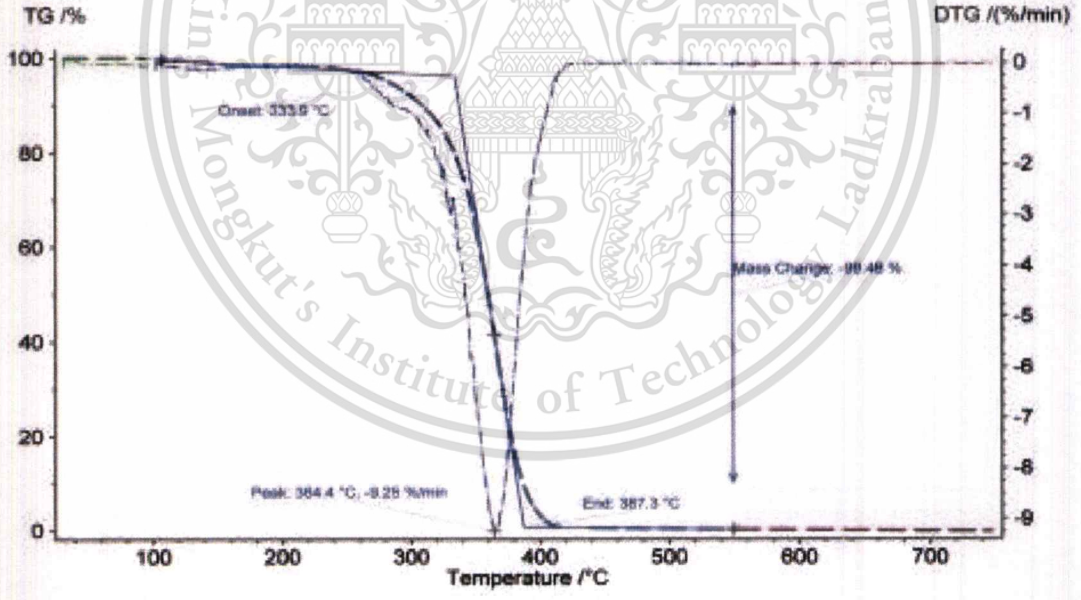


**Fig. F-9** TGA thermogram of M7B3-P1 nanocomposite film

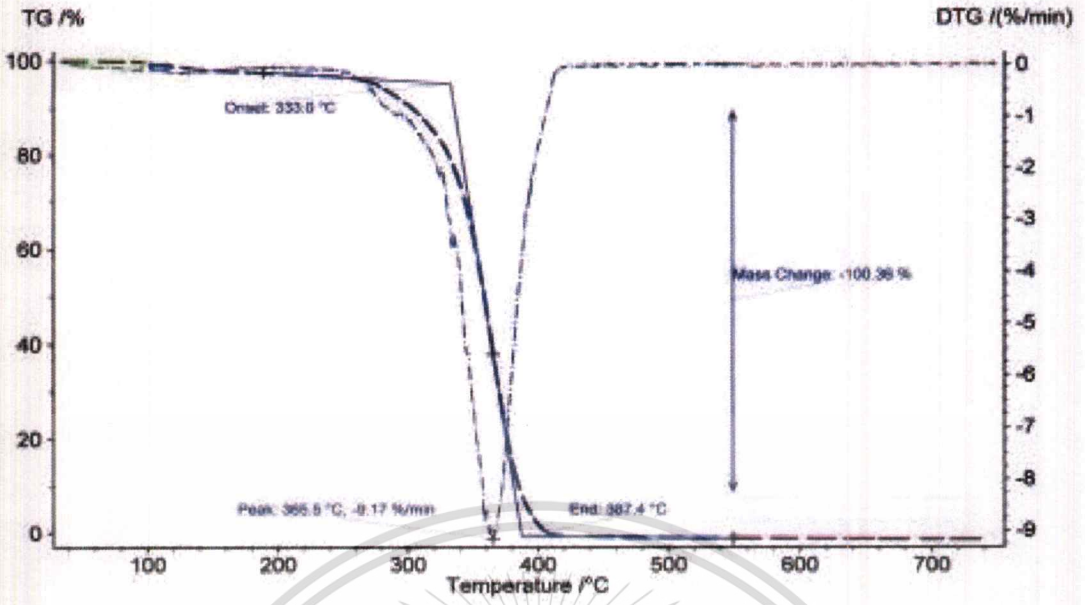


**Fig. F-10** TGA thermogram of M7B3-P2 nanocomposite film

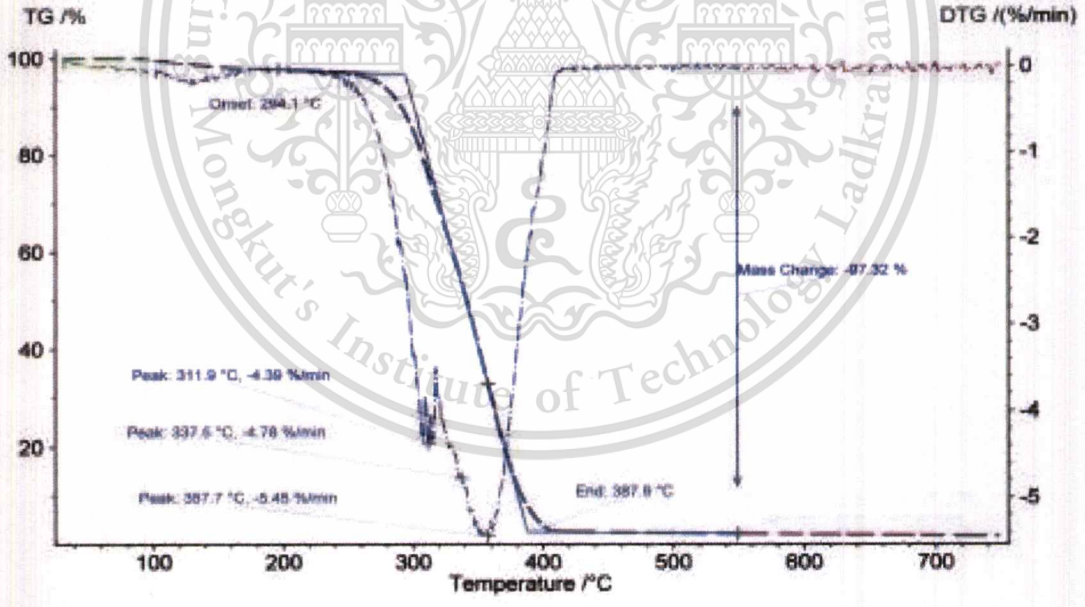


**Fig. F-11** TGA thermogram of M7B3-P3 nanocomposite film

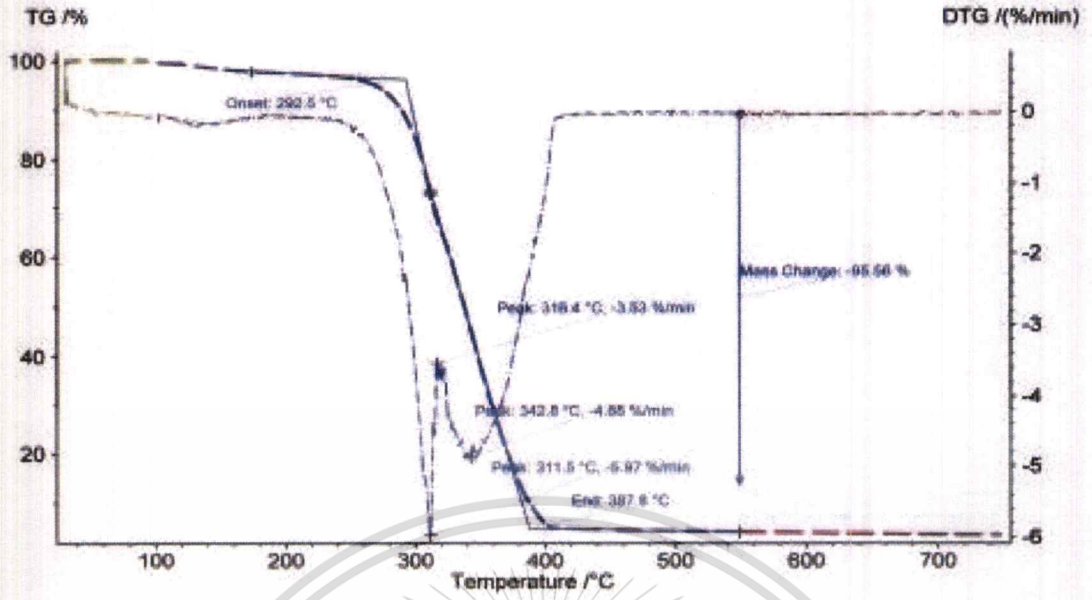


**Fig. F-12** TGA thermogram of M7B3-P6 nanocomposite film

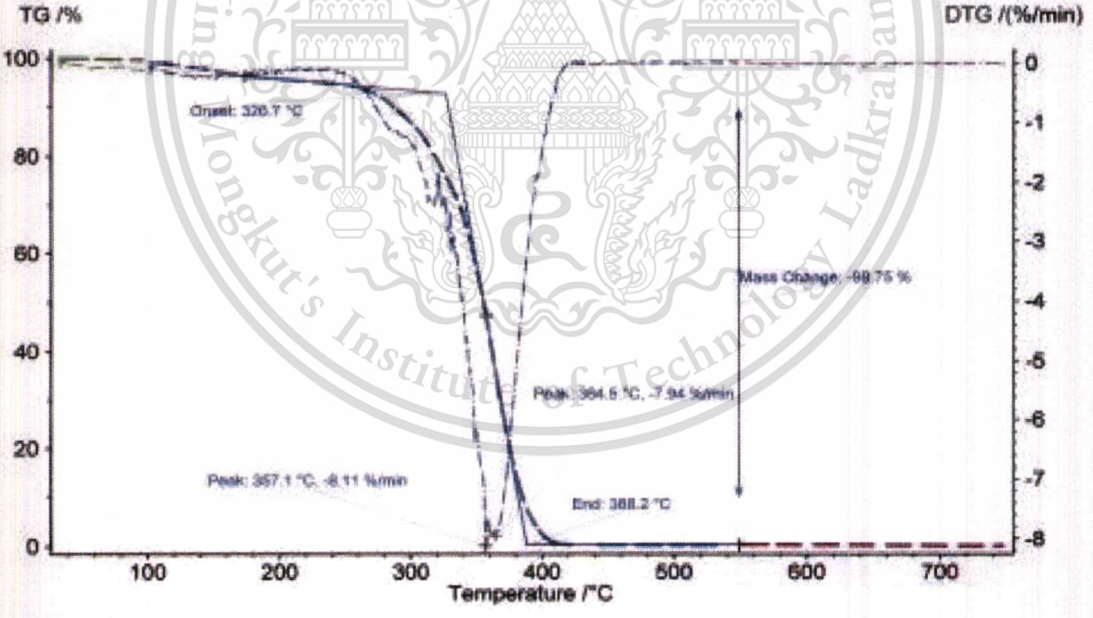


**Fig. F-13** TGA thermogram of M7B3-U2 nanocomposite film

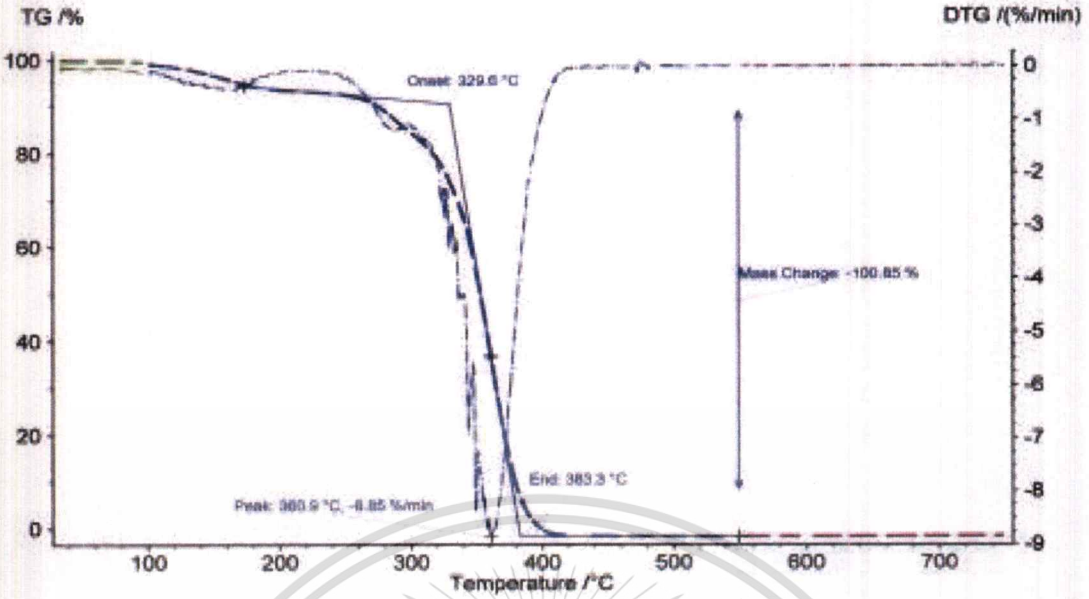


**Fig. F-14** TGA thermogram of M8B2 copolymer

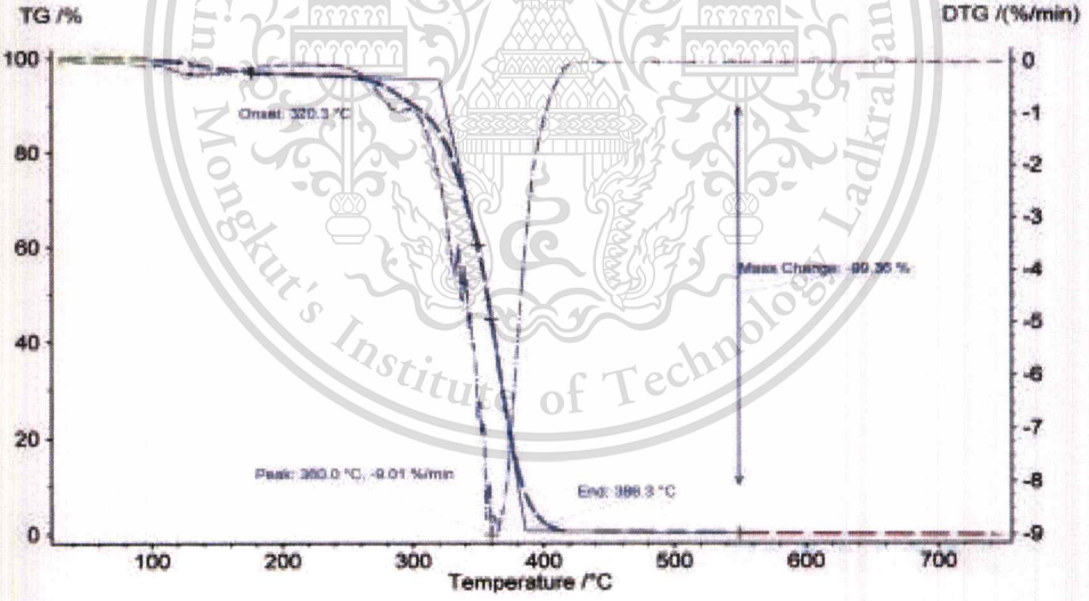


**Fig. F-15** TGA thermogram of M8B2-P1 nanocomposite film

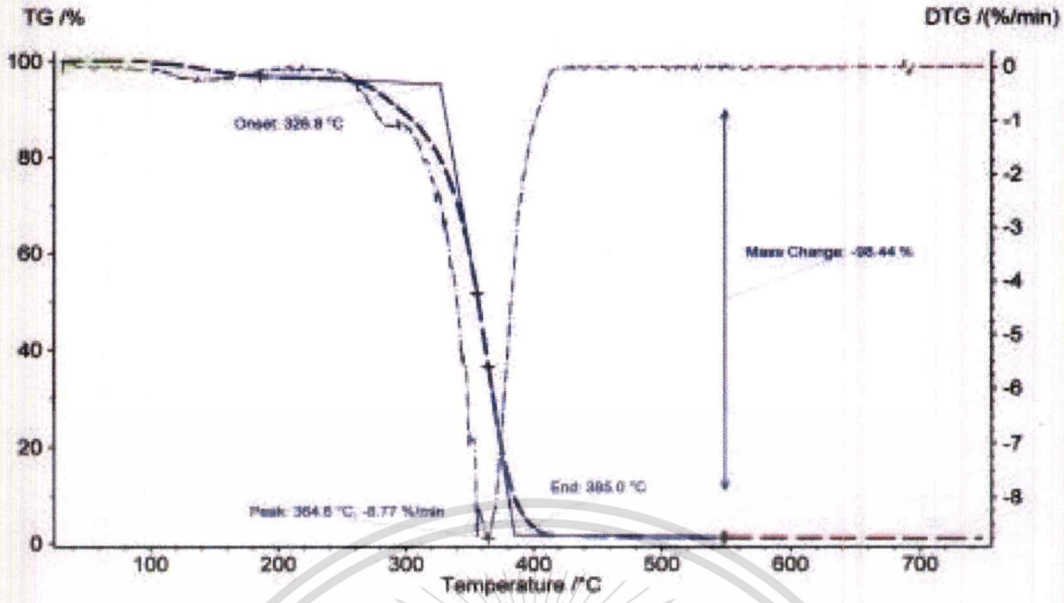


**Fig. F-16** TGA thermogram of M8B2-P2 nanocomposite film

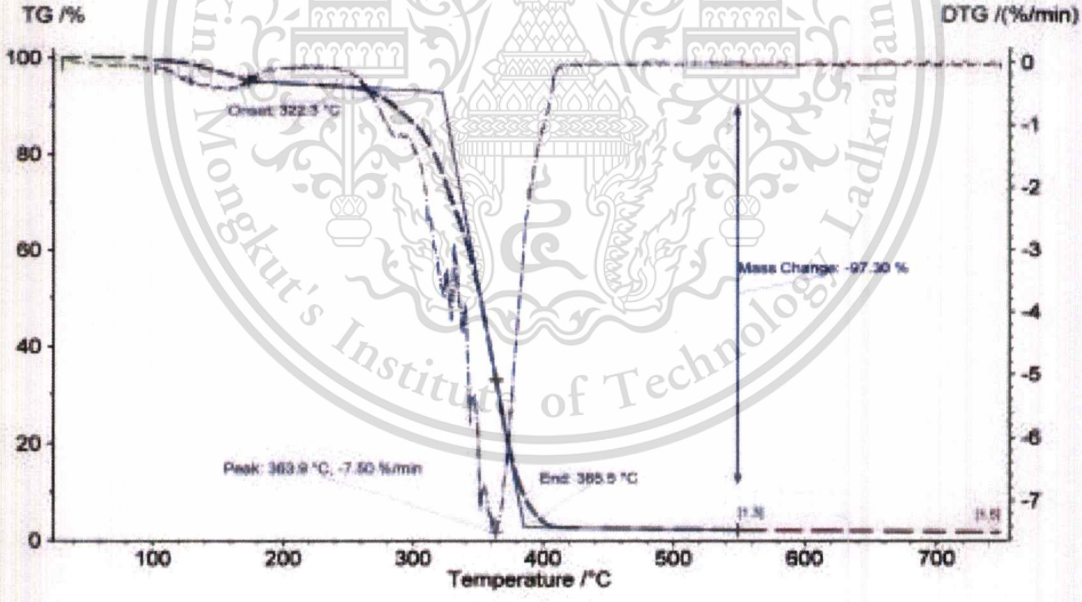


**Fig. F-17** TGA thermogram of M8B2-P3 nanocomposite film

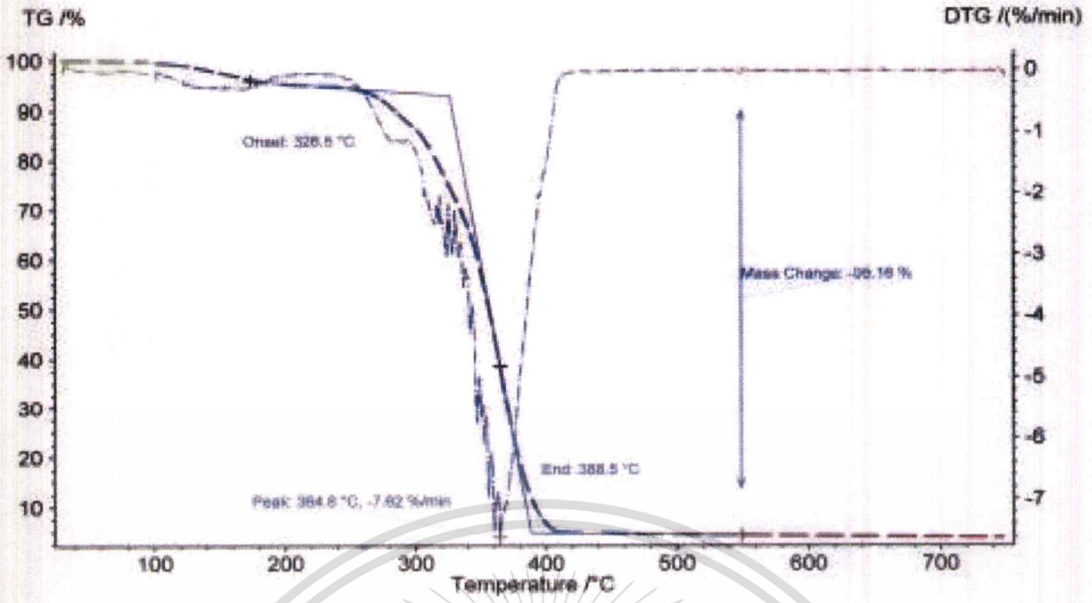


**Fig. F-18** TGA thermogram of M8B2-P6 nanocomposite film

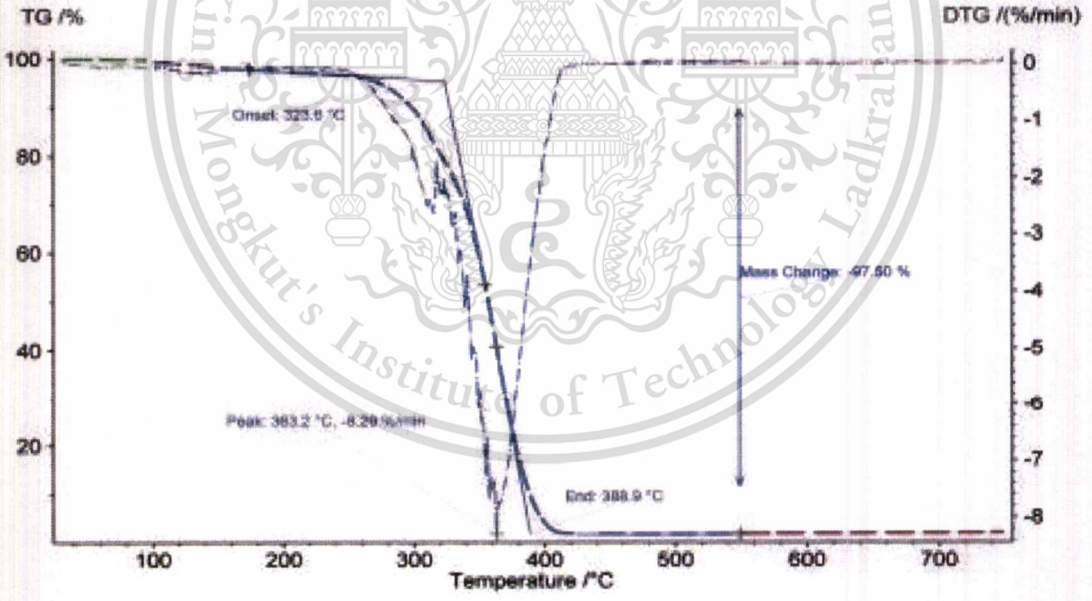


**Fig. F-19** TGA thermogram of M8B2-U2 nanocomposite film

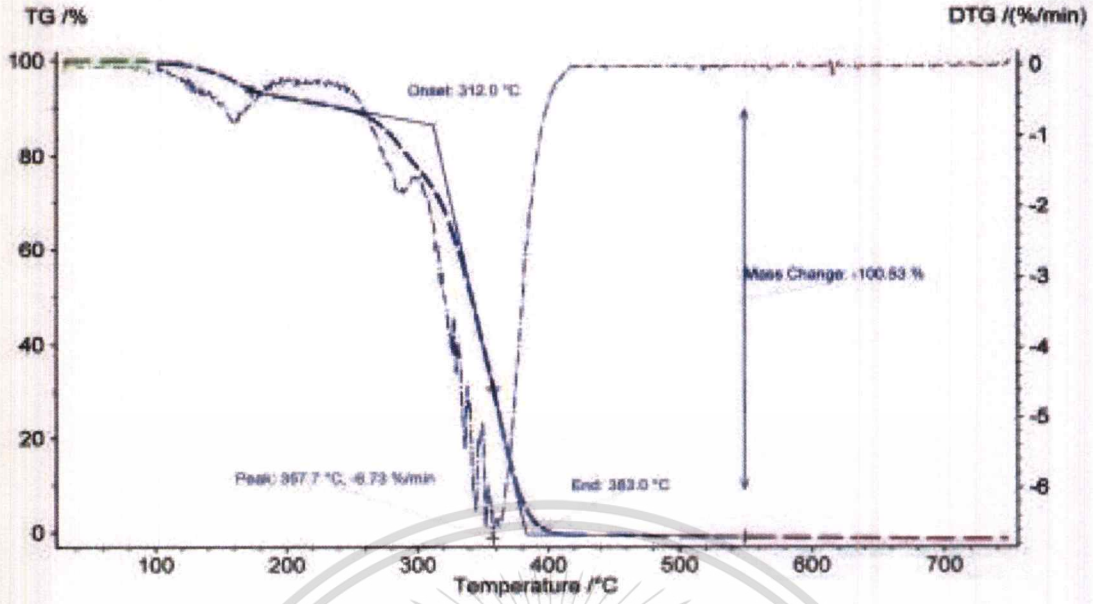


**Fig. F-20** TGA thermogram of M9B1 copolymer

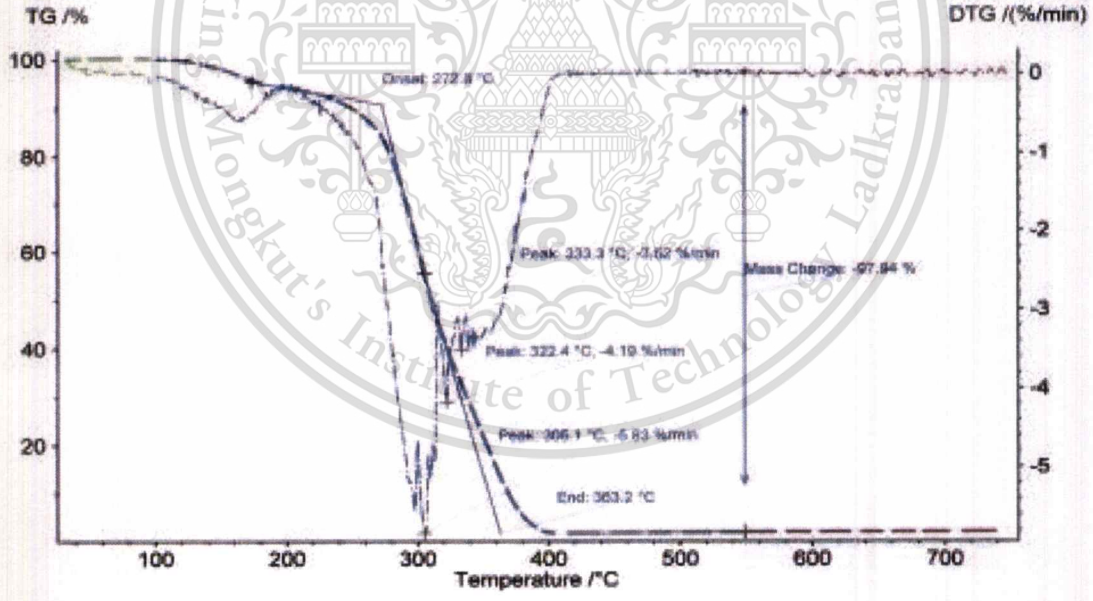


**Fig. F-21** TGA thermogram of M9B1-P1 nanocomposite film

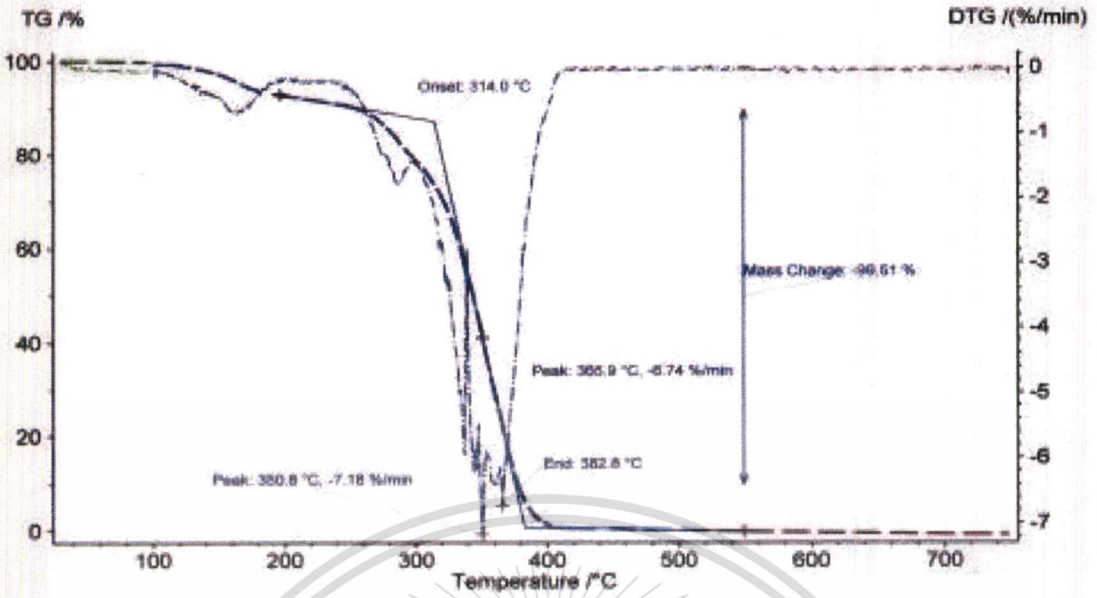


**Fig. F-22** TGA thermogram of M9B1-P2 nanocomposite film

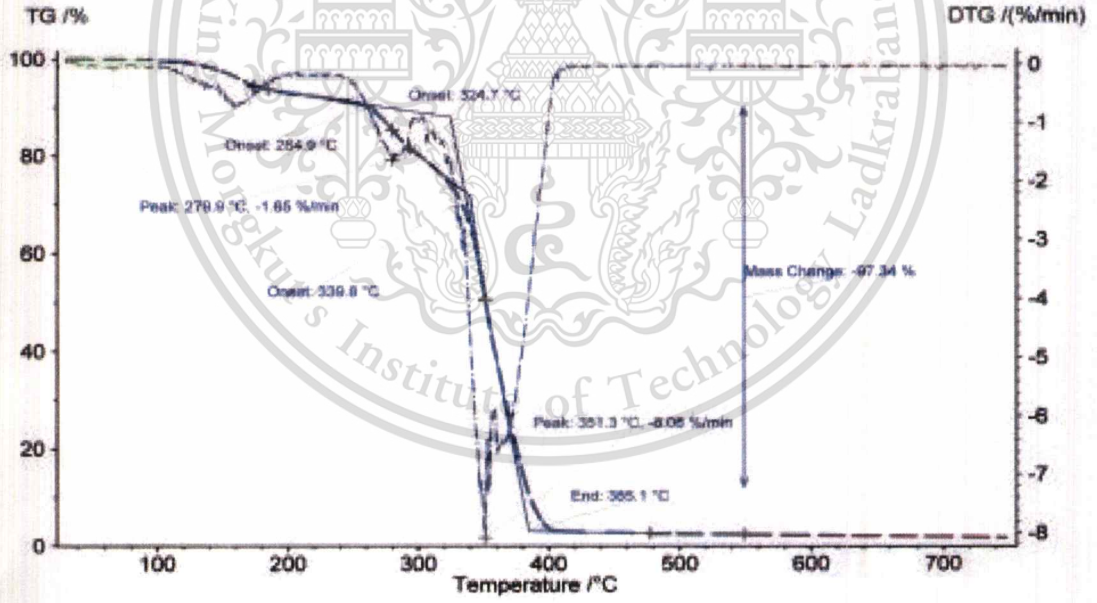


**Fig. F-23** TGA thermogram of M9B1-P3 nanocomposite film

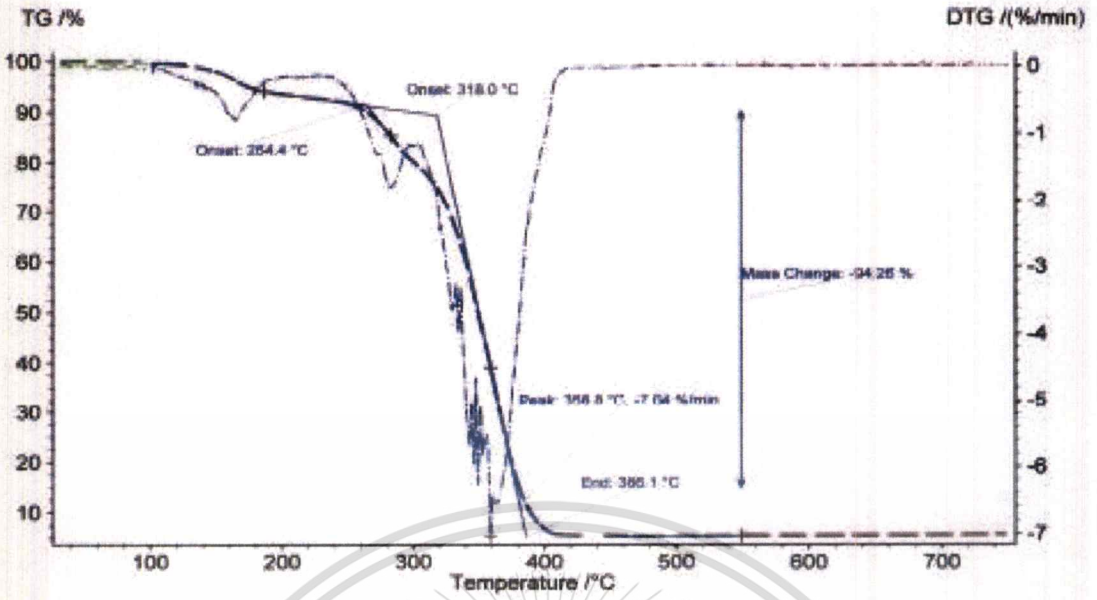


**Fig. F-24** TGA thermogram of M9B1-P6 nanocomposite film

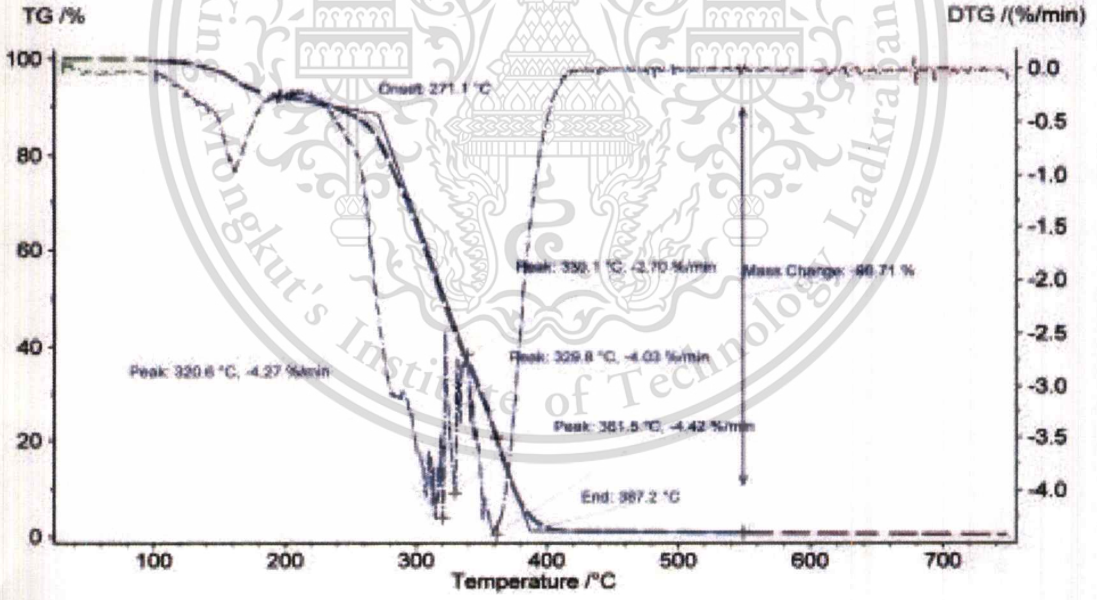


**Fig. F-25** TGA thermogram of M9B1-U2 nanocomposite film

# Appendix G

## Mechanical properties of P(MMA-*co*-BA) and P(MMA-*co*-BA)/ P-MMT nanocomposite films

**Table G-1** Effect of P-MMT and uMMT contents on tensile strength of P(MMA-*co*-BA)/P-MMT nanocomposite films

| Sample formula | Sample no. (MPa) | | | | | Mean (MPa) | SD (MPa) |
|---|---|---|---|---|---|---|---|
| | 1 | 2 | 3 | 4 | 5 | | |
| M6B4-P0* | 9.189 | 9.452 | 8.489 | 9.403 | 8.702 | 9.05 | 0.43 |
| M6B4-P1 | 13.73 | 12.39 | 12.93 | 12.9 | 12.32 | 12.85 | 0.57 |
| M6B4-P2 | 35.72 | 35.34 | 34.54 | 33.73 | 34.53 | 34.78 | 0.78 |
| M6B4-P3 | 54.82 | 51.31 | 52.38 | 51.51 | 53.31 | 52.67 | 1.44 |
| M6B4-P6 | 44.25 | 44.27 | 45.23 | 45.24 | 45.16 | 44.83 | 0.52 |
| M6B4-U2* | 18.06 | 20.43 | 18.56 | 17.45 | 17.55 | 18.41 | 1.21 |
| M7B3-P0 | 11.63 | 11.99 | 10.63 | 9.781 | 9.907 | 10.79 | 0.99 |
| M7B3-P1 | 21 | 21.27 | 21.07 | 20.52 | 20.93 | 20.96 | 0.28 |
| M7B3-P2 | 45.52 | 46.76 | 45.22 | 44.96 | 43.83 | 45.26 | 1.06 |
| M7B3-P3 | 45.47 | 43.79 | 44.2 | 44.8 | 41.79 | 44.01 | 1.39 |
| M7B3-P6 | 44.24 | 41.12 | 40.03 | 42.74 | 39.78 | 41.58 | 1.89 |
| M7B3-U2 | 35.88 | 36.69 | 35.57 | 35.53 | 35.28 | 35.79 | 0.55 |
| M8B2-P0 | 37.06 | 34.65 | 38.07 | 35.88 | 36.26 | 36.38 | 1.28 |
| M8B2-P1 | 42.97 | 42.59 | 41.5 | 41.7 | 40.81 | 41.91 | 0.87 |
| M8B2-P2 | 49.69 | 49.88 | 51.83 | 52.02 | 49.56 | 50.59 | 1.22 |
| M8B2-P3 | 42.01 | 41.22 | 42.38 | 45.16 | 44.12 | 42.98 | 1.62 |
| M8B2-P6 | 35.23 | 34.92 | 36.87 | 36.13 | 37.06 | 36.04 | 0.95 |
| M8B2-U2 | 46.68 | 46.12 | 45.62 | 45.4 | 46.73 | 46.11 | 0.60 |
| M9B1-P0 | 45.6 | 45.9 | 46.1 | 45.4 | 45.2 | 45.64 | 0.36 |
| M9B1-P1 | 46.99 | 47.39 | 49.12 | 46.86 | 48.3 | 47.73 | 0.96 |
| M9B1-P2 | 55.69 | 54.82 | 51.9 | 51.11 | 51.41 | 52.99 | 2.11 |
| M9B1-P3 | 62.65 | 59.64 | 60.24 | 61.09 | 63.84 | 61.49 | 1.73 |
| M9B1-P6 | 46.74 | 46.45 | 46.58 | 47.54 | 49.35 | 47.33 | 1.21 |
| M9B1-U2 | 47.23 | 49.8 | 51.15 | 45.02 | 47.17 | 48.07 | 2.41 |

* *P and U were the abbreviations for P-MMT and uMMT, respectively.*

**Table G-2** Effect of P-MMT and uMMT contents on Young's modulus of P(MMA-*co*-BA)/P-MMT nanocomposite films

| Sample formula | Sample no. (MPa) | | | | | Mean (MPa) | SD (MPa) |
|---|---|---|---|---|---|---|---|
| | 1 | 2 | 3 | 4 | 5 | | |
| M6B4-P0* | 246.5 | 150 | 214.5 | 191.5 | 183.5 | 197 | 35.98 |
| M6B4-P1 | 426.5 | 445.5 | 285.5 | 452 | 402.5 | 402 | 68.13 |
| M6B4-P2 | 930 | 985 | 935 | 945 | 955 | 950 | 21.79 |
| M6B4-P3 | 1740 | 1510 | 1650 | 1890 | 1850 | 1728 | 154.01 |
| M6B4-P6 | 1442 | 1253 | 1509 | 1469 | 1470 | 1429 | 101.03 |
| M6B4-U2* | 424.5 | 618 | 549.5 | 450 | 493 | 507 | 78.07 |
| M7B3-P0 | 291.5 | 315.5 | 306 | 254 | 270 | 287 | 25.35 |
| M7B3-P1 | 742 | 730.5 | 779.5 | 773.5 | 826 | 770 | 37.36 |
| M7B3-P2 | 1345 | 1315 | 1180 | 1295 | 1300 | 1287 | 62.91 |
| M7B3-P3 | 1215.5 | 1217 | 1426 | 1338.5 | 1181 | 1276 | 103.16 |
| M7B3-P6 | 1163 | 1095 | 1052 | 1384 | 1291 | 1197 | 138.19 |
| M7B3-U2 | 1180 | 1200 | 960 | 1050 | 1025 | 1083 | 103.30 |
| M8B2-P0 | 1012 | 790 | 965 | 850 | 800 | 883 | 99.99 |
| M8B2-P1 | 1288 | 1093 | 1151 | 1266 | 1324.5 | 1225 | 98.04 |
| M8B2-P2 | 1322 | 1348 | 1425 | 1615 | 1410 | 1424 | 114.95 |
| M8B2-P3 | 1377.5 | 1231.5 | 1351 | 1545 | 1410.5 | 1383 | 112.92 |
| M8B2-P6 | 1325.5 | 1216 | 1209.5 | 1194 | 1285.5 | 1246 | 56.61 |
| M8B2-U2 | 1453 | 1430 | 1280 | 1270 | 1320 | 1351 | 85.45 |
| M9B1-P0 | 1020 | 1070 | 1100 | 1250 | 1000 | 1088 | 98.84 |
| M9B1-P1 | 1535 | 1720 | 1560 | 1540 | 1305 | 1532 | 148.10 |
| M9B1-P2 | 1740 | 1840 | 1625 | 1485 | 1610 | 1660 | 135.23 |
| M9B1-P3 | 1725 | 1825 | 1700 | 1860 | 1760 | 1774 | 67.21 |
| M9B1-P6 | 1605 | 1480 | 1700 | 1720 | 1560 | 1613 | 99.47 |
| M9B1-U2 | 1405 | 1484 | 1505 | 1511 | 1622 | 1505 | 77.73 |

* *P and U were the abbreviations for P-MMT and uMMT, respectively.*

**Table G-3** Effect of P-MMT and uMMT contents on % elongation at break of P(MMA-*co*-BA)/P-MMT nanocomposite films

| Sample formula | Sample no. (%) | | | | | Mean (%) | SD (%) |
|---|---|---|---|---|---|---|---|
| | 1 | 2 | 3 | 4 | 5 | | |
| M6B4-P0* | 374.6 | 336.9 | 429.2 | 343 | 348.6 | 367 | 37.90 |
| M6B4-P1 | 251 | 224.7 | 286.8 | 315.7 | 252.4 | 266 | 35.42 |
| M6B4-P2 | 43.82 | 35.9 | 31.74 | 29.58 | 28.82 | 34 | 6.15 |
| M6B4-P3 | 6.456 | 6.854 | 6.882 | 6.403 | 7.533 | 7 | 0.45 |
| M6B4-P6 | 10.28 | 5.953 | 6.119 | 8.363 | 7.81 | 8 | 17.66 |
| M6B4-U2* | 241.2 | 259.5 | 271.3 | 266.4 | 203.7 | 248 | 27.48 |
| M7B3-P0 | 221.3 | 226.2 | 227.8 | 229.5 | 228.6 | 227 | 3.24 |
| M7B3-P1 | 50 | 59.41 | 57.24 | 79.6 | 68.83 | 63 | 11.45 |
| M7B3-P2 | 4.554 | 4.489 | 4.311 | 5.222 | 4.219 | 5 | 0.40 |
| M7B3-P3 | 7.523 | 6.951 | 6.791 | 5.725 | 6.851 | 7 | 0.65 |
| M7B3-P6 | 7.128 | 7.794 | 7.365 | 7.042 | 5.387 | 7 | 0.92 |
| M7B3-U2 | 105.2 | 134.8 | 185.1 | 124 | 169.3 | 144 | 32.86 |
| M8B2-P0 | 23.91 | 24.67 | 24.92 | 22.5 | 23.01 | 24 | 1.04 |
| M8B2-P1 | 4.524 | 4.529 | 4.626 | 4.639 | 4.323 | 5 | 0.13 |
| M8B2-P2 | 4.962 | 4.798 | 5.488 | 5.733 | 5.656 | 5 | 0.42 |
| M8B2-P3 | 4.087 | 4.272 | 3.779 | 4.214 | 4.647 | 4 | 0.31 |
| M8B2-P6 | 4.046 | 3.972 | 4.82 | 4.648 | 4.05 | 4 | 0.40 |
| M8B2-U2 | 8.03 | 6.801 | 6.381 | 6.969 | 8.973 | 7 | 1.05 |
| M9B1-P0 | 4.305 | 4.987 | 5.148 | 5.541 | 6.722 | 5 | 0.89 |
| M9B1-P1 | 4.844 | 4.282 | 4.78 | 4.351 | 5.7 | 5 | 0.57 |
| M9B1-P2 | 5.789 | 4.616 | 5.289 | 5.636 | 5.47 | 5 | 0.46 |
| M9B1-P3 | 6.147 | 5.347 | 5.515 | 5.283 | 6.12 | 6 | 0.42 |
| M9B1-P6 | 4.795 | 4.966 | 4.719 | 4.454 | 5.043 | 5 | 0.23 |
| M9B1-U2 | 5.869 | 6.962 | 6.455 | 5.206 | 5.185 | 6 | 0.78 |

* *P and U were the abbreviations for P-MMT and uMMT, respectively.*

# Author Biography

| | |
|---|---|
| **Name** | Mr.Sanit Sirapanichart |
| **Date of Birth** | September, 19th, 1984 |
| **Address** | 403/5 Adulyadej 7, Soi., Adulyadej, Rd., Muang, Udon Thani, Thailand 41000 |
| **Education** | 2008 B.Sc. (Petrochemical Technology) (GPA: 3.42) King Mongkut's Institute of Technology Ladkrabang, Thailand Research Topic: *Preparation of Organophosphate Modified Montmorillonite/Poly(methyl methacrylate) Nanocomposites* |
| **Award** | 2006 Scholarship for Good GPA Student, KMITL, Thailand |

**Conference and Publication**

1. S. Sirapanichart, S. Macksasitorn, S. Buakheio, P. Siriphannon, and P. Monvisade, **Preparation of Organophosphate Modified Montmorillonite/Poly(methyl methacrylate) Nanocomposites**, The 34th Congress on Science and Technology of Thailand (STT34) 2008.
2. Sirapanichart S., Khouchaf L., Siriphannon P., Monvisade P., Louarn G., and Elouadi B., **Chemical and Dielectric Study of PMMA/Montmorionite NanoComposite Films**, *Ferroelectrics*, 2010, 402:1, 47-54.
3. S. Sirapanichart, P. Monvisade, P. Siriphannon, and J. Nukeaw, **Poly(methyl methacrylate-co-butyl acrylate)/Organophosphate-modified Montmorillonite Composites**, *Iranian Polymer Journal*, 2011, 20:10, 803-811.

**Training Experience**

2007 Special training in "Occupational Healthy and Safety for Managers" at RMIT University, Australia